UNIVERSITEIT VAN PRETORIA
UNIVERSITY OF PRETORIA
YUNIBESITHI YA PRETORIA

Multicellular spheroids as a platform for cytotoxicity assessment of nanoparticles

by

Melissa Petzer

A dissertation submitted in fulfilment of the requirements for the degree

Magister Scientiae

in

Pharmacology

in the

Faculty of Health Sciences

at the

University of Pretoria

Supervisor

Prof W Cordier

Co-supervisors

Prof M Gulumian

Prof V Steenkamp

January 2023

1. Declaration

University of Pretoria

Faculty of Health Sciences

Department of Pharmacology

I, Melissa Petzer,

Student Number: 15027709

Subject of work: Dissertation

Title: Multicellular spheroids as a platform for cytotoxicity assessment of nanoparticles

Declare that:

1. I understand what plagiarism is and am aware of the University's policy in this regard
2. I declare that this dissertation is my own original work. Where other people's work has been used, this has been properly acknowledged and referenced in accordance with applicable requirements
3. I did not make use of work previously presented by another student and submitted it as my own
4. I have not allowed, and will not allow anyone to copy my work with the intention of passing it off as his, her, or their own work

Signature

Date

05/01/2023

---

2. Abstract

Nanoparticles are attractive candidates for drug development given their variable size, functionalisation, and reactivity with molecules. Gold nanoparticles possess the potential to elicit anticancer effects, though often these are determined in two-dimensional cell models that fail to represent the *in vivo* environment appropriately. Three-dimensional cultures, such as multicellular spheroids, offer greater representation, particularly due to their heterogenous phenotype and complex molecular architecture. This study aimed to develop an A549 alveolar carcinoma spheroid model to use as a mechanistic cytotoxicity testing platform for functionalised gold nanoparticles.

A549 multicellular spheroids were generated using an agarose micro-mould, with characterisation (morphology, acid phosphatase activity, protein content) over 21 days of growth. Cytotoxicity of 14 nm carboxyl-polyethylene glycol- and 20 nm amine-coated gold nanoparticles in spheroids were assessed on the seventh day post-seeding by determining the effect on morphology, acid phosphatase activity, protein content, caspase-3/7 activity and cell cycle alterations.

A549 spheroids were maintained over 21 days of growth, however they started to lose structural integrity on day 14. The 14 nm carboxyl-polyethylene glycol-liganded gold nanoparticles were not cytotoxic at a maximum concentration of 1.2 x 10^{12} nanoparticles/mL. The 20 nm amine-coated gold nanoparticles yielded dose- and time-dependent cytotoxicity, where decreased spheroid compactness was observed over a three-day exposure period at 4.5 x 10^{12} nanoparticles/mL. Over the same exposure time, no effect on the protein content was observed. Increased debris formation and deoxyribonucleic acid (DNA) fragmentation was observed through flow cytometric analysis, as well as a 75.00% decrease (significant, $p \leq 0.001$ in acid phosphatase activity, though no increase in caspase-3/7 activity occurred.

Spheroids were successfully formed and remained stable over the experimental period. Furthermore, differentiation between cytotoxic and non-cytotoxic gold nanoparticles, and further elucidation of its potential cytotoxic mechanism, was accomplished. Successful implementation of this method has therefore afforded greater representation of *in vitro* findings to the *in vivo* environment.

Keywords: alveolar carcinoma, gold nanoparticles, multicellular spheroid model, cytotoxicity

3. Research outputs

Poster presentation at national conference

Petzer M, Gulumian M, Steenkamp V, Cordier W. Multicellular spheroids as a platform for cytotoxicity assessment of nanoparticles. 54th Conference of the South Africa Society for Basic and Clinical Pharmacology, 22 October 2021 [Virtual].

Poster presentation at international conference

Petzer M, Gulumian M, Steenkamp V, Cordier W. Multicellular spheroids as a platform for cytotoxicity assessment of nanoparticles. 7th All Africa Congress of Basic and Clinical Pharmacology, 15 – 17 September 2021. [Virtual] [*Runner-up*: *Best Basic Pharmacology Poster*].

Publication

Fobian S-F, Petzer M, Vetten M, Steenkamp V, Gulumian M, Cordier W. Mechanisms facilitating the uptake of carboxyl-polyethylene glycol-functionalized gold nanoparticles into multicellular spheroids. Journal of Pharmacy and Pharmacology 2022 [https://doi.org/10.1093/jpp/rgac017].

4. Acknowledgements

I would like to thank the following individuals and institutions, without whom I would not have made it this far, be it in my education, or my life.

Seth-Frerich Fobian – for being the best research partner and a true friend. Working with you was an honour and a privilege.

Natie and Magriet Petzer – my parents, who have made me the woman I am today, and wholeheartedly supported me through every step of every journey I've embarked on, with zero hesitation.

Amoré Lacante – my sister and constant inspiration.

Zaudi Falzoné – my oldest friend and biggest cheerleader.

Shanique Coetzee – my best friend and constant support.

Andy Ellero – for emotional, laboratory and academic support too large to put into words.

The ICMM – for use of the CytoFlex flow cytometer.

Dr. Chrisna Durant – for training and protocol setup on the CytoFlex as well as training on data reading and interpretation.

Margo Nell – for the use of your lab in 2020 and exceptional insights into cell culture.

Funding for experimentation is hereby acknowledged from Brazil, Russia, India, China, South Africa (BRICS) in conjunction with the National Research Foundation (NRF) through the DST-NRF Innovation Masters Scholarship.

The almost four-year journey to finishing this degree taught me so many things, not all of them scientific or academic. I have been humbled by the opportunity to become a scientist; a privilege not obtainable to many women around the world. These women, who are yet to experience the beauty of learning, of knowledge and education in science, are what powered me to not give up, even when I really wanted to.

"I was taught that the way of progress was neither swift nor easy"

-Marie Curie

5. List of abbreviations, units, and symbols

2D	Two-dimensional
3D	Three-dimensional
Ac-DEVD-AMC	Acetyl-Asp-Glu-Val-Asp-7-amido-4-methylcoumarin
ADR	Adverse drug reaction
Amine-AuNP	Amine-liganded gold nanoparticles
APH	Acid phosphatase
ATCC	American Type Culture Collection
ATP	Adenosine triphosphate
Au	Gold
AuNP	Gold nanoparticle
BCA	Bicinchoninic acid
Br	Bromide
BSA	Bovine serum albumin
C	Carbon
CDA	Caspase-dependent apoptosis
CDK	Cyclin-dependent kinase
cells/mL	Number of cells per millilitre
cells/MCS	Number of cells per multicellular spheroid
cells/well	Number of cells per culture plate well
CIA	Caspase-independent apoptosis
CoA	Certificate of analysis
COOH	Carboxyl
CO_2	Carbon dioxide
CIE	Caveolae-independent endocytosis
CME	Caveolae-mediated endocytosis
Cu^{+}	Cuprous ions
Cu^{2+}	Copper ions
DAH	Differential adhesion hypothesis
DDS	Drug delivery system

DMEM	Dulbecco's Modified Eagle's Medium
DNA	Deoxyribonucleic acid
ECM	Extracellular matrix
EDTA	Ethylenediamine tetraacetic acid
FCS	Foetal calf serum
FI	Fluorescent intensity
g	Gravitational force
g	Grams
h	Hour
H	Hydrogen
KCl	Potassium chloride
kV	Kilovolt
LDH	Lactate dehydrogenase
M	Molar
MCS	Multicellular spheroid
min	Minutes
mg	Milligram
mL	Millilitre
N	Nitrogen
NSCLC	Non-small cell lung cancer
NaOH	Sodium hydroxide
NIOH	National Institute for Occupational Health
NP	Nanoparticle
NP/mL	Number of nanoparticles per millilitre
nm	Nanometre
O	Oxygen
OD	Optical density
PBS	Phosphate-buffered saline
PC	Phase-contrast
PCOOH-AuNP	Carboxyl-polyethylene glycol-liganded gold nanoparticles
PEG	Polyethylene glycol
PI	Propidium iodide

POC	Proof-of-concept
R&D	Research and development
RBC	Red blood cells
RIPA	Radioimmunoprecipitation assay
RLU	Relative light units
RNA	Ribonucleic acid
S	Sulphur
SCLC	Small cell lunch cancer
TEM	Transmission electron microscope
UV	Ultraviolet
USA	United States of America
V	Volume
% v/v	Percentage volume per volume
% w/v	Percentage weight per volume

Symbols

°C	Degrees Celsius
µ	Micro
µg	Microgram
µg/MCS	Microgram per multicellular spheroid
µL	Microlitre
µm	Micrometre
%	Percentage
π	P
®	Registered trademark
™	Trademark
iζ	Zeta

6. List of Figures

7. List of Tables

Table of contents

1. Chapter 1: Literature review

1.1. The drug development process

New treatments for diseases are continuously being sought, however, these require a strict pipeline of development to ensure their safe and efficacious use. The drug development process for a single drug is lengthy and can last up to 15 years.[1] Although this process is expensive, resource-intensive and far from ideal, the drug development process has shown significant improvement over the past few decades.[2-3] Hay *et al*. noted that the number of new compounds entering the development process increased by 62% between 2003 and 2013.[4] However, the rate of novel drug approval in this timeframe (2003 – 2013) was 25% less in comparison to the 1990's,[5] indicating a lower rate of approval regardless of the increased amount of drug candidates.

The amount of money invested in drug research and development (R&D) has significantly increased three-fold in cost between 1995 and 2014.[6] In 2010, it was estimated that $85 billion was spent on the development of new drugs,[7] which relates to a cost of $2.6 billion per individual drug.[8] Comparing this expenditure to the small number of new drugs that are approved and enter the market, it is estimated that $60 billion is 'lost' per year.[7]

There are two main reasons for drugs failing to complete the drug development process in modern R&D: a lack of efficacy or high toxicity.[3,9-10] Compounds need to be clinically effective against the targeted disease, while being safe for the patient to use (i.e. not exceeding an acceptable level of toxicity).[3] Kola reported that 60% of drug attrition was mainly due to either a lack of efficacy or excessive toxicity.[3] Cancer drug R&D has among the highest rates of drug attrition in therapeutic drug research.[10] In oncopharmacology, only 5% of drugs that showed efficacy in pre-clinical testing were marketed after phase III clinical trials.[11-12]

A review of small molecule drug discovery projects by AstraZeneca between 2005 and 2010 found that lack of safety of the molecule was the main reason for molecule attritions in the preclinical phase (82%).[13] Even if a drug is successfully marketed, it may still be withdrawn due to adverse drug reactions (ADRs) that are reported.[11]

Safety and efficacy screening needs to be prioritised in the design of models for pre-clinical studies.[14] Furthermore, some molecules that successfully passed through the pre-clinical phase of development are discarded at later stages of drug development.[1] Many compounds that showed activity in *in vitro* studies may fail to reproduce these effects *in vivo*.[15] There are various reasons why this phenomenon is observed.

One explanation for the disconnect between *in vitro* and *in vivo* results is the use of animal models. Animal models are a common preclinical *in vivo* tool used when progressing through the drug development pipeline from *in vitro* studies to *in vivo* human clinical trials.[16] In research fields where drug attrition rates are highest, like cancer R&D, it has been noted that the chosen *in vivo* animal models possess low similarity to the involved human pathophysiology.[10] An example of this is the widespread use of xenograft models in cancer drug R&D.[17] It is often observed in the xenograft model that, not only does the altered immunology of the mouse not resemble the human immunology, but also that the tumour cell line has little relevance to the human *in vivo* tumour.[10]

A better solution to the sub-optimal use of animal models is incorporating proof-of-concept (POC) in the preclinical phases of drug R&D study design.[10] The goal of POC is to determine at an early stage in the R&D pipeline what the probability of success of the drug might be in later clinical stages of testing.[18] This is especially important when testing new drug molecules, because it enables earlier decision making on whether it would be feasible to continue down the R&D pipeline.[10,19] The advantage of using POC is that it provides evidence that the molecule reaches its target in the body and indicates what the physiological response to the drug is.[10] Including POC could also reduce research costs - as more information is acquired in the earlier phases of R&D that determines how the rest of the phases will be designed or if development is halted.[19] In order for POC to be successful, the *in vitro* model chosen needs to be representative of the pathophysiology observed *in vivo*.[13] The low resemblance of classic *in vitro* assays to the physiological tissue is another explanation for the phenomenon of disconnect between *in vitro* and clinical outcomes in R&D.[15] A higher mimicry of the *in vivo* environment would allow for increased predictive power of *in vitro* cell-culture based studies, which could

subsequently reduce cost and other resources used at later stages of the drug development pipeline.[19]

1.2. *In vitro* cell culturing as a drug development model

Cell culture has been widely used as a modelling structure for studying the physiology and biochemistry of cells in drug development and screening.[20] Cell culture serves as an initial modelling system to show possible effects of a potential new drug in a physiological setting.[14] Various factors determine the most appropriate method for culturing, including the type of cell line and the new molecule/drug being screened.[14]

1.2.1. Two-dimensional cell culture model

The two-dimensional (2D) cell culture model is a well-established method used in pre-clinical screening, which consists of a monolayer of cells attached to a flat, artificial culture surface.[14,20] The formation of a monolayer incurs a forced morphology which is not natural for all cell types, especially cancerous cells.[20]

Although the 2D method is still widely used in cancer research, it has various limitations. The cells in 2D culture attach mainly to an artificial surface and interact with other cells at the periphery only, which is not consistent with the *in vivo* cancer phenotype.[20] Even though cultured cancer cells were derived from human primary tumours, these cells differ vastly from *in vivo* tumours.[12,14] There are various genes and receptors expressed in the *in vivo* tumour which are often not present in monolayer culture.[14] A549 *in vivo* tumours have been shown to have basal expression of genes that encode proteins like laminin and fibronectin. Fibronectin has been observed to be significantly reduced in 2D culture.[21] In monolayer cultures, the cells lack the cellular heterogeneity or mechanisms to enable drug resistance that is known to be a property of primary human tumours.[12,22]

Cells in 2D culture do not experience gravity in the same way as *in vivo* tumours and don't react to stimuli proportionately to the *in vivo* situation.[23-24] The environment around the *in vivo* tumour is very important due to interactions that occur between the environment and the tumour leading to resistance to drugs.[25] The 2D model cannot accurately simulate this natural *in vivo* environment of the cells, which often leads to poor outcomes in drug discovery.[26] Although the 2D cell culture model

provides a wealth of knowledge on mechanisms related to cancer growth and survival,[27] given their high drug failure rate, it reaffirms that this method cannot be solely relied upon in drug development.[11]

1.2.2. The extracellular matrix

The extracellular matrix (ECM) is defined as a network of molecules synthesised intracellularly and secreted extracellularly to support surrounding cells.[28-29] The ECM is a collection of proteins, polysaccharides, proteoglycans and glycoproteins.[29-30] Functions of the ECM include; intracellular communication, cell signalling, cellular differentiation, adhesion and maintenance of homeostasis.[31-32] A key feature of cancer is its ability to survive without adhesion to the ECM, which is why 2D culture was initially deemed useful. The role of the ECM in cancer is more complex than just adhesion to cells.[33] The ECM also provides biochemical cues that mediate cellular development.[34-35] These functions make the ECM a vital part of the *in vivo* tumour microenvironment that facilitate the progression of cancers.[12]

The ECM structure comprises the interstitial matrix and extracellular basement membrane (**Figure 1.1**).[29,36] The cells of the basement membrane are responsible for synthesis of ECM components that are secreted into the interstitial matrix, where they function as a tissue scaffold for cellular organisation.[29] The extracellular basement membrane is a specialised form of ECM which consists of various types of collagen, laminins, fibronectin and various linker proteins.[29,37] The basement membrane is a sheet-like ECM that provides anchorage for epithelial cells, allowing for support and maintenance of tissue polarity.[30] The main constituent of the interstitial matrix is collagen type I, which provides mechanical strength to the tissue.[37]

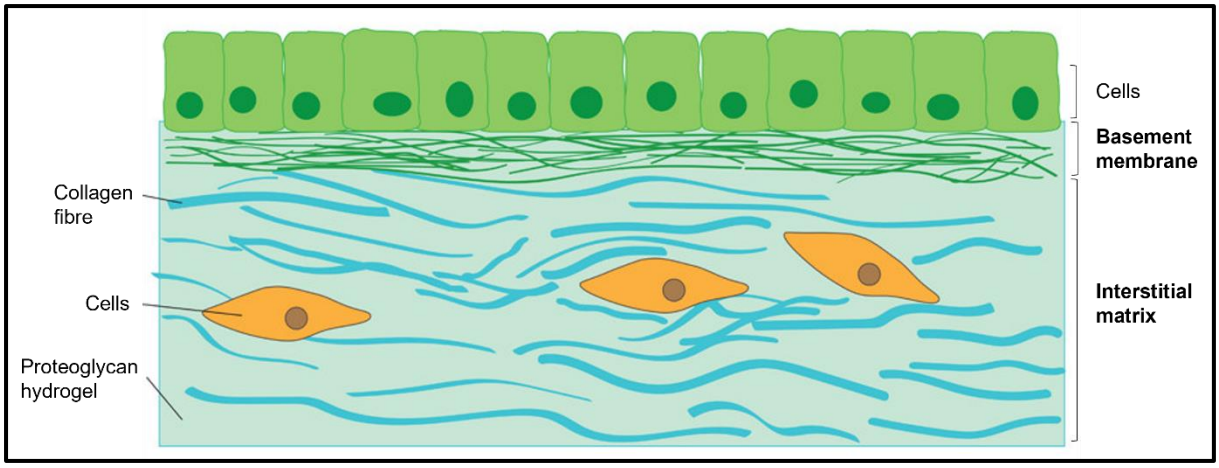

Figure 1.1: Structure of the extracellular matrix. Reprinted with permission and minor modification to annotations from Accounts of Chemical Research, Volume 51, Issue 7, Ieva Goldberga, Rui Li, Melinda J. Duer, Collagen structure-function relationships from solid-state NMR spectroscopy, Pages No. 1621-1629, Copyright (2018), with permission from American Chemical Society (Link: https://pubs.acs.org/doi/10.1021/acs.accounts.8b00092).

Dynamic remodelling of the ECM is an important process that mediates tissue homeostasis and development; as such neoplasms may form when the process occurs uncontrolled.[30,38] Dysregulation of the ECM can lead to cancer or accelerate the progression of existing cancer, and a distinctly remodelled ECM structure and composition is often observed in tumours (**Figure 1.2**).[32] In a standard cellular environment (non-cancerous), the primary constituents of the basement membrane consist of collagens IV and VI, and some fibrillar collagens.[32] In cancerous tissue, the basement membrane is more densely packed with fibrillar collagens (types I, III and V), which results in a rigid interstitial matrix.[32]

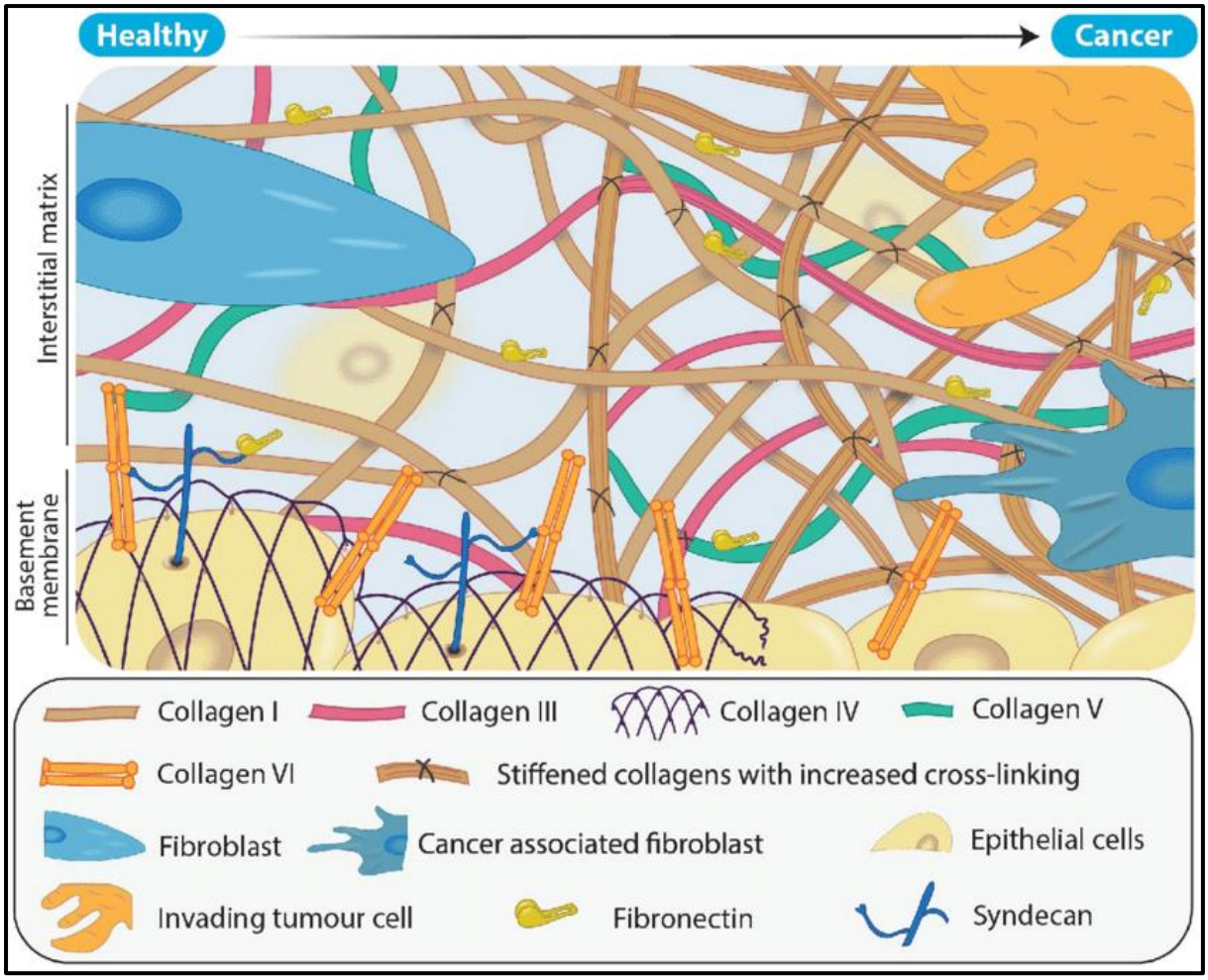

Figure 1.2: Differences in the remodelling and dysregulation of the extracellular matrix in healthy tissue versus cancerous tissue. Reprinted without any changes from Cancers, Volume 13, Issue 3, Yordanos F.I. Setargew, Kaitlin Wylie, Rhiannon D. Grant, Jessica L. Chitty, Thomas R. Cox, Targeting Lysyl Oxidase family mediated matrix cross-linking as an anti-stromal therapy in solid tumours, Pages No. 491-516, Copyright (2021). Use of this figure is authorised under terms of the Creative Commons CC by License.

1.2.3. Three-dimensional cell culture

Given the importance of the ECM and cellular heterogeneity in cancer, it is necessary to have representative *in vitro* models that can more accurately replicate the *in vivo* state.[20] *In vivo* tumours possess physical barriers and three-dimensional (3D) architecture which prevent drug penetration or confer biological heterogeneity through the solid tumour, leading to resistance.[12,22,39] Within the *in vivo* environment, cancer cells attach to one another as opposed to an artificial surface observed in 2D culturing, resulting in a 3D unit; the tumour.[15] Since tumours grow as 3D structures *in vivo,* a 2D *in vitro* cell culture model is less representative thereof.[26] As such, 3D cell culturing methods have been developed in order to resemble the *in vivo* environment more closely and allow for more relevant biological assessments.[15,40] By using more advanced techniques, such as 3D cultures, it is possible to close the gap between

traditional 2D cell culture models and *in vivo* models.[26,41] A 3D culturing environment produces more ECM, allows for cellular interaction and heterogeneity, and ultimately greater representation of drug-induced efficacy and toxicity.[42] As such, 3D cellular models tend to show greater chemoresistance than cells cultured in a 2D model.[26,43-44]

The 3D cell culture recreates an environment in which cell-cell and cell-ECM interactions occur, which is similar to what happens *in vivo*.[45] As opposed to 2D cell culture,[46] cells grown in a 3D culture can undergo self-assembly, where they attach to one another to form, among other types, multicellular spheroids (MCSs).[40] Formation of MCSs by self-assembly supports the differential adhesion hypothesis (DAH), where it is postulated that cellular rearrangement occurs during tumour development because the inherently motile cells constantly exchange weaker cellular adhesions for stronger versions.[47] The final cellular arrangement is achieved once all of the cellular attachments are of the strongest type possible for the cells.[47] As MCSs grow, zonal differentiation occurs where a distribution of cell types are observed in the various regions of the spheroid, similar to what is found in solid tumours (**Figure 1.3**).[48] This mimicry of the *in vivo* tumour microenvironment occurs due to the formation of molecular gradients, such as nutrient availability and cellular waste removal.[49] Traditional 2D culture comprises mostly viable cells, since dead cells would detach from the artificial surface, while 3D culture contains cells in various growth stages, not just viable, proliferating cells.[26,50-51] This cellular heterogeneity within the MCS is essential for the model to be an accurate representation of *in vivo* tumours,[12,51] and thus different regions can be broadly described.

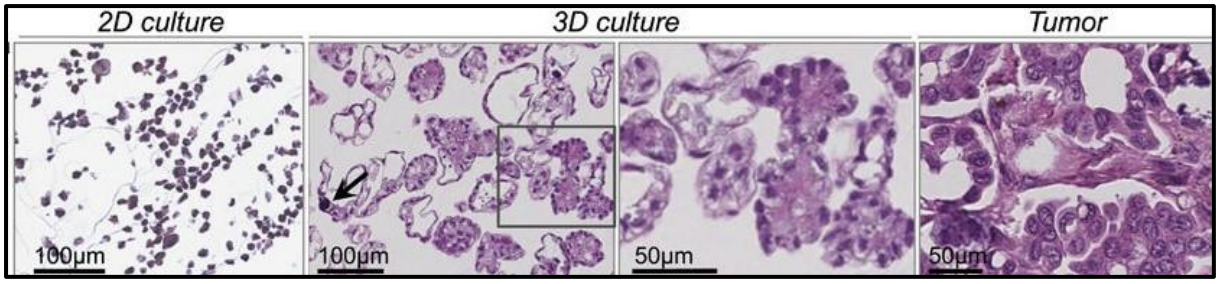

Figure 1.3: Micrographs highlighting the increased comparability of three-dimensional cultures of epithelial ovarian cancer cells to *in vivo* tumours when compared to two-dimensional cultures. Reprinted from Laboratory Investigation, Volume 93, Issue 5, Janet M. Lee, Paulette Mhawech-Fauceglia, Nathan Lee, Christina L Parsanian, Yvonne G. Lin, *et al.*, A three-dimensional microenvironment alters protein expression and chemosensitivity of epithelial ovarian cancer cells in vitro, Pages No. 528-542, Copyright (2013), with permission from Springer Nature.

The MCS is generally divided into three distinct zones (**Figure 1.4**).[52] The necrotic core (**Section 1.2.3.1**), which is surrounded by the internal quiescent zone (**Section 1.2.3.2**), where there is very limited oxygen and nutrients available, and the external proliferative zone (**Section 1.2.3.3**), representing the outermost layer.[53] This zonal differentiation is most commonly observed in MCSs once they reach a diameter of around 500 µm.[54-55]

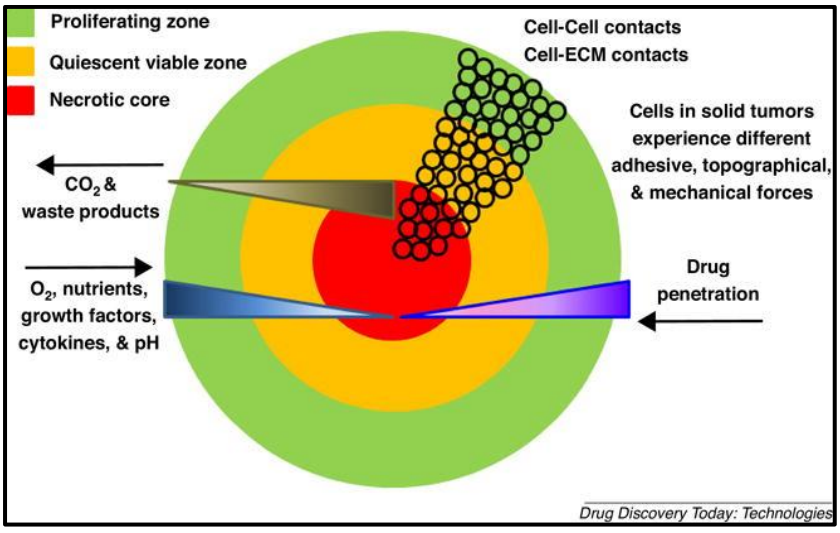

Figure 1.4: Schematic representation of the zonal differentiation observed in multicellular spheroids. Reprinted without any changes from Drug Discovery Today: Technologies, Volume 23, Shilpa Sant, Paul A. Johnston, The production of 3D tumor spheroids for cancer drug discovery, Pages No. 27-36, Copyright (2017), with permission from Elsevier.

1.2.3.1. Necrotic core

Sub-populations of cells within the MCS core are classified as anoxic, hypoxic, and necrotic. The availability of nutrients and oxygen diminishes in the inner region of the MCS, while the accumulation of waste products increases as the distance from the outermost layer increases with growth of the MCS (**Figure 1.4**).[27,51-52,55-56] The

innermost core is referred to as the necrotic zone.[55] Cellular necrosis occurs due to the depletion of oxygen (leading to hypoxia) and the build-up of metabolic waste as MCS size increases.[57] Cells in the core are more resistant to chemotherapy, in part due to the reduced drug penetration in the deeper layers, the high levels of necrosis, and the reduced proliferative capacity of cells.[39,51-52,57]

1.2.3.2. Quiescent zone

The MCS core is surrounded by cells that are still viable, but are proceeding through various stages of cell death, commonly referred to as the peri-necrotic zone.[55] Many cells in this region are apoptotic.[55] Oxygen is not completely diminished in this region, but the availability thereof is reduced (**Figure 1.4**), leading to a semi-hypoxic environment which triggers changes in cellular gene expression.[52,55,57] This results in an altered metabolism with subsequent increased lactic acid by-product formation and reduced pH levels.[55] The reduced access to nutrients and waste accumulation deters growth in this region.[57] Cells in this environment are less likely to actively proliferate and grow, and thus are ideal targets for cancer drug development, given their representation of the *in vivo* environment that is more resistant to chemotherapy.[51,58] Although drugs have reduced penetration in this area, it is not as low as within the core.[39] Whilst these cells are viable, they do not all actively proliferate, which leads to this section being termed the quiescent zone.[59] These cells possess reduced metabolic capacity, which confirms the heterogenous cellular phenotypes of such models.[57]

1.2.3.3. Proliferative zone

Cells in the outer region of the spheroid actively grow and proliferate due to abundant access to oxygen and nutrients.[52] Since the majority of chemotherapeutic drugs target proliferating cells, the outermost layer is considered the most susceptible due to its proliferative state and ability to easily expel waste.[51,55,58] Cells in this region are able to interact with the external environment; including other cells, the ECM and soluble factors.[55,57] These interactions can lead to chemotherapeutic resistance within the outer layer of the spheroid, even though drugs have good penetration in this layer.[52] These interactions with the external environment have been observed *in vivo* and are known to contribute to chemotherapeutic resistance.[25]

The role of the ECM in tumour progression has been discussed in **Section 1.2.2**, but it also contributes to drug resistance.

1.3. Chemotherapeutic resistance

Cancer cells have been known to adapt in the presence of chemotherapeutic agents in order to evade destruction.[60] Some chemotherapeutic agents target cancer cells by the induction of apoptosis or preventing proliferation.[33] Furthermore, cells may alter their cell cycling and apoptotic processes to prevent degradation.[61] Many chemotherapeutic agents target only actively proliferating cells.[62] Changes to the microenvironment, such as cellular interactions, ECM components, protein expression and mutations may lead to reduced chemotherapeutic response.[33,61] The ECM may alter cellular signalling,[43,61] offer a protective role to solid tumours,[33] and mediate cellular proliferation and differentiation, thus allowing certain cancers to evade chemotherapeutic effects.[39] For example, ovarian cancer cells grown in a 2D model have been found to be more susceptible to paclitaxel-induced apoptosis due to reduced B-cell lymphoma (Bcl)-2 gene expression, compared to 3D models.[43] In the MCS, the formation of the ECM and its associated structural and adhesive proteins and components allows these influences and interactions to occur *in vitro,* thereby creating an accurate model for the *in vivo* situation.[39]

Chemoresistance is a major roadblock in cancer treatment,[33,60] and acquired resistance has been observed in several types of cancer.[63] Tumours also possess some level of innate resistance to chemotherapy,[63] due to physical barriers which prevent drug penetration through the solid tumour.[39] One way to overcome this physical barrier is to improve the delivery of chemotherapeutic agents into the tumour by using nanomedicine.[64]

1.4. Nanoparticles

1.4.1. Nanoparticles and nanomedicine

Nanoparticles (NPs) are particles with at least one dimension smaller than 100 nm.[65] Nanotechnology has been applied to medicine in order to mimic or alter biological processes, leading to the formation of nanomedicine.[66] In pharmaceutical science, NPs are an attractive field of study with regards to drug delivery and therapeutic treatment.[67] In oncopharmacotherapy, for example, the non-specific nature of

chemotherapeutic drugs often leads to severe side effects. Functionalising NPs with specific groups would allow for a more targeted approach,[68-69] whereby drugs are delivered to specific locations within the body, reducing non-specific effects, improving efficacy, and decreasing side effects.[67]

One of the most appealing applications of NPs in medicine is the ability to target specific cells or tissues by functionalisation.[66-67] Nanomedicine has played a central role in the fight against the COVID-19 pandemic. The vaccines developed by Moderna and Pfizer BioNTech against COVID-19 make use of NP technology. Nanoparticle vaccines have the potential to provide broader antibody-based responses to infection, which is paramount considering the current ongoing COVID-19 pandemic being driven by the constant formation of new variants.[70] Nanoparticle vaccines possess added advantages, which include the potential to modify NP properties as new variants emerge, as well as the potential for targeted antigen delivery via various routes.[71] In a docking study carried out in 2020, it was found that iron oxide NPs, which were approved by the United States Federal Drug Administration (FDA) for anaemia treatment,[72] could be effective in treating COVID-19 infection by interacting with the spike protein binding domains of the SARS-CoV-2 virus.[73]

Another application of NPs in the medical field is the design of specialised drug delivery systems (DDSs) that improve the solubility, *in vivo* stability and biodistribution of the drug.[64] The DDSs can also create drug reservoirs which allow for sustained drug release over extended periods of time, thereby maintaining the drug at a therapeutically effective concentration for a longer period of time.[64] Using specialised DDSs could be one way in overcoming the physical barriers of the solid tumour in cancer treatment. Delivery of particles into cells by NPs occurs by attaching the molecule (in this case a drug molecule) onto the surface of the NP. Once the system enters the cell, the drug molecules will detach from the NP surface.[74]

Targeting of NPs may be an active process via conjugation of the particle to a tissue-specific ligand, or a passive process whereby the NP enters the target tissue via leaky junctions.[75] Nanoparticles can be targeted to the tissue of interest by conjugating the NP to a ligand that targets receptors on the particular tissue (**Figure**

1.5).[76] In this way, NPs have the ability to increase the efficacy and reduce ADR of the therapeutic agent.[69] Types of ligands used in conjugation are small molecules, protein domains, nucleic acids, polypeptides and antibodies.[77] Each of these ligand types confers unique advantages and disadvantages and are chosen based on the specific targeting needs of the NP. Multiple ligands of the same type or different types have been used in combination.[69]

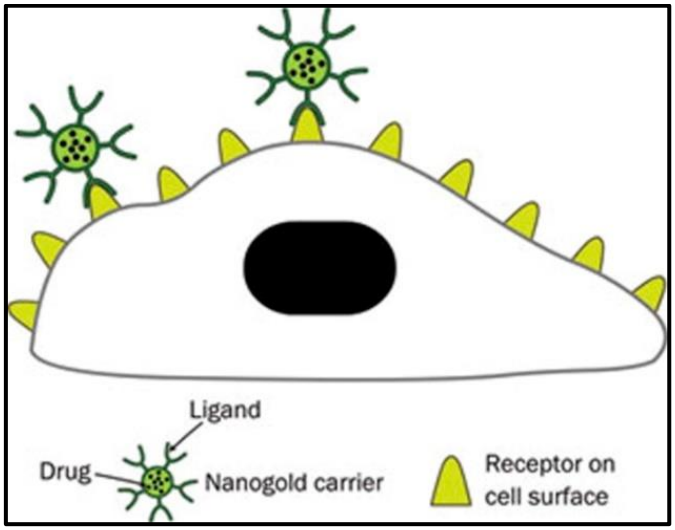

Figure 1.5: Nanoparticle functionalised to target a specific receptor on a cell surface. Reprinted from Acta Pharmacologica Sinica, Volume 32, Issue 8, Zhao-zhin J. Lim, Jia-en J. Li, Cheng-teng Ng, Lin-yue L. Yung, Boon-huat Bay, Gold nanoparticles in cancer therapy, Pages No. 983-990, Copyright (2011), with permission from Springer Nature.

In order for the functional groups to conjugate with a chosen ligand, the NP surface needs to be altered. Alteration occurs most often via covalent reactions, although non-covalent reactions may also be used.[78] The covalent reactions include reactions with carbonyl, amine and sulfhydryl reactive groups, as well as click chemistry.[78] These processes can lead to toxicity via rapid kidney infiltration or accumulation in specific organs.[79] This highlights the need for toxicity screening platforms when testing NPs for various biological applications. A commonly used strong non-covalent reaction is the interaction between (strept)avidin and biotin which is a very strong reaction.[78]

Liposomes are spherical vesicles that are made up of one or multiple phospholipid bilayers.[80] Liposomes have also been used in the targeting of NPs and offers an advantage as the structure of the liposome is similar to the cell membrane of the targeted cells.[66] As such, lipid-lipid exchanges are enhanced, allowing for enhanced delivery of the drug into the target cell membrane.[81-82] Doxil® was the first FDA-

approved nano-drug, which used polyethylene glycol (PEG)-liganded nano-liposomes to encapsulate doxorubicin to target the drug specifically to only the cancer cells. This resulted in reduced side effects and prolonged drug circulation time, thereby increasing chemotherapeutic efficacy.[83]

Additionally, NPs may function as theragnostics,[84] which allows for both diagnosis and treatment of a disease in a sequential manner.[85] Using a combined treatment strategy is beneficial, since results from diagnostic tests are used to design a treatment plan and also monitor the treatment response.[86] Theragnostics is an attractive field in cancer treatment as it aims to reduce treatment delay and make patient care better and easier for healthcare professionals.[85]

The focus of this study was on gold nanoparticles (AuNPs). Various AuNPs have been used to synthesise miniature sensors that are used to detect chemical and biological agents in the fields of biomedicine, forensics, environmental and anti-bioterrorism.[87] Since these sensors need to be very sensitive, AuNPs are excellent scaffolds for synthesising such sensors. This sensitivity is due to their unique physical and chemical properties, the variety of simple methods of synthesising AuNPs, their stability as well as their biocompatibility with stabilising ligands.[88]

Gold nanoparticles have been a focus of study in the medical field for many years, as far back as the use of gold (Au) salts for arthritis in traditional Chinese medicine.[89-90] The diverse options for conjugating and stabilising AuNPs for medical applications has made them a promising vehicle for disease treatment, such as DDS in cancer treatment.[90] They are known to have unique photo-optical properties, making them useful in the field of biomedical optical imaging.[87,90] It has also been shown that AuNPs can increase the efficacy of radiation therapy in some cancers.[91]

Two AuNPs were used in this study: i) 14 nm citrate-stabilised and carboxyl-polyethylene glycol (PCOOH)-liganded AuNPs (PCOOH-AuNPs), and ii) 20 nm amine-liganded AuNPs (amine-AuNPs). The cell line chosen for this study was the A549 alveolar carcinoma cell line due to its relevance in previous research conducted by the research group in pulmonary cells,[92] while showing evidence of successful 3D culturing.[93-94]

Globally, lung cancer is still a big contributor to cancer-related mortality.[95] It was estimated that 236 740 new cases of lung cancer would be diagnosed in the United

States in 2022.[96] That is an increased incidence when compared to the 2019 estimation of 228 150 new cases.[97] Lung cancer is defined as either small cell lung cancer (SCLC) or non-small cell lung cancer (NSCLC), with the latter making up the majority of cases.[96] 61% of patients with stage III NSCLC are treated with chemotherapy and radiation, whereas earlier stages of disease are treated with surgery.[96] Immunotherapy has been a large focus in the treatment of lung cancer since its approval as treatment by the FDA in 2015. 33% of newly diagnosed stage IV NSCLC cases were being treated with immunotherapy in 2018, compared to 12% in 2016.[96]

Immunotherapy has many risks associated when it is used as a treatment for cancer. It was found that the risk of developing an adverse reaction after receiving immunotherapy for NSCLC was 52.5%.[98] Suresh, et al. found that checkpoint inhibitor pneumonitis occurred in 19% of patients receiving immune checkpoint immunotherapy for NSCLC.[99]

Inhalation toxicology is a risk faced by gold miners who are exposed to gold dust during the mining and refining process.[100] The skin and lungs are in constant contact with the environment, which increases the exposure time to the gold dust and therefore also the potential toxicity. The skin is a good barrier, but the lungs are vulnerable.[101] Various studies have shown increased incidence of lung cancers in gold mine workers, but the presence of other hazardous materials such as arsenic and lead in these mines have made it difficult to establish the level of risk associated with gold exposure.[100]

Due to the global burden of lung cancer and heightened risk of occupational AuNP exposure in the South African mining sector, pulmonary cell lines need to be investigated.[101]

1.4.2. Nanoparticle properties

Various physical properties of NPs influence their biological activities, which may either be beneficial or detrimental.

1.4.2.1. Size

Nanoparticles vary in size and this affects how the body identifies and distributes them within the body.[102] The surface-to-volume ratio of NPs is very important when

assessing drug delivery and toxicity. As the size of the NP decreases, the surface-to-volume ratio increases. With regards to the latter, this results in more of the active drug being near the surface of the particle, allowing for faster drug release.[103] It has been reported that NPs ≥200 nm are usually recognised as foreign by the immune system.[104] Therefore to avoid immune destruction and to obtain effective drug release, smaller NPs are preferred, such as the 14 nm and 20 nm AuNPs used in this study. However, when the NP becomes very small, the high surface-to-volume ratio might lead to excessive reactivity, which is a concern for experimentation and safety.[102] This, again, emphasises the need for toxicity screening platforms when investigating NPs to select appropriate candidates.

Aggregation is a concern when evaluating small NPs, since it complicates the exploration of possible applications and reactivity of the synthesised NPs, and also affects how the NPs are transported.[105-106] Nanoparticles tend to aggregate into clusters due to particle-particle attachment because of short-range thermodynamic interactions.[106] There are two different types of aggregation: homoaggregation, where clustering of similar particles occurs, and heteroaggregation, where dissimilar particles aggregate.[106] Strategies have been employed to prevent aggregation of NPs, including altering the surface charges of the particles.[105]

1.4.2.2. Surface properties

Surface characteristics of NPs can be chemically altered to create a function-appropriate NP.[107] Changing the surface properties can assist in avoiding immune destruction of the NP. Hydrophobic particles are more likely to be cleared from the body by the immune system; thus altering the surface of the NP and making it more hydrophilic, will make it less likely to be cleared by the immune system.[108] Coating the NPs in polymers, surfactants or copolymers, like polyethylene glycol (PEG), has proven advantageous in this regard.[109-110] The NPs used in this study were carboxyl-PEG, and amine-liganded AuNPs, respectively. Polyethylene glycol is hydrophilic and hinders the binding of plasma proteins, thereby preventing immune clearance.[111-112] Amine ligands have shown to be excellent stabilising agents in the synthesis of NPs from noble metals.[113-114]

1.4.2.3. Nanoparticle interference during analysis

The physicochemical properties of NPs imbue them with various effects; unfortunately, these properties also allow for interference with various analytical assays.[115] Importantly, the sample preparation of assays may render these interferences potentially greater or less depending on, for example, the inclusion and number of washing steps and potential low internalisation within cells.[115-116]

Since NPs have the ability to interfere with biochemical assays, it is proposed to use label-free screening methods, where possible.[116] This does not imply that fluorometric and colorimetric analyses cannot be performed when screening for toxicity of NPs. Chemiluminescence assays have been successfully used in cytotoxicity screening of NPs, and thus offer a potential route of experimentation. For all assays, interference should be determined and proven negligible.[117]

1.4.3. Nanoparticle uptake

Nanoparticle uptake into cells occurs via both active and passive processes,[92] and is dependent on the cell type. All cell types do not possess the receptors and mechanisms that enable uptake or biological activity of NPs, and thus cell-type specific modalities need to be employed.[118] It has been reported that passive uptake into red blood cells (RBCs) occurs due to their lack of endocytic mechanisms.[119] Active uptake into most cell types occurs via receptor-mediated endocytosis, either as pinocytosis or phagocytosis.[92,120] Pinocytosis typically mediates the uptake of fluids and small particles, while phagocytosis takes place for larger particles.[92,120] Pinocytosis includes micropinocytosis, clathrin- and caveolin-mediated endocytosis, and clathrin-and caveolin-independent endocytosis (**Figure 1.6**).[92,120-121]

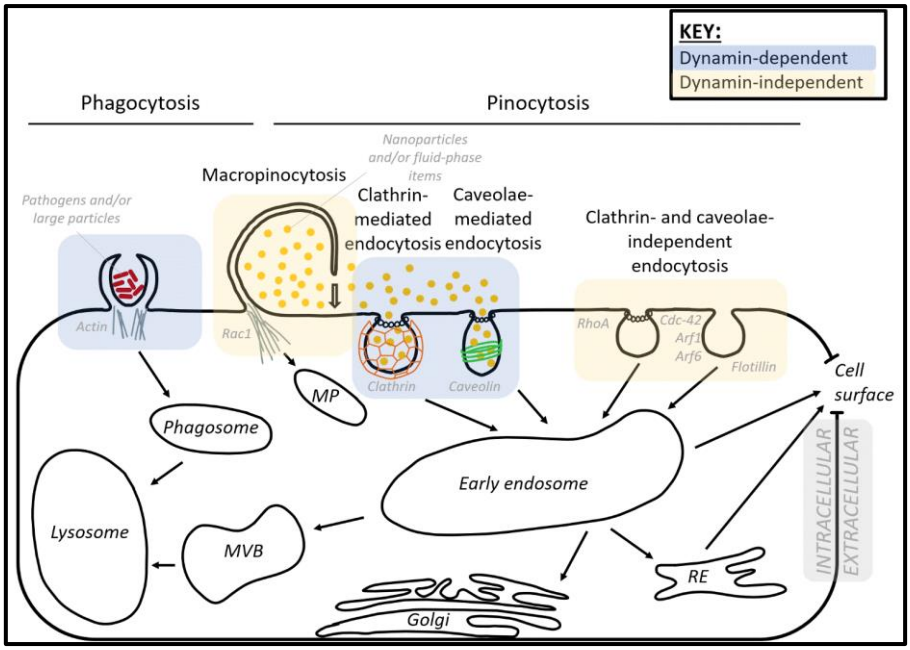

Figure 1.6: Illustration of the possible cellular uptake pathways. Reprinted without any changes from Journal of Pharmacy and Pharmacology, Volume 20, Seth-Frerich Fobian, Melissa Petzer, Melissa Vetten, Vanessa Steenkammp, Mary Gulumian, Werner Cordier, Mechanisms fascilitating the uptake of carboxyl-polyethylene glycol-functionalised gold nanoparticles into multicellular spheroids, Pages No. 1 -14, Copyright (2022). Use of this figure is authorised under terms of the Creative Commons CC by Licence.

The properties of NPs also highly influence their uptake into cells. The uptake of NPs between 20 and 50 nm is faster than larger NPs.[122] The functionalisation[123] and surface charge also affect uptake,[124] stressing the importance of full characterisation.

Albanese and Chan described cell-type specific uptake of AuNP aggregates, where increased uptake was observed in the MDA-MB-435 human melanoma cell line, while it was decreased in HeLa adenocarcinoma and A549 human alveolar adenocarcinoma cell lines.[125] Furthermore, uptake was decreased for monodispersed AuNPs.[125] This could be due to differential mechanisms that cell types employ in order to facilitate AuNP uptake.[125] Uptake will also differ in a 2D model, compared to a 3D model, particularly as the former comprises a single layer rather than heterogenous phenotypes and an ECM.[20,26,45]

Studies to determine the uptake mechanism of AuNPs into cells have shown variable results due to different NPs, cell types and exposure parameters. Uptake may be via clathrin-mediated endocytosis,[126-127] caveolin-mediated endocytosis[128] or phagocytosis-mediated,[129] which will invariably alter their downstream effects. A 2019 study by Vetten and Gulumian (which formed the foundation for this study) found that the PCOOH-AuNPs were taken up by BEAS-2B human bronchial

epithelial cell monolayers via caveolae-independent endocytosis (CIE).[92] In A549 MSCs (used in the present study), Fobian *et al*. found the major pathway to be caveolae-mediated endocytosis (CME),[121] suggesting alternative pathways dependent on the cell type and/or culture conditions. These findings support the theory of cell-type specific uptake,[125] as well as the increased physiological relevance of 3D models, compared to 2D.[15,26,40-41]

1.4.4. Nanoparticle toxicity

There has been concern regarding the toxicity risks posed by NPs and this has resulted in their use being limited.[123,130-131] A tiered approach has been suggested when testing NP toxicity.[132] These tiers consist of in-depth NP characterisation, after which the compounds are subjected to *in vitro* tests. If these tests show promising results, a more robust *in vitro* study should be employed to establish the level of toxicity. This approach provides more reliable data before the costly *in vivo* testing process is started.[133] Doing so with a MCS model, further increases the representability thereof, particularly as the uptake of NPs to inner regions would be greatly impacted by its heterogenous nature.[12,52]

Without functionalisation, NPs have shown to be non-specific and not able to reach their desired target, resulting in excessive cytotoxicity.[123] Oxidative stress has been noted by some NPs in keratinocytes,[134] macrophages and monocytes.[135] Inflammation has been reported to occur as a result of NPs that are present in the cell while being chemically inactive.[74] The aforementioned findings emphasise the need for toxicity screening when working with NPs.

When synthesising NPs from noble metals, the most common ways they are stabilised is by functionalising them with polymers or ligands.[114] Functionalisation of NPs can enhance them for the desired action, stabilise them, as well as reduce the risk of cytotoxicity.[114,123] Polymer-linkage has been shown to increase the stability as well as reduce the toxicity of iron oxide NPs,[136] and quantum dot NPs.[137] Such PEGylated NPs show reduced cytotoxicity compared to non-functionalised counterparts.[123]

Gold has traditionally been considered a chemically-inactive metal valued for its medicinal properties.[138] The AuNPs display dissimilar and diverse characteristics

when compared to their bulk counterparts, and thus it is not possible to extrapolate and predict the behaviour of AuNPs without formal assessment. Although some AuNPs have been described to lack toxicity,[64,139-140] biocompatibility still needs to be considered during drug development, and these compounds cannot be assumed to be safe until tested.[74] Cells might be exposed to the AuNPs for extended periods of time due to particle internalisation.[139,141] The propensity to incur cytotoxicity may be different depending on the non-specific or specific effects of AuNPs. Furthermore, AuNPs have caused cellular damage via the induction of oxidative stress and subsequent up-regulation of inflammatory genes.[142]

1.5. The cell cycle

1.5.1. Phases of the cell cycle

Cells pass through the cell cycle as they grow and proliferate, which involves complex and controlled processes mediated by proteins and control points.[143-144] By completing the cell cycle, the cell is able to duplicate itself. The time to achieve this is referred to as the doubling time.[59] The eukaryotic cell cycle is divided into the interphase and mitotic (M) phase.[59] Interphase is the initial phase of the cell cycle, the process of growth and deoxyribonucleic acid (DNA) replication, which is followed by mitosis; the formation of two cells from one.[59] In cancer research, the cell cycle is studied in order to find targets for new drugs.[145] Interphase is sub-divided into more phases (**Figure 1.7**): G_1, S, G_2, M and sometimes, G_0.[59,144,146]

The first phase is the G_1-phase, also referred to as the first gap.[146] The cell is biochemically active during this phase and very subtle microscopic changes can be observed.[59] DNA repair and cell growth occurs in the G_1-phase. The S-phase follows the G_1-phase and constitutes DNA synthesis.[144,146] After the S-phase, the G_2-phase is reached, where the proteins necessary for further replication are synthesised, and the cell replenishes its energy stores.[59] The G_2-phase is also a gap phase where,[146] as in the G_1-phase, cell growth and DNA damage repair mechanisms are active.[147]

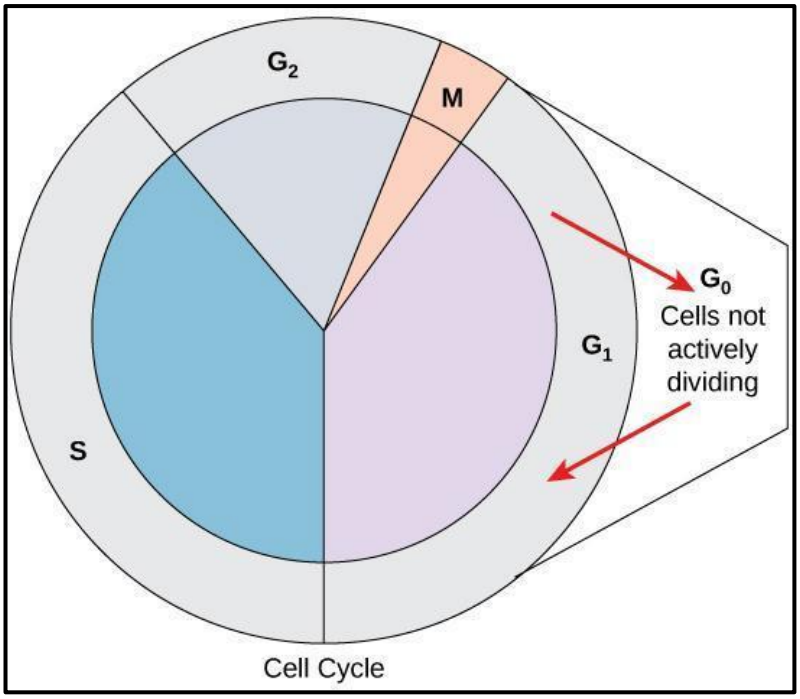

Figure 1.7: The phases of the cell cycle. Reprinted from Fundamentals of Cell Biology, Shoshana Katzman, Jennifer Hurst-Kennedy, Alessandra Barrera, Jennell Talley and Rebecca Higgins, Chapter 13: The Cell Cycle and its Regulation, Copyright (2020). Use of this figure is authorised under terms of the Creative Commons CC by License.

After the G_2-phase, cells are usually advanced to the M-phase, where mitosis takes place by progressing through prophase, metaphase, anaphase, and telophase.[59] Mitosis is the phase where the replicated chromosomes segregate into separate nuclei.[144] After completing mitosis, cytokinesis takes place as the so-called final step in mitotic division, where the cytoplasm physically separates and two individual cells are formed.[144]

The G_0-phase, which constitutes quiescent cells, is not present in all cells.[146,148] These cells aren't actively dividing, nor preparing to divide, so technically they have exited the cell cycle.[59] This is a temporary exit and cellular signals can trigger the cell back into the G_1-phase to continue with cellular cycling.[59] The outer layers of the MCS have a higher constituent of actively proliferating cells,[149] while cells closer to the spheroid core have less actively proliferating cells, and higher numbers of quiescent cells (cells in the G_0-phase).[42] Immediately surrounding the MCS core are high numbers of cells in the G_1-phase.[149] The ability of a cell to progress through the cell cycle depends on its location within the MCS.[42,150] This also influences the expression of cell cycle-related proteins.[42] It has also been reported that smaller MCSs container higher numbers of actively proliferating cells than larger MCSs.[42]

1.5.2. Cell cycle control

The tight internal control of the cell cycle is what makes it such an attractive target in cancer research, since most therapies are targeted to actively proliferating cells.[62] Two groups of proteins are essential for cell cycle control; cyclins and cyclin-dependent kinases (CDKs).[59,144,146-147] These proteins' expression levels fluctuate throughout the various steps of the cell cycle, and this expression is influenced by internal and external triggers.[59] There are three main checkpoints in the cell cycle which maintain ordered progression of cells through the cell cycle.[147]

The G_1-S checkpoint occurs at the end of the G_1-phase and establishes the integrity of the DNA synthesised in the G_1-phase.[59] This step ensures that the newly synthesised DNA is not damaged and can be replicated in the S-phase.[146] If damaged DNA is found, the cell will attempt to repair this damage.[147] This checkpoint is often referred to as the restriction point, from where the cell is committed to the cell cycle.[59] If there is damage that has occurred that can't be repaired, the cell cycle will arrest at this checkpoint.[147]

The G_2-M checkpoint occurs at the end of the second gap and establishes whether all the chromosomes have been duplicated, and the DNA is not damaged.[59,147] Should the DNA be damaged, repair will be attempted.[59] Should either of these requirements not be met, the cell cycle will arrest, and the cell will not enter into mitosis.[147]

The M-checkpoint happens near the end of metaphase.[59] It is often referred to as the spindle checkpoint,[147] since it checks that the newly formed sister chromatids are attached to spindle microtubules.[59] If this checkpoint is failed the cell will be eliminated by apoptosis.[147]

Deregulation of the cell cycle results in unchecked growth and DNA replication.[62] Cell cycle deregulation is commonly observed in human cancer.[151] Other than the internal checkpoints, the cell cycle is also regulated by phosphorylation of cyclins and CDKs that serve as signals to drive the cell through the phases.[152] These checkpoints create various potential treatment opportunities through the cell cycle of cancerous cells.

1.6. Apoptotic cell death

Apoptosis and necrosis are two of the most widely-described mechanisms of cell death.[153] Other modes of cell death are known, and include necroptosis and autophagy.[154]

Apoptosis, also termed “programmed cell death”, is associated with maintenance of physiological homeostasis, and also disease progression.[155] Since apoptosis is a well-organised cellular death mechanism, it requires energy (in the form of adenosine triphosphate [ATP]) to activate the different pathways.[153] There are key morphological features that characterise apoptosis, including shrinkage of the cell, membrane blebbing, and fragmentation of nuclear DNA.[156] Membrane blebbing is followed by “budding” where cell fragments are separated into apoptotic bodies.[157]

Cysteine-aspartic proteases (or caspases) are proteolytic enzymes that are known to be involved in many cellular processes, most notably apoptosis and inflammation.[158] Several caspases have been identified since their discovery, and they have been given unique numbers to differentiate them from one another. It is known that mammalian caspases-2, -3, -7, -8, -9 and -10 are involved in apoptosis.[158] The specifics of their role in apoptosis has been split into initiators (caspases-2, -9, -8 and -18) and executioners (caspases-3, -6 and -7).[159]

Apoptosis can be classified as intrinsic or extrinsic (**Figure 1.8**). Extrinsic apoptosis is caused by external stress factors which are recognised by transmembrane receptors and is a caspase-dependent apoptosis (CDA) process.[160] Intrinsic apoptosis is caused by intracellular stress, such as DNA damage or oxidative stress.[157] Factors that activate apoptosis can be cell-type specific, e.g. corticosteroid medications which results in apoptosis in thymocytes, but not other cells.[157]

Intrinsic apoptosis can either be CDA, or caspase-independent apoptosis (CIA).[160] As the names suggest, these pathways differ based on the need of caspase enzymes in the induction of cell death. The binding of ligands are the initial stimuli for activation of the process.[157] Apoptosis is regulated by various external and internal ligands that result in the activation of the suitable pathway (**Figure 1.8**).[161]

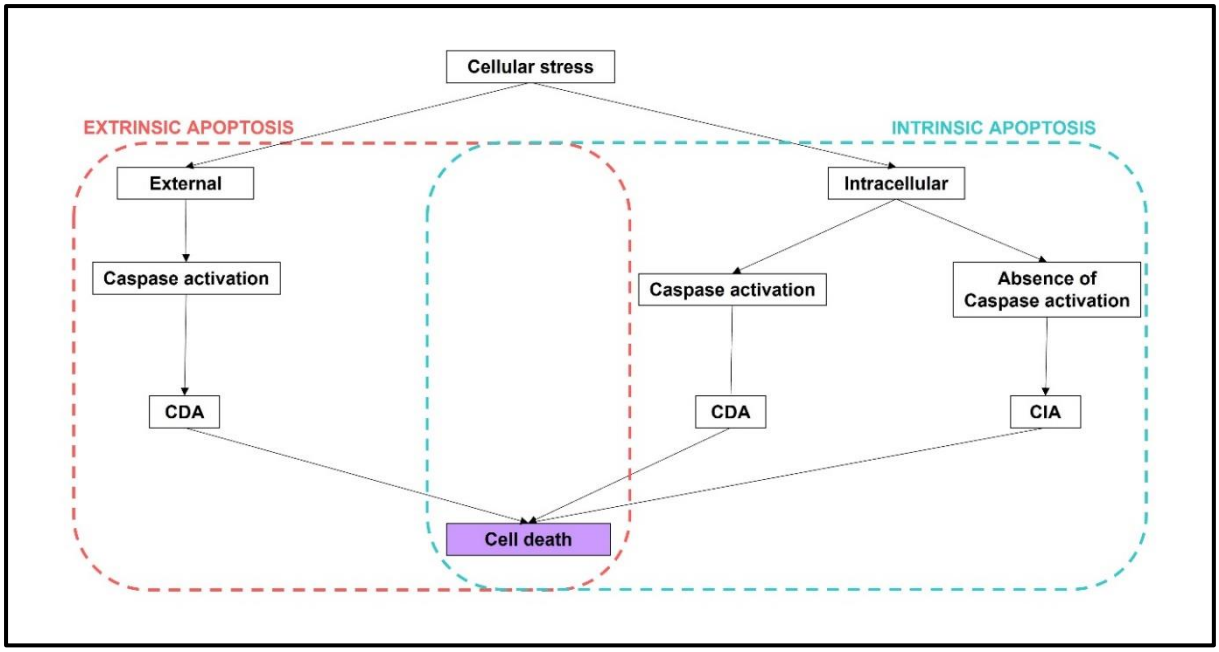

Figure 1.8: Summary of the different apoptosis pathways activated when the cell is placed under stress. Original image. CDA: caspase-dependent apoptosis; CIA: caspase-independent apoptosis.

The activation of caspases results in the induction of pro-apoptotic pathways that promote cell death (**Figure 1.8**).[162] The caspase-dependent pathway can be initiated by various factors, like pathogens, DNA, ribonucleic acid (RNA) or chemotherapeutic agents. The type of receptor and the ligand involved will influence the cell death pathway that is used by the cell.[161]

The ligand-binding that initiates apoptosis will determine whether the intrinsic or extrinsic apoptotic pathway is followed. The intrinsic or mitochondrial pathway relies on the permeabilisation of the mitochondrial membrane.[163] This occurs by pro-apoptotic factors congregating on the mitochondria and inducing permeabilisation of the membrane. This process is regulated by proteins from the Bcl-2 protein family and mitochondrial lipids.[156]

Many cancer therapies are cell cycle-specific and target actively proliferating cells.[62,145,157] Proteins fluctuate during the cell cycle, and thus chemotherapies can enable cell cycle arrest at specific points by targeting these proteins.[59,62] This strengthens the need for a 3D model to test whether NPs can induce apoptosis in A549 cells since the expression of proteins in 3D cultures is more representative of the *in vivo* situation than in 2D cultures.[12,14,45-46,164] An *in vitro* study by Ahamed *et al.* found that apoptosis was induced in A549 human epithelial lung cells by nickel ferrite NPs via increased reactive oxygen species (ROS) and activation of caspases.[165]

Titanium dioxide NPs have been reported to display pro-apoptotic activity in normal human lung fibroblasts and epithelial breast cells, though only at less than 100 nm sizes.[166]

1.7. Aim and objectives

The study aimed to establish a 3D model using A549 human alveolar adenocarcinoma cells as a platform for cytotoxicity evaluation of 14 nm citrate-stabilised carboxyl-polyethylene glycol-liganded AuNPs and 20 nm amine-liganded AuNPs.

The objectives of this study were to:

1 Establish A549 spheroids using low adherence culturing methods;
2 Assess the growth, viability and protein content of spheroids using phase contrast microscopy, the acid phosphatase assay and the bicinchoninic acid assay, respectively;
3 Determine whether the AuNPs interfere with any of the biological fluorescent and chemiluminescent assays; *and*
4 Elucidate nanoparticle cytotoxicity using morphological changes (phase contrast microscopy), biochemical parameters (acid phosphatase assay and bicinchoninic acid assay), cell cycle analysis and caspase-3/7 activity analysis.

2. Chapter 2: Materials and methods

Ethical clearance

This project, and the entirety of the experimentation referred to herein, was approved by the Research Ethics Committee of the University of Pretoria, Faculty of Health Sciences (REC 690/2019; **Appendix I**).

Reagents

Reagents were procured, prepared and stored as per **Appendix II**. Sterility data and certificates of analysis (CoA) for the AuNPs are provided in **Appendix III**.

2.1. Synthesis and characterisation of gold nanoparticles

2.1.1. Carboxyl-polyethylene-glycol liganded gold nanoparticles

The 14 nm citrate-stabilised carboxyl-polyethylene glycol-liganded AuNPs (PCOOH-AuNPs) were synthesised as described by Vetten and Gulumian,[92] using established methods.[167-168] The AuNPs were synthesised by Mintek and functionalised at the National Institute for Occupational Health (NIOH) under sterile conditions. The AuNPs were prepared using sodium citrate as the reducing agent. A trisodium citrate aqueous solution was added to a boiling aqueous solution of tetrachloroaurate and the mixture was boiled under reflux for 15 minutes (15 min). The suspension was then left to cool to room temperature and stirred overnight, after which it was filtered with a 0.25 µm sterile syringe filter. The PEG-liganded AuNPs were prepared using ligand-exchange where citrate is replaced, resulting in a generic formula:

$$Au\text{-}S\text{-}(CH_2)_{11}\text{-}(C_2H_6O_2)_n\text{-}Functional\ group$$

For the synthesis of PEG-COOH, the AuNPs were saturated with the relevant PEG-ligands possessing carboxyl functional groups leading to:

$$Au\text{-}S\text{-}(CH_2)_{11}\text{-}(C_2H_6O_2)_n\text{-}COOH$$

The characterisation of the AuNPs was carried out by Mintek. The size and shape of the AuNPs was determined using a FEI Tecnai T12 transmission electron microscope (TEM), which operates at 120 kV. The AuNPs were placed on formvar-

coated copper grids and dried, then measured using ImageJ in order to obtain the average particle diameter.

The absorbance spectra of the AuNPs were determined using a CECIL CE3021 spectrophotometer using wavelengths between 400 nm and 800 nm. The zeta-potential of the AuNPs was determined using Zetasizer Nano ZS at 25°C. The pH was measured at 37°C.

2.1.2. Amine-liganded gold nanoparticles

The 20 nm amine-liganded AuNPs were synthesised from gold NPs with a core size >10 nm (Au-20; NSNP204-206) via the reduction of Au^{3+} to Au^{0} with sodium citrate.[169] The citrate reduction process involved hot gold chloride and sodium citrate as reactants. In this reaction, the citrate molecules acted as both reducing and stabilising agents, allowing for the formation of the colloidal gold. The bifunctional ligands of the type XRSH (X = COOH, $N(CH_3)_3$, and CH_3) were used in order to replace the citrate ligands on the nanoparticles surface.[169]

Au-20-ammonium (NSNP205): *N*,*N*,*N*-trimethyl(11-mercaptoundecyl)ammonium bromide was used to exchange citrate ligands from citrate AuNPs. The dark red NSNP205 was stable in water suspension containing 0.5 M potassium chloride (KCl). If the KCl concentration was too low, the colour of the suspension became blue with aggregation of NSNP205. Surface ligands (chemical composition): $HS(CH_2)_{11}N(CH_3)_3Br$.[169]

2.2. Maintenance of cell cultures

2.2.1. A549 alveolar carcinoma cell line

A549 cells (ATCC® CCL-185™) were cultured in 75 cm^2 cell culture flasks in Dulbecco's Modified Eagle's Medium (DMEM) supplemented with penicillin-streptomycin solution (1%), glutamine (1%), and foetal calf serum (FCS; 10%) in a humidified atmosphere at 37°C and 5% CO_2. The DMEM was replaced as needed until ±80% confluence was reached.

The cell culture was washed with sterile phosphate-buffered saline (PBS), and the cells were chemically detached with TrypLE™ Express for approximately 5 min at 37°C. Cells were decanted into 15 mL centrifugation tubes and 10% FCS-

supplemented DMEM added to deactivate the TrypLE™ Express. The cells were harvested by centrifugation at 200 *g* for 5 min, and the pellet was resuspended in 1 mL 10% FCS-supplemented DMEM. Cells were counted using the trypan blue (0.1% w/v in PBS) exclusion assay with a haemocytometer and diluted to the required cellular concentration (7.5 x 10^5 cells/mL) for MCS generation in 10% FCS-supplemented DMEM.

2.2.2. Multicellular spheroid generation

Various methods exist for generating 3D cell cultures. Traditionally, these methods rely on the use of pre-designed scaffolds, which are often disadvantageous due to their lack of essential biological signalling.[170] Self-assembly methods are preferred since these processes are relatable to what is seen *in vivo*,[171] and comprise various molecular role players, such as cadherins, which further determine the way in which attachment occurs, and MCSs can form without additional matrix material.[170-171] Self-assembly does not face the limitations that scaffold-based methodology does, in that it has the inherent ability for ECM recapitulation and interactions between cells and the ECM, as well as compatibility with a wide variety of high-throughput biological assays.[172-173] Two methods of MCS generation were assessed: a standard liquid overlay and a bulk generation liquid overlay method. Multicellular spheroids were originally formed using the liquid overlay technique as described by Friedrich *et al.,*[174] and modified for use by Fobian *et al*.[121]

An agarose solution (4%) was diluted to a 1.6% solution by adding of FCS-free DMEM (150 mL). Agarose (50 µL, 1.6%) was used to coat the bottoms of 96-well plate wells. The plates were swirled after the agarose was added to assure level coverage of the bottom of the well and a concave plug. The agarose was left to cool and solidify for a few min to create a low-attachment surface. The outermost wells of the plate were filled with sterile PBS (200 µL) to prevent edging effects. After optimisation, the ideal density of the MCSs was found to be 7.5 x 10^4 cells/MCS. Cells (100 µL, 7.5 x 10^5 cells/mL) were seeded onto the agarose plug to achieve 7.5 x 10^4 cells/well. Plates were incubated at 37°C and 5% CO_2 for 72 h to allow the cells to form MCSs. After MCSs had established, 50% of the DMEM (50 µL) was replaced every two to three days. The MCSs were grown for up to 21 days.

A bulk generation platform was used to further refine the 3D model initially co-established by Fobian *et al*.[121] A non-adherent microwell system was used to generate MCSs,[170,175-176] and used for subsequent experimentation. The 9x9 array negative polydimethylsiloxane moulds were autoclaved prior to each generation of microwells to ensure sterility. To create the microwell system, a sterile liquid agarose solution (1.6%, 500 µL) was pipetted into the mould to create an agarose platform with 81 microwells (**Figure 2.1**). Special care was taken to avoid any air bubbles when pipetting the molten agarose. Once the agarose had gelled, the microwell was carefully separated from the mould and placed in a 12-well plate. Each microwell was calibrated by filling it with DMEM (160 µL) and letting it equilibrate for at least 1 h. The DMEM was replaced with 160 µL cell suspension (3.8 x 10^6 cells/mL). Plates were incubated at 37°C and 5% CO_2 for 24 h, keeping the plates as still as possible. After 24 h, DMEM (1 mL) was pipetted alongside the mould to ensure nutrient transfer. Medium was replenished every 4 to 7 days after the MCSs had formed. The MCSs were grown for up to 21 days, with formation, growth, and viability assessed as described in Section 2.5 at regular intervals (4, 7, 11, 14, 18 and 21 days).

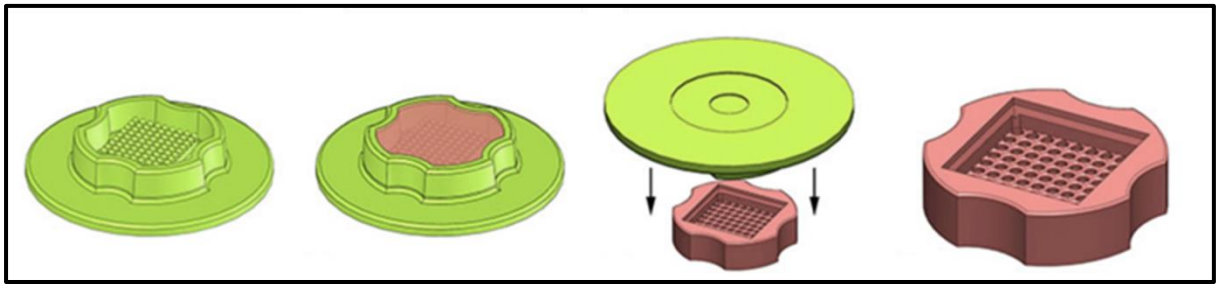

Figure 2.1: Graphic of the creation of the agarose microwell system. Reprinted from The European Research Journal, Volume 4, Issue 3, Ozan Karaman, Ziysan B. Yarah, Determination of the minimum serum concentration to develop scaffold-free micro-tissue, Pages 145-151, Copyright (2017), with permission from ProQuest Central.

2.3. Determination of spheroid formation, growth, and viability

2.3.1. Characterisation of multicellular spheroid formation

After MCS seeding and establishment, a Carl Zeiss Axiovert 200 M inverted microscope (Carl Zeiss Inc, Oberkochen, Germany) and a 5x magnification was used to visualise the A549 MCSs on days 4, 7, 11, 14, 18 and 21.

Phase-contrast (PC) microscopy is a contrast-enhancing technique that is used to visualise clear, high-quality, detailed images of specimens, with the added benefit of being able to visualise live cells as it does not require the specimen to be killed, fixed or stained for visualisation.[177] Phase shifts of light passing through a transparent

sample are converted into differences in intensity of the image, enabling the visualisation of transparent objects.[178] Micrographs were taken at selected intervals to determine the volume and diameter of the MCSs using ImageJ. The volume of the MCSs was calculated using the following equation as a measure of growth:[179]

$$Spheroid\ volume\ (V) = 0.5\ x\ (length)\ x\ (width)^2$$

The percentage change in the volume of MCSs over different days was calculated. For example, the change in the percentage in MCS volume between Day 4 and Day 7 was calculated using the formula:

$$\%\ change\ in\ spheroid\ volume = \frac{V\ on\ day\ 7 - V\ on\ day\ 4}{V\ on\ day\ 4} \times 100$$

The circularity index of the MCSs was measured. A circularity index of 1.0 is a perfect circle and 0.0 is an elongated polygon shape.[180] ImageJ was used to measure the circularity index using the following formula:

$$Circularity = 4\pi \left(\frac{area}{perimeter^2}\right)$$

2.3.2. Multicellular spheroid viability via acid phosphatase assay

The acid phosphatase (APH) assay is a cellular viability assay that measures cytosolic APH activity.[181] In viable cells, *p*-nitrophenyl phosphate is hydrolysed to *p*-nitrophenol by APH.[181] The assay was modified by pooling three MCSs and using a concentrated assay buffer.

Washed, pooled MCSs were re-suspended in 100 µL PBS and 100 µL assay buffer (containing para-nitrophenylphosphate [4 mg/mL] and Triton X-100 [0.2% v/v] in citrate buffer [0.1 M]) at 37°C for 90 min. After incubation, 10 µL sodium hydroxide (1 M, NaOH) was added to each well and the absorbance was read at 405 nm (reference: 630 nm) with an ELX800 UV microplate reader (BioTek Instruments Inc, Highland Park, USA) within 10 min of adding NaOH. All the absorbance values were blank-subtracted and the APH activity was calculated as a percentage using the following formula:

$$APH\ activity\ (\%\ relative\ to\ Day\ 4) = \frac{ODsample}{Average\ OD4} \times 100$$

Where '*ODsample*' refers to the corrected optical density of the sample and '*OD4*' is the corrected optical density of Day 4 MCSs.

2.3.3. Protein content via bicinchoninic acid assay

The bicinchoninic acid (BCA) assay was used to quantify the amount of protein present in the MCSs. The stable BCA reagent forms a purple complex with cuprous ions (Cu^{+}) in an alkaline environment. The Cu^{+} are produced when proteins react with copper ions (Cu^{2+}). The intensity of the colour produced by this reaction increases proportionately to protein concentration.[182]

Eight MCSs were pooled and washed twice with PBS (100 µL) with centrifugation at 200 *g* for 5 min in a 1.5 mL tube. The MCSs were lysed using 100 µL radioimmunoprecipitation assay (RIPA) buffer (50 mM Tris-hydrochloride [pH 7.4], 150 mM sodium chloride, 1% Triton X-100, 1% sodium deoxycholate, 0.1% w/v sodium dodecyl sulphate, 1 mM ethylenediamine tetraacetic acid [EDTA] and 0.02% w/v Roche cOmplete™ protease inhibitor cocktail). The MCSs were vortex-mixed, sonicated on ice for 5 min, and centrifuged at 16,000 *g* for 10 min. The lysate (as supernatant) was collected and stored at -80°C until use.

A clear 96-well flat-bottom plate was used to conduct the assay. An aliquot (5 µL) of the standard (bovine serum albumin [BSA]; 0.1, 0.2, 0.25, 0.5, 1.0, 1.5 and 2 mg/mL in PBS) or MCS lysate was added to the wells together with 195 µL BCA working solution (Appendix II). The plate was shaken for 10 min at room temperature, and incubated at 60°C for 30 min. The plate was cooled to room temperature, and the absorbance measured with an ELX800UV microplate reader using a 570 nm filter. Lysate protein content (mg/mL) was interpolated from the BSA standard curve, and dilutions considered to determine individual spheroid content (µg/MCS).

The percentage change in the protein content was calculated by dividing the difference in the average protein content between different days by the protein content on an earlier day. For example, the change in the percentage protein content between Day 4 and Day 7 was calculated using the formula:

$$\%\ change\ in\ protein\ content = \frac{Protein\ (Day\ 7) - Protein\ (Day\ 4)}{Protein\ (Day\ 4)}\ x\ 100$$

2.4. Assessment of nanoparticle interference

As NPs may interact with various assay substrates, thereby affecting the experimental results,[92,183-184] it is important to assess whether interference occurs.

The AuNPs were provided at stock concentrations of 2.5 x 10^{12} NP/mL (14 nm PCOOH-AuNP) and 1.8 x 10^{14} NP/mL (20 nm amine-AuNP) from the supplier as a red-coloured liquid suspension. As AuNPs may react with various substrates and diluted in unique spectral properties, interference studies were conducted to ensure validity of experimentation. This was done by diluting the AuNPs to in-reaction concentrations and assessing whether shifts in absorbance or fluorescence at the relevant wavelengths in a cell-free environment occurred. Before initialising any fluorometric assay, interference between the AuNPs and assay substrates or any possible fluorophore quenching was established.

2.4.1. Acid phosphatase assay

2.4.1.1. Inherent effect on optical density

The AuNPs were diluted to the desired concentrations (6 x 10^{11} NP/mL PCOOH-AuNP, 1.2 x 10^{12} NP/mL PCOOH-AuNP and 4.5 x 10^{12} NP/mL amine-AuNP) in both distilled water and FCS-free DMEM (to a final volume of 100 µL) in a clear, flat-bottom 96-well plate. The inherent behaviour of the AuNPs was assessed by measuring the absorbance at 405 nm (reference: 630 nm), which is the wavelength where the assay substrate conversion occurs, with an ELX800 UV microplate reader. Controls included distilled water and FCS-free DMEM.

Given the experimental setting of interference assessment, less wash steps were performed during the interference testing than during cellular assessment. As such, AuNP loss prior to conducting the cellular assays was not considered. The consequence of this would be that less AuNPs would be available during the assay than what is present during interference testing, further decreasing the likelihood of interference with the spectroscopic method or substrate/product.

2.4.1.2. Effect in the presence of assay substrates

The AuNPs were diluted to the desired concentrations (6 x 10^{11} NP/mL PCOOH-AuNP, 1.2 x 10^{12} NP/mL PCOOH-AuNP and 4.5 x 10^{12} NP/mL amine-AuNP) in PBS

to a final volume of 100 µL to simulate the APH assay protocol. The APH assay buffer (Appendix II, 100 µL) was added to the PBS-diluted AuNPs (100 µL). The AuNPs were then incubated at 37°C for 90 min, after which 10 µL NaOH (1 M) was added. Absorbance was read at 405 nm (reference: 630 nm) within 10 min of adding NaOH. An APH assay buffer control was included.

2.4.2. Bicinchoninic acid assay

2.4.2.1. Inherent effect on optical density

The AuNPs were diluted to the desired concentrations (6 x 10^{11} NP/mL PCOOH-AuNP, 1.2 x 10^{12} NP/mL PCOOH-AuNP and 4.5 x 10^{12} NP/mL amine-AuNP) in both distilled water and FCS-free DMEM (to a final volume of 100 µL) in a clear, flat-bottom 96-well plate. The inherent behaviour of the AuNPs was assessed by measuring the absorbance using a 570 nm filter, which is the wavelength where the assay substrate conversion occurs. Controls included distilled water and FCS-free DMEM blanks.

Given the experimental setting, less wash steps were performed during the interference testing than during cellular assessment. As such, AuNP loss prior to conducting the cellular assays was not considered. The consequence of this would be that less AuNPs would be available during the assay than what is present during interference testing, further decreasing the likelihood of interference with the spectroscopic method or substrate/product.

2.4.2.2. Effect in the presence of assay substrates

The AuNPs were diluted to the desired concentrations (6 x 10^{11} NP/mL PCOOH-AuNP, 1.2 x 10^{12} NP/mL PCOOH-AuNP and 4.5 x 10^{12} NP/mL amine-AuNP) in PBS to a final volume of 5 µL to simulate the BCA assay protocol. The BCA working solution (Appendix II, 195 µL) was added to the PBS-diluted AuNPs (5 µL). The plate was shaken for 10 min at room temperature, and incubated at 60°C for 30 min. The plate was cooled to room temperature, and the absorbance measured using a 570 nm filter, which is the wavelength where the assay substrate conversion occurs. The BCA assay working solution control was included.

2.4.3. Propidium iodide

Possible interference of the AuNPs with PI was determined, as PI may quench due to the presence of AuNPs.[185] Furthermore, it was imperative to ascertain whether the AuNPs would register as debris during flow cytometric analysis.

2.4.3.1. Autofluorescence of nanoparticles

The AuNPs were diluted to the desired concentrations (6 x 10^{11} NP/mL PCOOH-AuNP, 1.2 x 10^{12} NP/mL PCOOH-AuNP and 4.5 x 10^{12} NP/mL amine-AuNP) in both distilled water and FCS-free DMEM (to a final volume of 100 µL) in black, clear-bottom 96-well plates. The inherent fluorescence of the AuNPs was assessed by reading the fluorescent intensity (FI) using the excitation wavelength of 385 nm and emission wavelength of 590 nm. Controls included distilled water and FCS-free DMEM.

Given the experimental setting, less wash steps were performed during the interference testing than during cellular assessment. As such, AuNP loss prior to conducting the cellular assays was not considered. The consequence of this would be that less AuNPs would be available during the assay than what is present during interference testing, further decreasing the likelihood of interference with the spectroscopic method or substrate/product.

2.4.3.2. Possibility of propidium iodide fluorescent quenching by nanoparticles

The AuNPs were diluted to the desired concentrations (6 x 10^{11} NP/mL PCOOH-AuNP, 1.2 x 10^{12} NP/mL PCOOH-AuNP and 4.5 x 10^{12} NP/mL amine-AuNP) in PBS to a final volume of 100 µL to simulate the PI staining protocol.

Two concentrations of PI were tested at higher concentrations than would be used in the experimental procedure. A stock solution of PI was diluted in PBS (2 mg/mL and 5 mg/mL in-reaction) and added to the PBS-diluted AuNPs. The plate was incubated for 40 min at 37°C, and the FI was measured using the excitation wavelength of 385 nm and emission wavelength of 590 nm. A PBS blank was included.

2.4.3.3. Possibility of nanoparticle identification as debris during flow cytometry

Upon standardisation of the AuNP concentration across the PCOOH and amine-types, two more amine-AuNP concentrations were added: 2.3 x 10^{12} NP/mL amine-AuNP and 1.1 x 10^{12} NP/mL amine-AuNP. The possibility of the AuNPs being picked up as debris during flow cytometry was also assessed.

The AuNPs were diluted to the desired concentrations (6 x 10^{11} NP/mL PCOOH-AuNP, 1.2 x 10^{12} NP/mL PCOOH-AuNP, 4.5 x 10^{12} NP/mL amine-AuNP, 2.3 x 10^{12} NP/mL amine-AuNP and 1.1 x 10^{12} NP/mL amine-AuNP) in FCS-supplemented PBS (1%, final volume 600 µL) in a 1.5 mL centrifuge tube. The AuNPs were centrifuged at 200 *g* for 5 min. While vortex-mixing, ice-cold absolute ethanol (1.4 mL) was added to the tube in a drop-wise fashion. The AuNPs were incubated overnight in a refrigerator. The AuNPs were washed and resuspended in 500 µL staining solution (80 µg/mL PI, 0.1% Triton X-100 and 100 µg/mL DNA-free RNase in PBS) for 40 min at 37°C. The samples were analysed using a Beckman CytoFLEX flow cytometer (Beckman Coulter, South Africa) and the appropriate band pass filter.

2.4.4. Caspase-3/7 assay

The interference study aimed to establish whether the presence of AuNPs would interfere with the assay substrate in a cell-free environment. The AuNPs were diluted to the desired concentrations (6 x 10^{11} NP/mL PCOOH-AuNP, 1.2 x 10^{12} NP/mL PCOOH-AuNP, 4.5 x 10^{12} NP/mL amine-AuNP, 2.3 x 10^{12} NP/mL amine-AuNP and 1.1 x 10^{12} NP/mL amine-AuNP) in distilled water and FCS-free DMEM (up to a final volume of 25 µL per well) in a black, clear-bottom 96-well plate. The plate was incubated on ice for 30 min. Substrate buffer (Appendix II, 100 µL) was added to each well and the plate was further incubated at 37°C for 4 h after which the FI was measured at excitation wavelength of 340 nm and emission wavelength of 450 nm, as this is where the fluorescent substrate would be excited and emitted under test conditions. An assay buffer blank was included.

2.5. Cytotoxicity assessment of gold nanoparticles

2.5.1. Gold nanoparticle exposure

The MCSs were deemed appropriate to use at Day 7 as they were compact and maintained their morphological features, and this corresponded with the age of MCSs used in the uptake studies by Fobian *et al*.[121] Mature MCSs were carefully removed from the mould into a standard liquid-overlay 96-well plate. The MCSs were exposed to 100 µL of either FCS-free DMEM (negative control), saponin (1%, positive control) or AuNPs (6 x 10^{11} NP/mL PCOOH-AuNP, 1.2 x 10^{12} NP/mL PCOOH-AuNP, 4.5 x 10^{12} NP/mL amine-AuNP, 2.3 x 10^{12} NP/mL amine-AuNP and 1.1 x 10^{12} NP/mL amine-AuNP) for 24, 48 and 72 h at 37°C and 5% CO_2. After incubation, MCSs were washed three times with sterile PBS (100 µL) and the cytotoxicity of the AuNPs were assessed using the assays described in **Sections 2.7.2.** to **2.7.4**.

2.5.2. Nanoparticle effect on growth and viability of spheroids

The effect on MCS growth, protein content and viability after exposure to the AuNPs was determined as per **Section 2.5**, using the controls mentioned in **Section 2.7.1**.

2.5.3. Cell cycle analysis

Flow cytometry-mediated cell cycle analysis enables the quantification of cellular distribution through different phases of the cell cycle based on differential propidium iodide staining.[186] Given the difference in DNA content between cells in the G0/G1, S, and G2/M-phase, potential effects on proliferation can be determined,[186] although it does require cells to be in a single-cell suspension to pass through the flow cytometer and allow for accurate analysis. As such, MCSs required dissociation prior to staining and analysis.

In order to use CytoExploreR to analyse flow cytometry data, gates needed to be established for the datasets. To establish these gates, MCSs were treated in order to arrest cells in specific phases of the cell cycle. On Day 7 post-MCS formation, MCSs were treated as follows: FCS-depletion for 24 h to simulate G_1-phase block, by removing all culture medium from the well and replacing with 100 µL FCS-free medium.[187] 40 µM methotrexate (100 µL, in PBS) for 24 h to simulate S-phase block and 80 µM curcumin (100 µL, in PBS) for 24 h to simulate G2/M-block.[188] These

controls were known to cause cell-cycle arrest at the relevant phases and the experimental procedure was optimised for use on MCSs. Controls for cell cycle analysis included untreated MCSs (negative control), 1% DMSO (100 µL, in PBS as vehicle control) and 100 µM cisplatin (100 µL, in PBS as positive control).

2.5.3.1. Multicellular spheroid dissociation

The MCSs were dissociated according to the methods described by Grasser *et al*.[189] with minor modifications as per optimisation results. Thirty MCSs were pooled in a 1.5 mL tube and suspended in PBS (1 mL). The tube was centrifuged at 200 *g* for 5 min and the PBS removed. This washing process was repeated twice. The MCSs were dissociated by adding 900 µL Accutase® and gentle pipetting to facilitate mixing and initial dissociation. The tube was placed in a 37°C heated plate shaker for 10 min, after which the mixture was gently aspirated ten times to facilitate dissociation.

In the event that the MCSs do not completely dissociate after one dissociation cycle, Grasser *et al*. determined that up to four cycles could be repeated without sustaining cellular damage.[189] After optimisation, it was established that two dissociation rounds were sufficient to obtain a uniform single cell suspension from the pooled MCSs. The solution was transferred to a 15 mL centrifugation tube and the Accutase® solution was deactivated with FCS-supplemented PBS (10%, 2 mL). The cell suspension was centrifuged at 200 *g* for 5 min. The supernatant was discarded, and the cell pellet resuspended in FCS-supplemented PBS (1%, 1 mL).

2.5.3.2. Fixation and propidium iodide staining for analysis

The dissociated cellular suspension was centrifuged at 200 *g* for 5 min, after which the supernatant was decanted, and the pellet re-suspended in FCS-supplemented PBS (1%, 600 µL). While vortex-mixing, ice-cold absolute ethanol (1.4 mL) was added to the tube in a drop-wise fashion to fix the cells. The solution was incubated overnight in a refrigerator. Fixed cells were washed and re-suspended in 500 µL staining solution (80 µg/mL PI, 0.1% Triton X-100 and 100 µg/mL DNA-free RNase in PBS) for 40 min at 37°C. The samples were analysed using a Beckman CytoFLEX flow cytometer (Beckman Coulter, South Africa) using the appropriate band pass filter. The CytoFlex flow cytometer was on loan from the Institute of Cellular and Molecular Medicine (University of Pretoria) to carry out the analysis using an

optimised protocol set up by Dr Chrisna Durant. Deconvolution software (Kaluza, version 2.1) was used to measure DNA distribution, and CytoExploreR (R-script) was used to analyse data.

2.5.4. Apoptotic analysis via caspase-3/7 activity

As a surrogate for potential induction of apoptosis, caspase-3/7 activity was measured using the acetyl-Asp-Glu-Val-Asp-7-amido-4-methylcoumarin (Ac-DEVD-AMC) conversion assay. Ac-DEVD-AMC is a synthetic tetrapeptide substrate that is cleaved by activated caspases-3/7 to free the bound fluorogenic 7-amido-4-coumarin (AMC).[190] As caspase-3/7 is only activated via pro-apoptotic pathways, fluorescence indicates an induction of programmed cell death.[190] Cisplatin (10 and 100 µM) served as a positive control.

Four pooled MCSs were placed in a 1.5 mL tube and washed with PBS (1 mL) twice at 200 *g* for 5 min. Cold lysis buffer (Appendix II, 100 µL) was added to the MCSs and incubated on ice with gentle aspiration every 10 min until lysis was observed. After optimisation, it was found that MCS lysis occurred after approximately 30 min. The cell lysate (25 µL per well) was pipetted from the tube into the well of a black-walled, clear-bottom 96-well plate, and substrate buffer added (Appendix II, 100 µL). The plate was incubated at 37°C for 4 h and the FI was measured at an excitation wavelength of 340 nm and an emission wavelength of 450 nm. The caspase-3/7 activity was measured as follows:

$$Caspase\text{-}3/7\ activity\ (fold\text{-}change) = \frac{FI\ sample}{FI\ control\ average}$$

2.6. Substantiating methods designed for 2D in 3D culture

2.6.1. Acid phosphatase assay optimisation

At first the protocol for monolayer was repeated using single MCSs (data not shown). The assay buffer was at the same concentration than in monolayer (containing para-nitrophenylphosphate [2 mg/mL] and Triton X-100 [0.1% v/v] in citrate buffer [0.1 M])

Due to the nature of MCSs and the distribution of cells within the MCS, the ELX800 UV microplate reader (BioTek Instruments Inc, Highland Park, USA) could not differentiate MCSs treated with saponin from control MCSs.

After various rounds of optimisation, the best method was found to be pooling three spheroids together per well, as well as using a stronger assay buffer. Spheroids were resuspended in 100 µL PBS and 100 µL assay buffer (containing para-nitrophenylphosphate [4 mg/mL] and Triton X-100 [0.2% v/v] in citrate buffer [0.1 M]) at 37°C for 90 min. After incubation, 10 µL sodium hydroxide (1 M; NaOH) was added to each well and the absorbance was read at 405 nm (reference: 630 nm) with an ELX800 UV microplate reader (BioTek Instruments Inc, Highland Park, USA) within 10 min of adding NaOH.

2.6.2. Bicinchoninic acid assay optimisation

It has been discussed that the nature of MCSs would mean there is less viable cells in the MCSs than would be in monolayer culture. Therefore, there is less protein expression in the inner layer of the MCS. The BCA assay is one of the most sensitive assays for protein quantification, but it still has a minimum threshold of 0.5 µg/mL.[191] Since the MCSs in this study were relatively small, the individual protein content of each MCS was below the minimum threshold of the BCA assay and pooling MCSs was used as a method to optimise the assay for use in 3D culture.

2.6.3. Optimisation of MCS dissociation and flow cytometry

It has been discussed that the nature of MCSs would mean there is less viable cells in the MCSs than would be in monolayer culture. Since flow cytometry requires a large number of single cells for accurate analyses, pooling MCSs was necessary to have a large enough sample. Additionally, dissociation was needed to ensure that single cell suspension was available.

2.6.4. Ac-DEVD-AMC conversation assay optimisation

It has been discussed that the nature of MCSs would mean there is less viable cells in the MCSs than would be in monolayer culture. Pooling of MCSs made it possible for enough viable cells to be present that could undergo conversion of Ac-DEVD-AMC to AMC and be picked up by the reader.

2.7. Statistical analysis

Data from the results of all assays was captured using Microsoft® Excel® and analysed statistically using GraphPad Prism® 5. Statistical analyses for all assays, apart from the cell cycle distribution, was done by performing a Kruskall-Wallis with post-hoc Dunn's test. Cell cycle results obtained from flow cytometry was analysed using two-way analysis of variance facilitated by R with the use of CytoExploreR, an R script developed by Dillon Hammill. Significance was defined as $p < 0.05$.

Each experiment was carried out using a minimum of three biological and technical replicates, allowing for at least nine data points to be generated per sample. Data on the diameter and volume of the spheroids obtained from microscopy results was processed using ImageJ. Results were reported as the mean ± the standard error of the mean (SEM).

3. Chapter 3: Results

3.1. Characterisation of gold nanoparticles

The PCOOH-AuNPs and amine-AuNPs were characterised by Mintek to determine their size, concentration, ultraviolet absorbance, and surface charge in distilled water (**Table 3.1**).

Table 3.1: Nanoparticle characteristics.

Property	PCOOH-AuNP	Amine-AuNP
Size (nm)	14 ± 2	20
Concentration (NP/mL)	2.5×10^{12}	1.8×10^{14}
UV absorbance maximum (nm)	523	530
Surface charge in distilled water (mV)	-58.2	+42.8 ± 10

3.2. Establishing a 3D model for A549 multicellular tumour spheroids

The standard liquid overlay and bulk-generation methods described in **Section 2.4.2** were compared and it was evident that the MCSs generated by the micro-moulds were more reproducible and possessed less heterogeneity in shape and size (**Figure 3.1**). Morphologically, MCSs underwent less change between Day 7 and Day 10 in the micro-mould group (**Figure 3.1 B**) than the traditional group (**Figure 3.1 A**) and were more consistent in shape and size. As such, the MCSs generated by the micro-mould method were taken forward for experimentation.

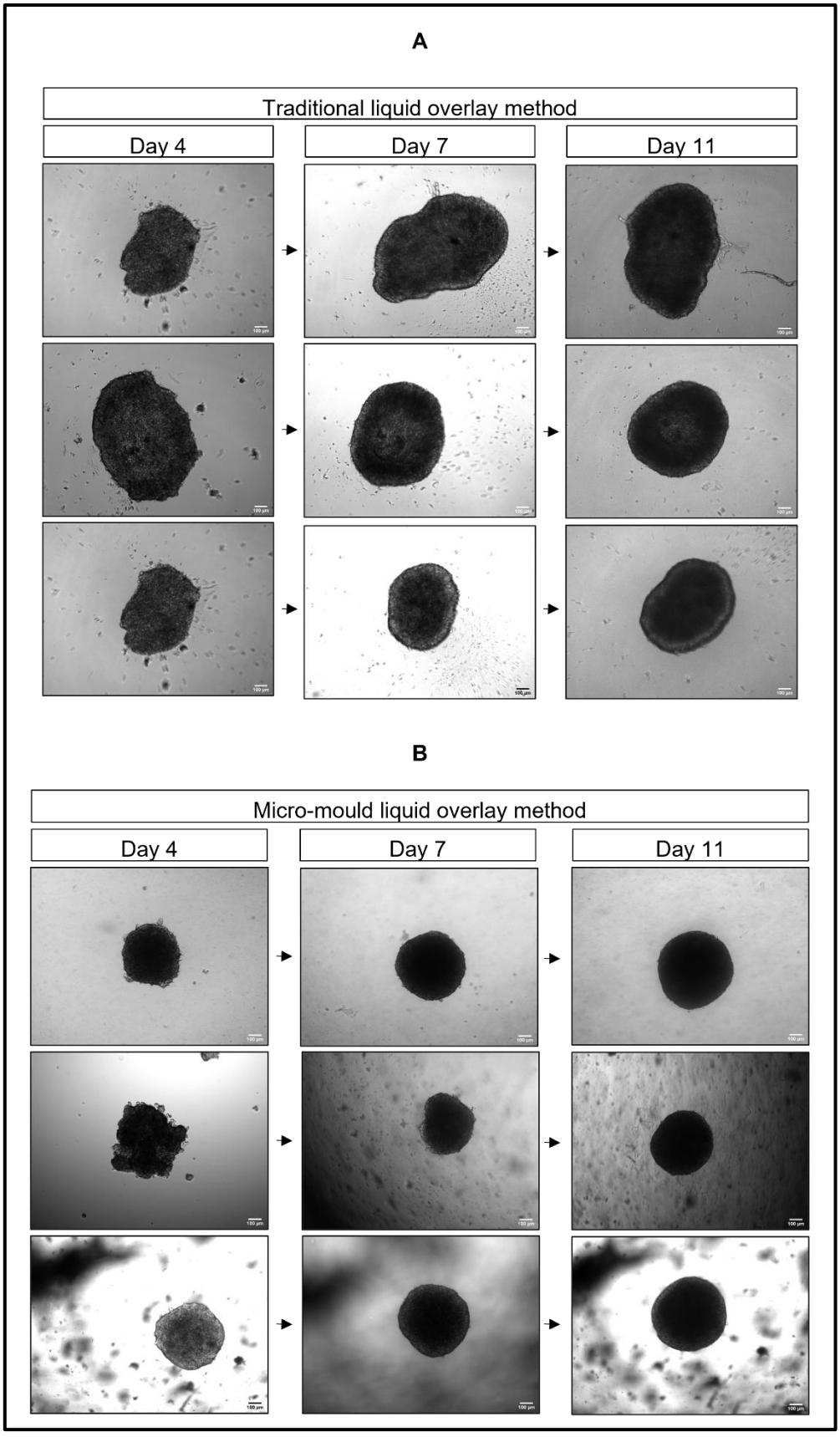

Figure 3.1: Comparison between traditional (A) and micro-mould (B) methods of generating A549 multicellular spheroids. Scale bar = 100 µm. Triplicate images at 4x magnification are shown for the respective day. These images show the micro-mould method produced more reproducible MCSs and was therefore chosen as the method of MCS formation for establishment of the model.

The A549 MSCs successfully formed by Day 4 when using the micro-mould liquid overlay method and were maintained for 21 days. Phase contrast images of multiple passages/batches of spheroid generation is included for reference in **Appendix IV**.

From Day 4 to Day 7 there was a significant ($p < 0.0001$) increase in circularity from 0.6 ± 0.02 to 0.9 ± 0.01 (**Figure 3.2**), after which it remained stable till Day 14. From Day 14 to 18 there was a steady decrease to 0.8 ± 0.03, where the circularity stabilised again until Day 21. Microscopy confirmed the spheroid structure with clearly defined edges alongside circularity, as well as a high opacity, indicating compaction (**Figure 3.2**).

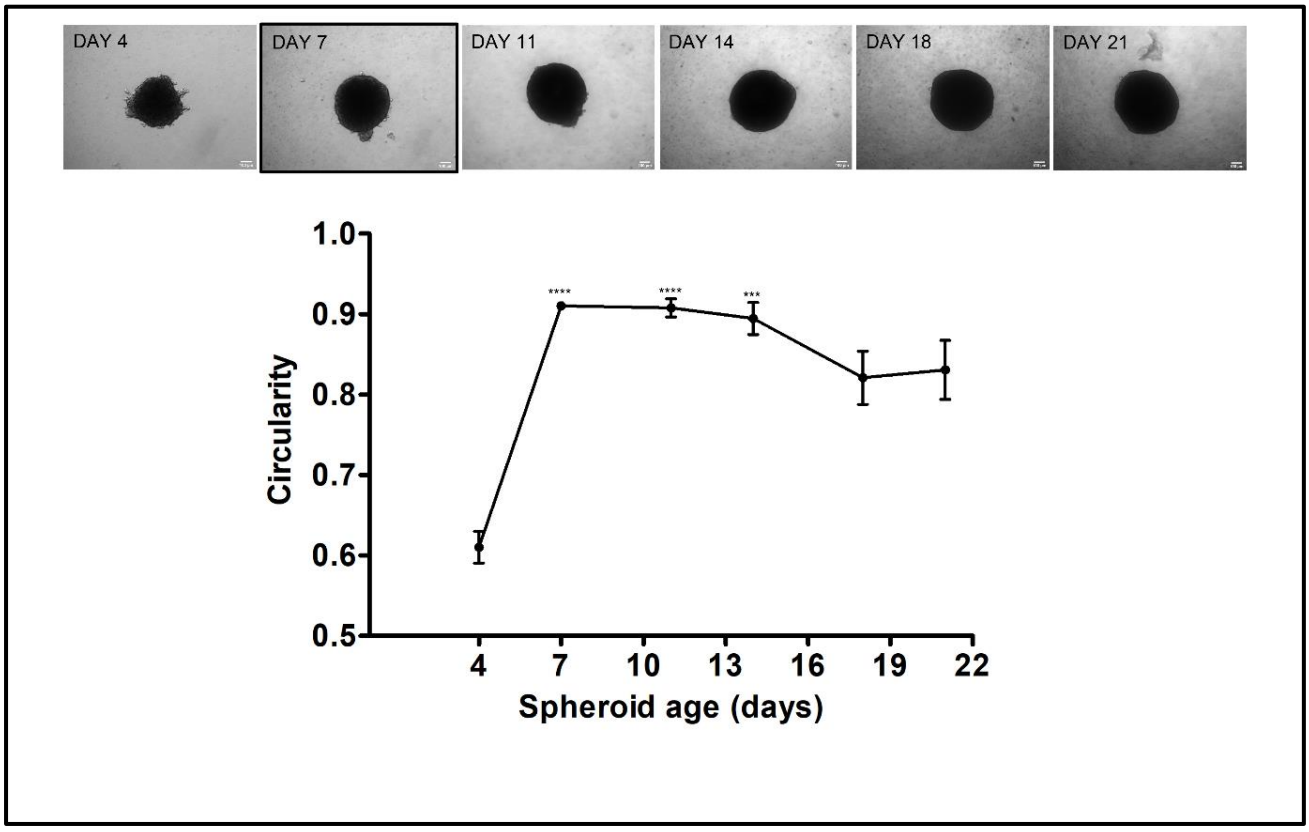

Figure 3.2: Changes in multicellular spheroid circularity over the 21-day measurement period, with phase-contrast microscopy images included for visualisation. The Day 7 spheroid is outlined to indicate this as the chosen day for nanoparticle exposure. Scale bar = 100 µm. Significance indicated as ***p ≤ 0.001; ****p ≤ 0.0001.

The spheroid volume initially decreased non-significantly ($p > 0.05$) from 2.64 x 10^8 µm^3 ± 0.49 µm^3 on Day 4 to 2.41 x 10^8 µm^3 ± 0.37 µm^3 on Day 7 (**Figure 3.3**). Thereafter, the volume decreased from Day 11 to Day 18, reaching 1.86 x 10^8 µm^3 ± 0.10 µm^3, before marginally increasing to 2.00 x 10^8 µm^3 ± 0.06 µm^3 on Day 21 (**Figure 3.3**).

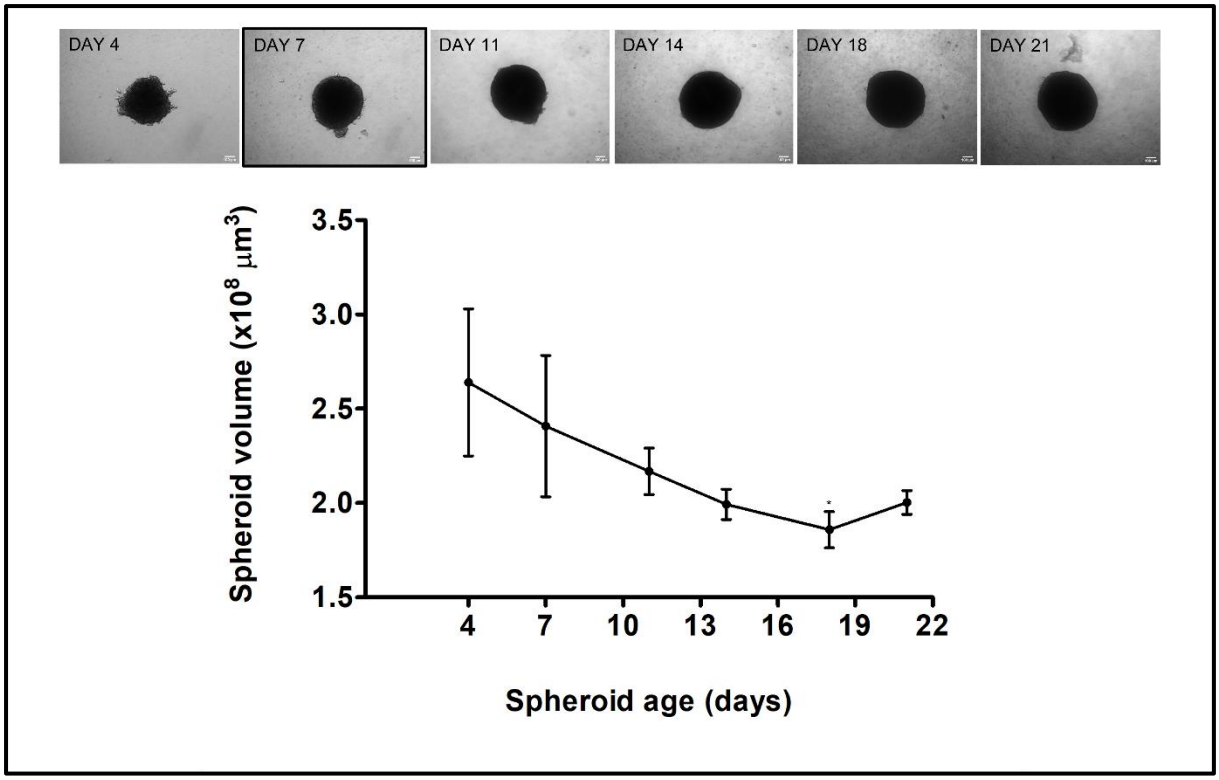

Figure 3.3: Changes in multicellular spheroid volume over the 21-day measurement period, with phase-contrast microscopy images included for visualisation. The Day 7 spheroid is outlined to indicate this as the chosen day for nanoparticle exposure. Scale bar = 100 µm. Significance indicated as *p ≤ 0.05.

Spheroid diameter increased over the 21-day measurement. The diameter remained relatively unchanged from Day 4 to Day 7, after which a significant increase ($p < 0.001$) was observed until Day 11, where the diameter reached 643.92 µm ± 16.67 µm. After this time point, the increase became less pronounced, but continued until Day 21, with a final diameter of 759.61 µm ± 29.61 µm (**Figure 3.4**).

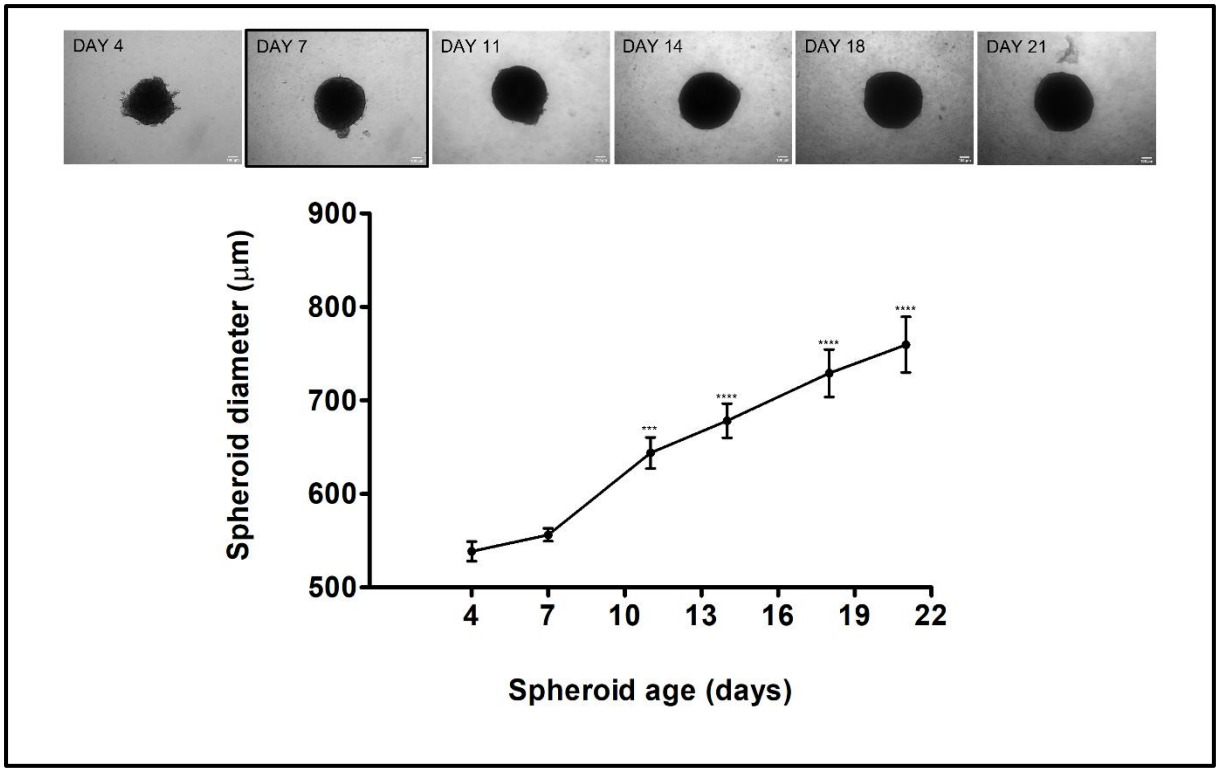

Figure 3.4: Changes in multicellular spheroid diameter over the 21-day measurement period, with phase-contrast microscopy images included for visualisation. The Day 7 spheroid is outlined to indicate this as the chosen day for nanoparticle exposure. Scale bar = 100 µm. Significance indicated as ***p ≤ 0.001; ****p ≤ 0.0001.

Day 7 was identified as the optimum day for AuNP exposure since the MCSs were fully formed, and displayed the least variable diameter, volume, and circularity for the three-day maximum exposure period. Additionally, spheroids maintained structural integrity and viability for long enough to permit exposure to AuNPs for three days.

3.3. Multicellular spheroid viability

The APH activity initially increased ($p > 0.05$, non-significant) from Day 4 to 7, after which it plateaued until Day 14 (**Figure 3.5**). A sharp increase in activity was observed at Day 18, which then reduced back to an activity showing a similar trend to that seen for Day 11. Protein content initially increased by 30.00% from 2.5 µg ± 0.02 µg on Day 4 to 3.2 µg ± 0.03 µg on Day 7. Protein content continued to increase thereafter until Day 18, where it started to decrease and reached 0.6 µg ± 0.07 µg at Day 21 (**Figure 3.5**).

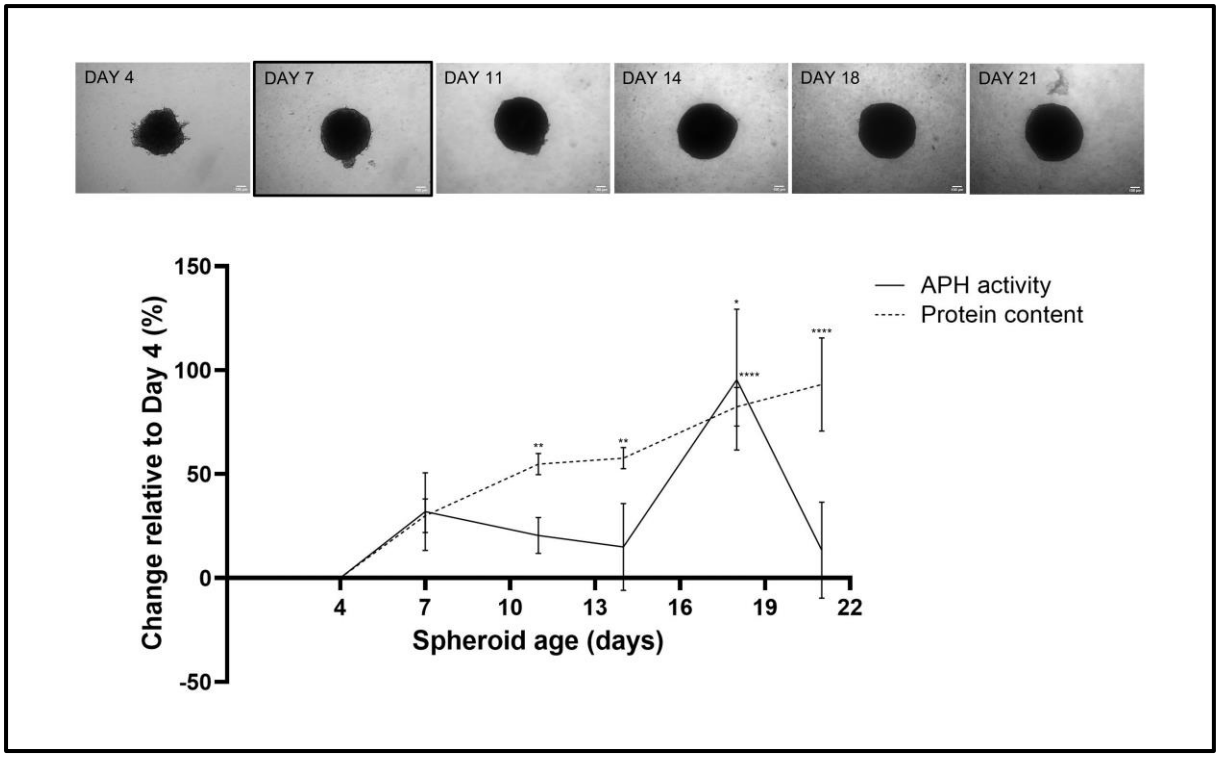

Figure 3.5: Growth and viability measurements of A549 multicellular spheroids over 21 days, including microscopy images for visualisation, showing continuously increasing protein content, along with initially increasing acid phosphatase (APH) activity, followed by a reducing trend, with the exception of Day 18. The Day 7 spheroid is outlined to indicate this was the chosen day of nanoparticle exposure supported by the viability results. Scale bar = 100 µm. Significance indicated as *p ≤ 0.05; **p ≤ 0.01; ****p ≤ 0.0001.

Taking into consideration the stability of the model at Day 7, particularly pertaining to its structural integrity and viability, it was selected as the most appropriate time of exposure to facilitate a long enough experimental window.

3.4. Nanoparticle interference studies with assay substrates

To determine whether the AuNPs would affect any of the experimental procedures, interference studies were conducted. Apart from the optical properties of the AuNPs, the potential to alter substrate conversion or fluorescence intensity of fluorophores was also assessed.

3.4.1. Acid phosphatase assay

3.4.1.1. Inherent effect on optical density

The AuNPs displayed an increased absorbance when diluted in water (72.78% with 6 x 10^{11} NP/mL PCOOH-AuNP, 143.54% with 1.2 x 10^{12} NP/mL PCOOH-AuNP and 150.43% with 4.5 x 10^{12} NP/mL amine-AuNP), compared to only water (**Figure 3.6**

A). These increases in absorbance were non-significant ($p > 0.05$), for all but the 4.5 x 10^{12} NP/mL amine-AuNP group ($p = 0.01$), however the latter was considered negligible since the assay protocol does not include water.

A marginal increase in absorbance was observed when AuNPs were diluted in DMEM (7.80% for 6 x 10^{11} NP/mL PCOOH-AuNP, 21.32% with 1.2 x 10^{12} NP/mL PCOOH-AuNP and 41.17% with 4.5 x 10^{12} NP/mL amine-AuNP), compared to only DMEM (**Figure 3.6 A**). These increases in absorbance were non-significant ($p > 0.05$), for all but the 4.5 x 10^{12} NP/mL amine-AuNP group ($p = 0.01$). Although an increase was noted, it should be considered that in the cellular system, excess NPs that were not taken up by the cells are washed out of the external environment, thus decreasing their presence.

To indicate how marginal of an increase this was, the negative control in a cellular environment, where the assay is conducted in a medium-free environment, had an average absorbance value of 0.157, which is correlated to an increase of 220.41%, compared to water alone, and 15.44% compared to DMEM alone.

3.4.1.2. Effect in the presence of assay substrates

When comparing the observed absorbance of the AuNPs with the assay reagents (**Figure 3.6 B**), no significant spontaneous conversion of the substrate was observed ($p > 0.05$), except for the 1.2 x 10^{12} NP/mL PCOOH-AuNP, which showed an increased absorbance of 127.27%, compared to only the assay buffer. Although this result was significant ($p < 0.05$), it should be noted that in the experimental setting, wash steps will decrease the concentrations of the AuNPs, particularly as a low uptake into cells can be expected based on prior experimentation.

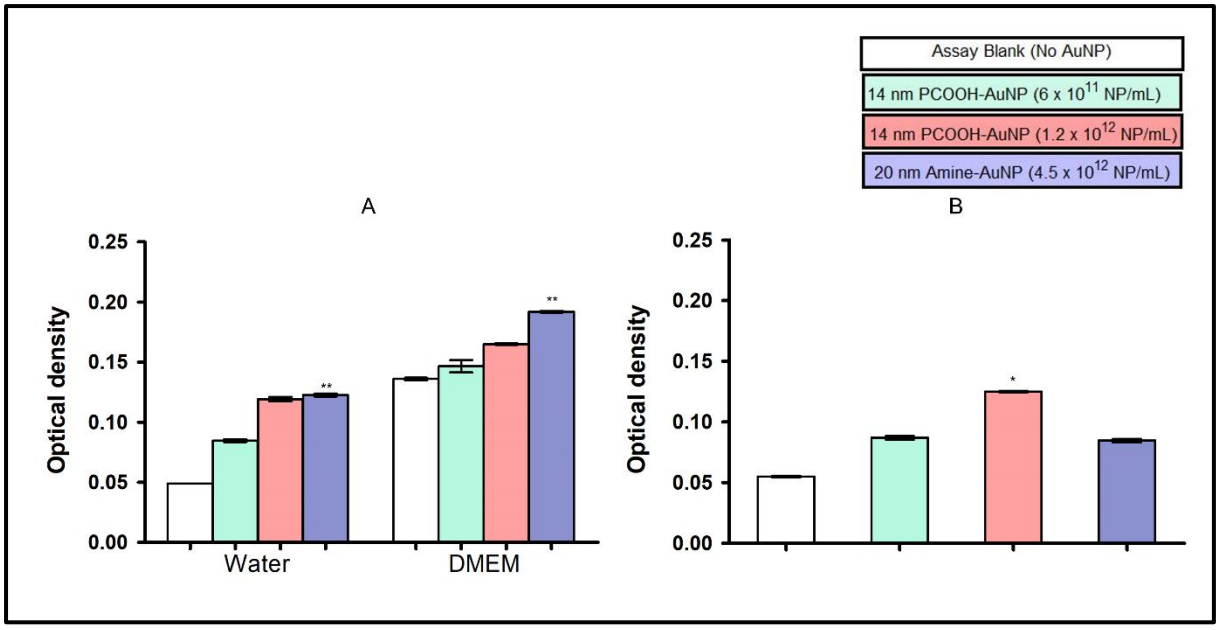

Figure 3.6: Absorbance values of gold nanoparticles in water and medium free from foetal calf serum (A) and interference of gold nanoparticles with the acid phosphatase assay substrate in a cell-free environment (B). Blank absorbance values were included for scale. The measurement was carried out at a wavelength of 405 nm. Significance indicated as *p ≤ 0.05; **p ≤ 0.01.

3.4.2. Bicinchoninic acid assay

3.4.2.1. Inherent effect on optical density

The AuNPs displayed an increased absorbance when diluted in water (71.30% with 6 x 10^{11} NP/mL PCOOH-AuNP, 155.65% with 1.2 x 10^{12} NP/mL PCOOH-AuNP and 193.91% with 4.5 x 10^{12} NP/mL amine-AuNP), compared to that of water only (**Figure 3.7 A**). These increases in absorbance were non-significant ($p > 0.05$), for all but the 4.5 x 10^{12} NP/mL amine-AuNP group ($p = 0.01$), but was considered negligible since the assay protocol does not include water only. Although the assay protocol involves a number of wash steps, these were not included in the interference study due to the high probability that the AuNPs would be washed away.

The change in absorbance was marginal in the presence of AuNPs with DMEM. An absorbance increase of 0.53% with 6 x 10^{11} NP/mL PCOOH-AuNP, 12.82% decrease with 1.2 x 10^{12} NP/mL PCOOH-AuNP and 22.72% increase with 4.5 x 10^{12} NP/mL amine-AuNP was noted when compared to DMEM only (**Figure 3.7 A**). Changes in absorbance were non-significant ($p > 0.05$) for all three AuNPs and considered negligible due to the extensive washing involved in the assay protocol,

which was not possible with the interference study due to the high probability of AuNPs being washed away, if not taken up by the cells.

3.4.2.2. Effect in the presence of assay substrates

When comparing the observed absorbance of the AuNPs with the assay reagents (**Figure 3.7 B**), no statistically significant ($p > 0.05$) spontaneous conversion of the substrate was observed, except for a 16.67% increase caused by the 4.5 x 10^{12} NP/mL amine-AuNPs when diluted in the buffer ($p = 0.01$). Although the assay protocol involves a number of wash steps, these were not included in the interference study due to the high probability that the AuNPs would be washed away and thus, this increase was considered non-relevant.

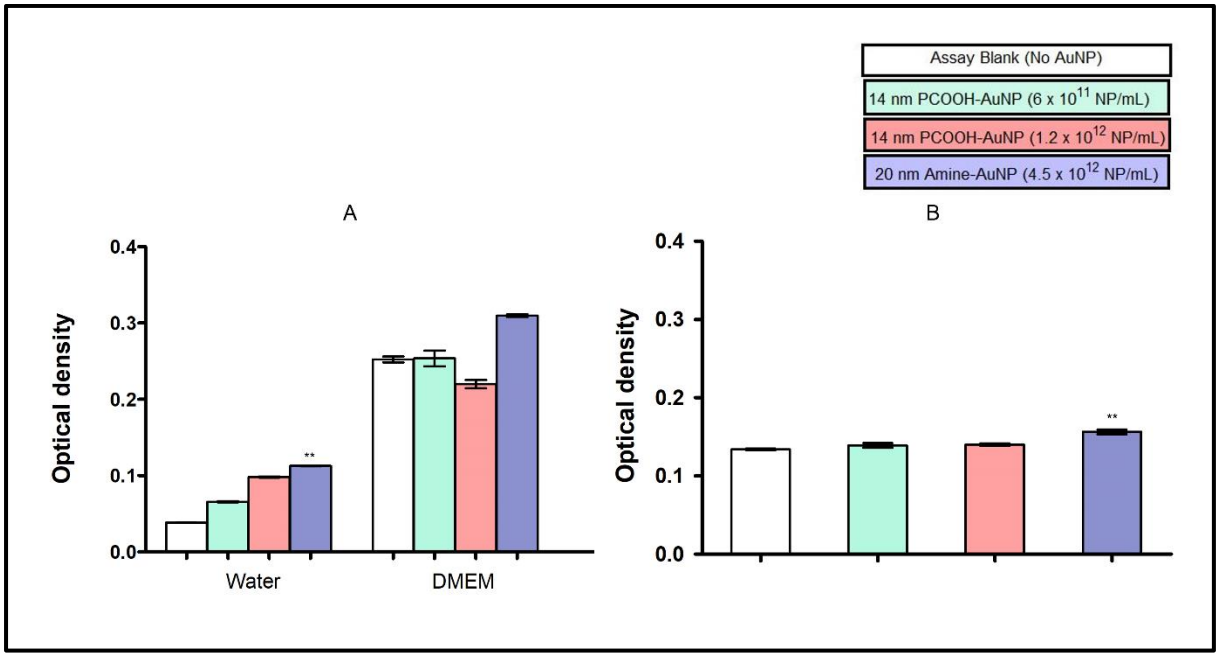

Figure 3.7: Absorbance values of gold nanoparticles in water and medium without foetal calf serum (A) and interference of gold nanoparticles with the acid phosphatase assay substrate in a cell-free environment (B). Blank absorbance values were included for scale. The measurement was carried out at a wavelength of 405 nm. Significance indicated as *p ≤ 0.05; **p ≤ 0.01.

3.4.3. Propidium iodide

3.4.3.1. Autofluorescence of nanoparticles

The AuNPs displayed a decrease in fluorescence when diluted in water (with 10.58% for 6 x 10^{11} NP/mL PCOOH-AuNP, 14.81% with 1.2 x 10^{12} NP/mL PCOOH-AuNP and 14.81% with 4.5 x 10^{12} NP/mL amine-AuNP), compared to water only (**Figure 3.8 A**). All decreases were non-significant ($p > 0.05$) and considered negligible

except for the 4.5 x 10^{12} NP/mL amine-AuNPs, where there was a significant ($p = 0.02$) decrease in fluorescence, which was considered negligible due to the extensive washing that occurs during cellular assays.

When AuNPs were present in DMEM, fluorescence was decreased (with 20.35% for 6 x 10^{11} NP/mL PCOOH-AuNP, 39.63% with 1.2 x 10^{12} NP/mL PCOOH-AuNP and 12.94% with 4.5 x 10^{12} NP/mL amine-AuNP), compared to DMEM only (**Figure 3.8 A**). Although the fluorescent decrease observed with 1.2 x 10^{12} NP/mL PCOOH-AuNP was significant ($p < 0.05$), it was considered negligible due to the extensive washing that occurs during cellular assays.

3.4.3.2. Possibility of propidium iodide fluorescent quenching by nanoparticles

The AuNPs did not cause relevant quenching of PI, at either the low (2 mg/mL) or high (5 mg/mL) concentrations of PI (**Figure 3.8 B**). The marginal quenching effects observed were non-significant ($p > 0.05$), except for the quenching by 4.5 x 10^{12} NP/mL amine-AuNPs at 2 mg/mL PI ($p < 0.05$) and 1.2 x 10^{12} NP/mL PCOOH-AuNP at 5 mg/mL PI ($p < 0.05$). The effect was considered low enough for the analysis to continue, since the in-reaction concentration of PI in the protocol was much lower than the concentrations tested, as well as the extensive washing prior to taking the readings.

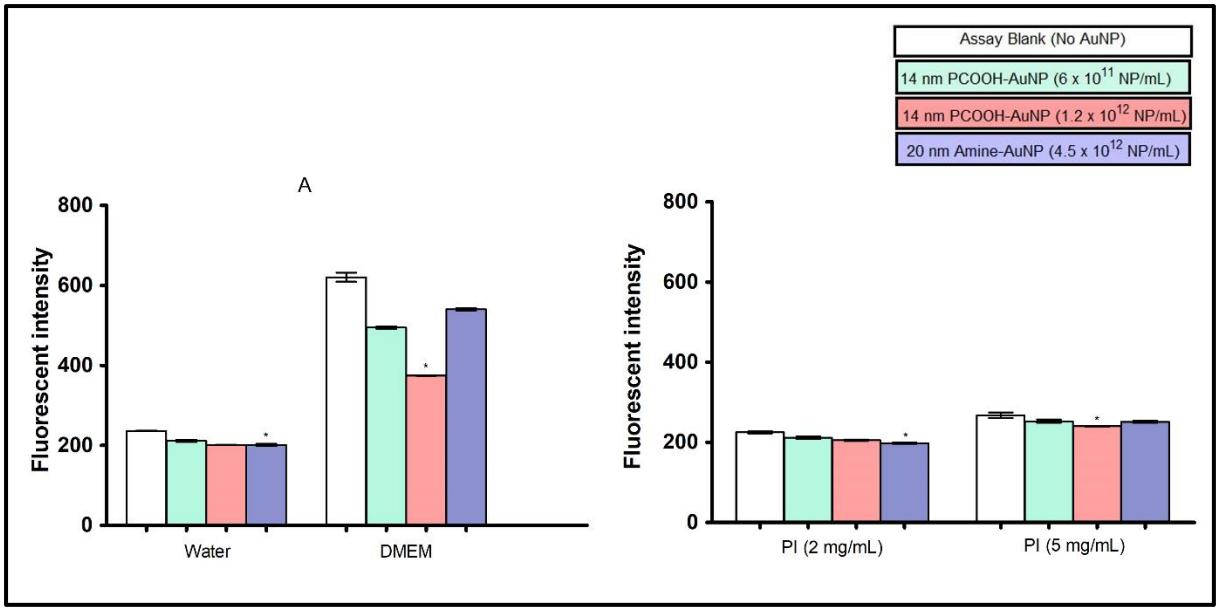

Figure 3.8: Fluorescent intensity of the gold nanoparticles in water and medium devoid of foetal calf serum (A) and quenching of propidium iodide (PI) at high concentration by gold nanoparticles (AuNP) (B). Blank values were included for reference. The 385±40, 590±35 filter set (nm; excitation, emission wavelengths ± bandpass filter ranges) was used. Significance indicated as *p ≤ 0.05.

3.4.3.3. Possibility of nanoparticle identification during flow cytometry

Interference studies were undertaken using the CytoFlex flow cytometer to determine whether the AuNPs would be picked up as fluorescent debris during flow cytometry (**Figures 3.9** and **3.10**) or interfere with PI fluorescence. The analysis was performed with AuNPs were at maximum concentrations; 1.2 x 10^{12} NP/mL PCOOH-AuNP (**Figure 3.9**) and 4.5 x 10^{12} NP/mL amine-AuNP (**Figure 3.10**) for 24 h. It was found that in the absence of cells (green and red graphs on **Figures 3.9** and **3.10**), the AuNPs were not picked up as being part of the cell cycle. Cell cycle activity was only observed in groups that contained cells (yellow and blue on **Figures 3.9** and **3.10**). Propidium iodide concentrations were comparable to the experimental protocol.

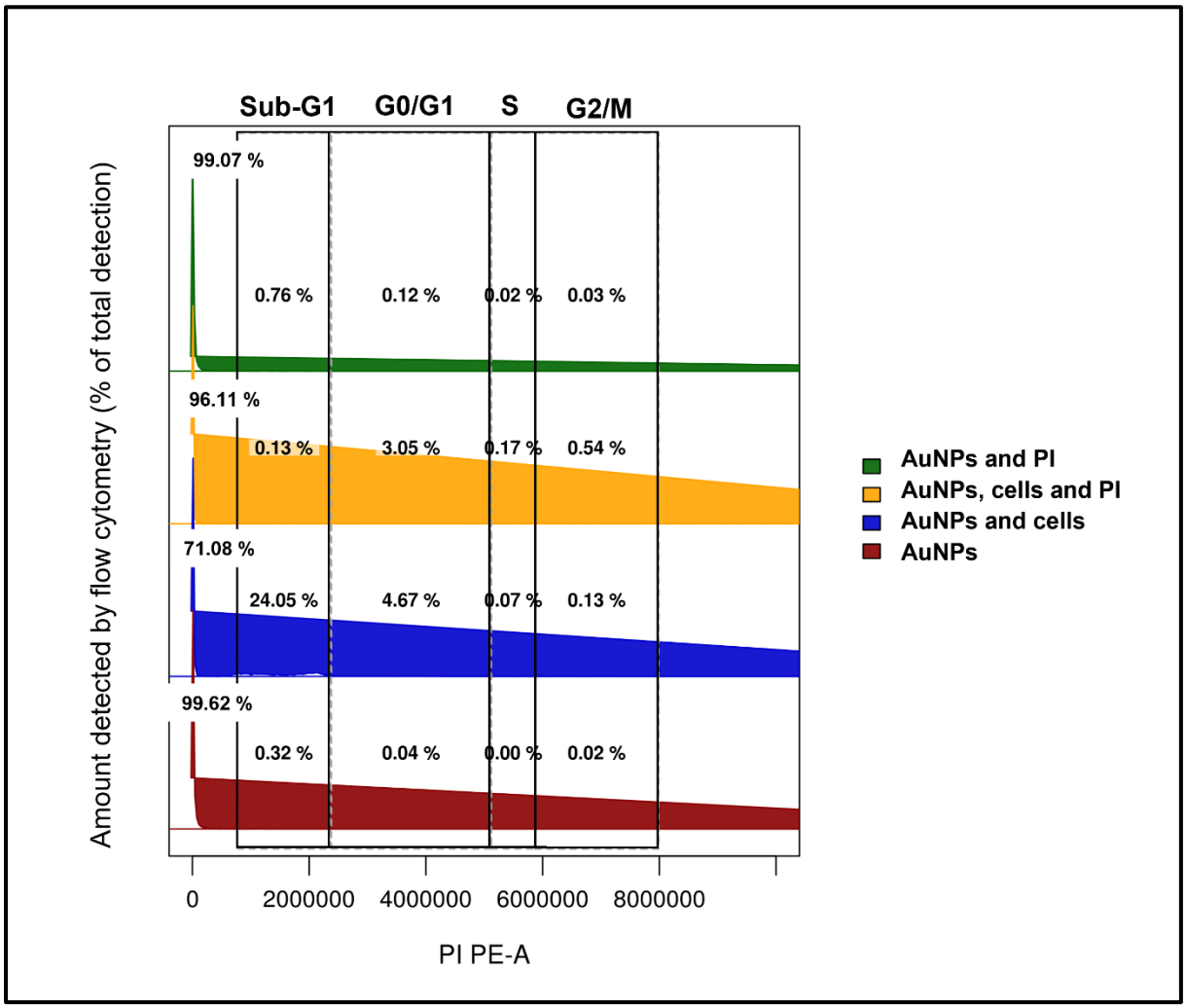

Figure 3.9: Percentage of material picked up by CytoFlex flow cytometer to determine whether PCOOH-AuNPs would interfere with propidium iodide (PI) during experimental analysis.

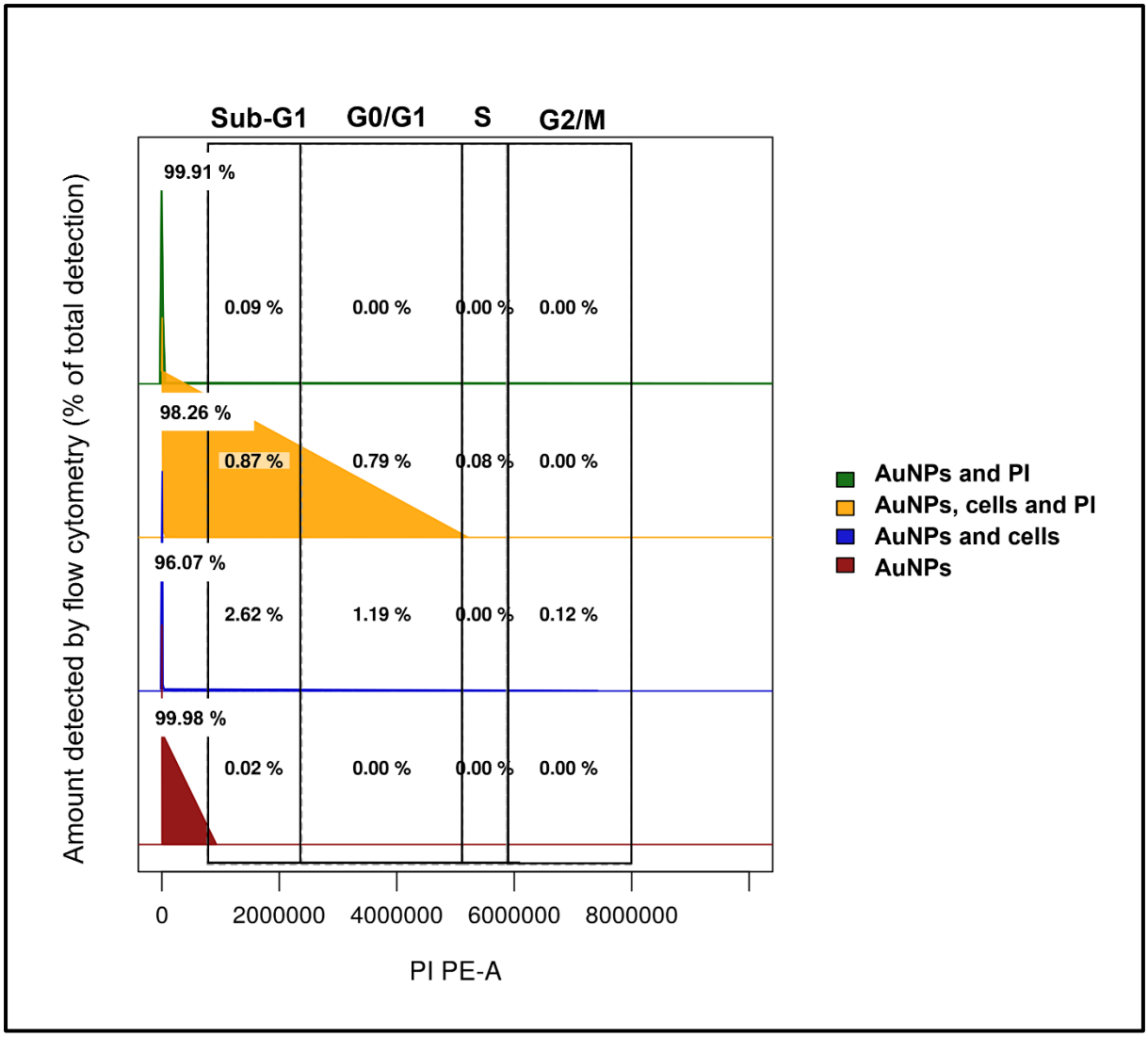

Figure 3.10: Percentage of material picked up by CytoFlex flow cytometer to determine whether amine-AuNPs would interfere with propidium iodide (PI) during experimental analysis.

3.4.4. Caspase-3/7 assay

There was a non-significant decrease in fluorescence ($p > 0.05$), of 40.00% for 6 x 10^{11} NP/mL PCOOH-AuNP, 35.15% with 2.3 x 10^{12} NP/mL amine-AuNP and 49.99% with 4.5 x 10^{12} NP/mL amine-AuNP when diluted in water, compared to water only (**Figure 3.11**). There was a significant ($p < 0.01$) decrease in fluorescence by 56.56% with 1.2 x 10^{12} NP/mL PCOOH-AuNP (**Figure 3.11**). Although it might have been of concern since the assay was performed in a water-based solution, it was considered negligible due to the extensive washing involved in the assay protocol, which was not possible with the interference study due to the high probability of AuNPs being washed away, if not taken up by the cells.

A non-significant ($p > 0.05$) decrease in fluorescence was noted for both AuNPs (low concentrations) when diluted in DMEM, compared to DMEM only (**Figure 3.11**). There were significant decreases in fluorescence ($p < 0.05$) for both groups (**Figure 3.11**) at high concentrations. The latter was considered negligible especially considering the number of wash-steps involved, implying that there would essentially be no DMEM present at the time at which the fluorescence was read. There was extensive washing involved in the assay protocol, which was not possible with the interference study due to the high probability of AuNPs being washed away, if not taken up by the cells.

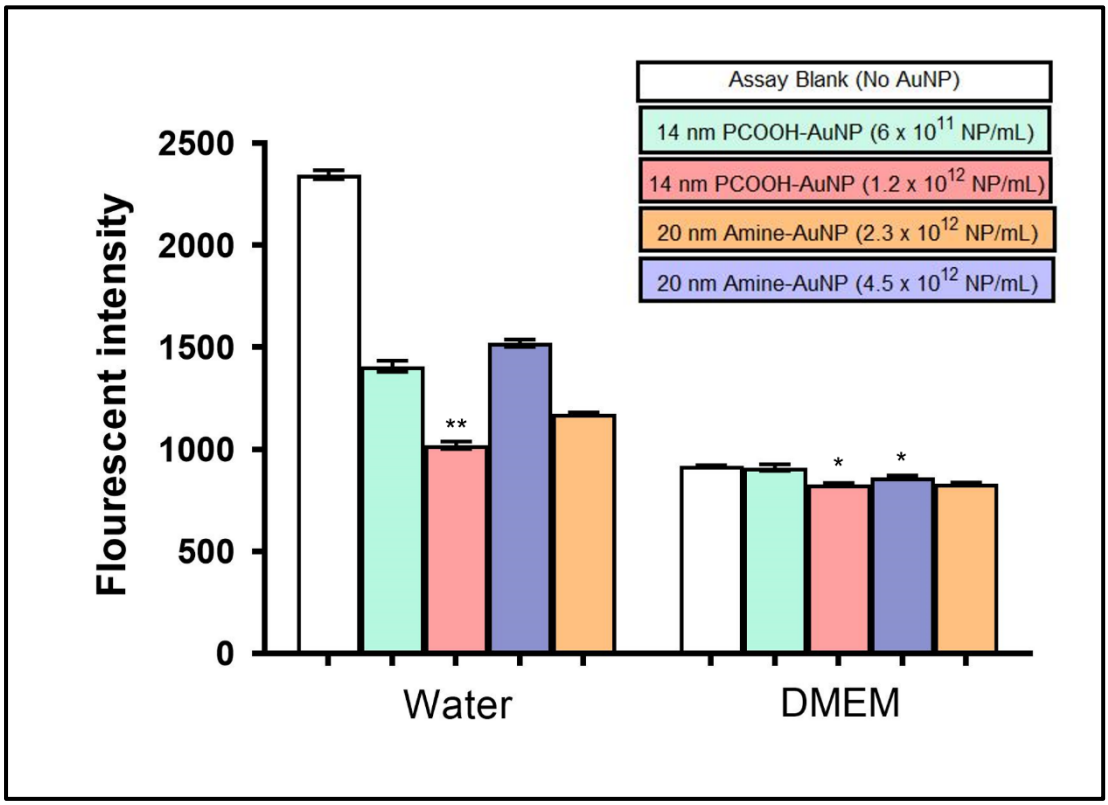

Figure 3.11: Fluorescent intensity of the caspase-3/7 assay substrate in the presence of gold nanoparticles (AuNP) in water and medium free from foetal calf serum. Blank values were included for reference. The 340±11, 450±50 filter set (nm; excitation, emission wavelengths ± bandpass filter ranges) was used. Significance indicated as *p ≤ 0.05; **p ≤ 0.01.

.

3.5. Cytotoxicity measurement of gold nanoparticles

3.5.1. Morphological effect of gold nanoparticles on A549 spheroids

Phase contrast (PC) microscopy images of the effects of the different AuNPs on the MCSs at Day 7 are provided in **Appendix IV**. The PCOOH-AuNPs, for the most part, did not alter the morphology of the MCSs at any concentration, while the amine-

AuNPs yielded morphological changes after 24 h. Amine-AuNP-treated MCSs were less compact, displayed an increase in debris formation, and lost structural integrity.

3.5.1.1. Circularity

The positive control significantly ($p < 0.01$) decreased the circularity of the MCSs by 15.13% after 24 h, after which it plateaued at 72 h (**Figure 3.12**), most likely as a result of loss of structural integrity. The PCOOH-AuNPs non-significantly ($p > 0.05$) decreased circularity (**Figure 3.12**), suggesting little alterations at the concentrations tested. The effect was not dependent on time of exposure. The amine-AuNPs significantly ($p < 0.001$) decreased circularity by 38.84% after 24 h (**Figure 3.12**), and then plateaued, suggesting a loss of shape and structural integrity.

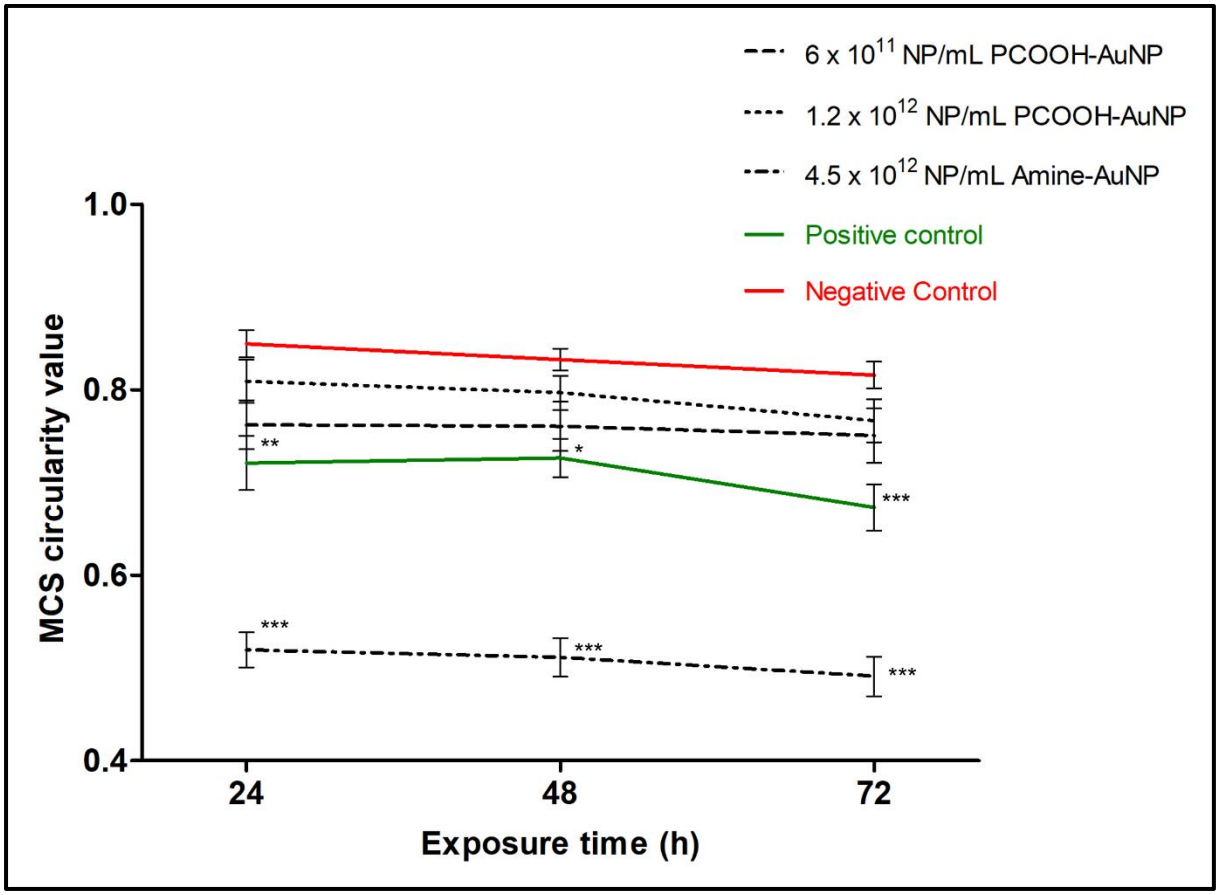

Figure 3.12: Effect of gold nanoparticles on the circularity index of multicellular spheroids over a 72 h exposure period. The positive control (1% saponin [indicated as a solid green line]) and the negative control (untreated multicellular spheroids [indicated as a solid red line]) were included for interpretation. Significance indicated as *p ≤ 0.05; **p ≤ 0.01; ***p ≤ 0.001.

3.5.1.2. Volume

The positive control increased MCS volume by 18.35% after 48 h, compared to the negative control, however, this was non-significant ($p > 0.05$) (**Figure 3.13**), suggesting reduced compaction of the spheroid and possible release of cellular connections. The PCOOH-AuNPs at the lowest concentrations (6 x 10^{11} NP/mL) caused a slight increase in volume after 48 h of 11.34% (non-significant, $p > 0.05$), which may indicate release of cellular connections and loss of structural integrity. This effect, however, was not seen at the higher concentration PCOOH-AuNP (1.2 x 10^{12} NP/mL), indicating that there is indeed loss of cellular connections due to the PCOOH-AuNPs. The amine-AuNPs caused a 10.24% increase in volume after 24 h. The effect was similar to that of the positive control (**Figure 3.13**), except that the effect occurred after a shorter exposure period.

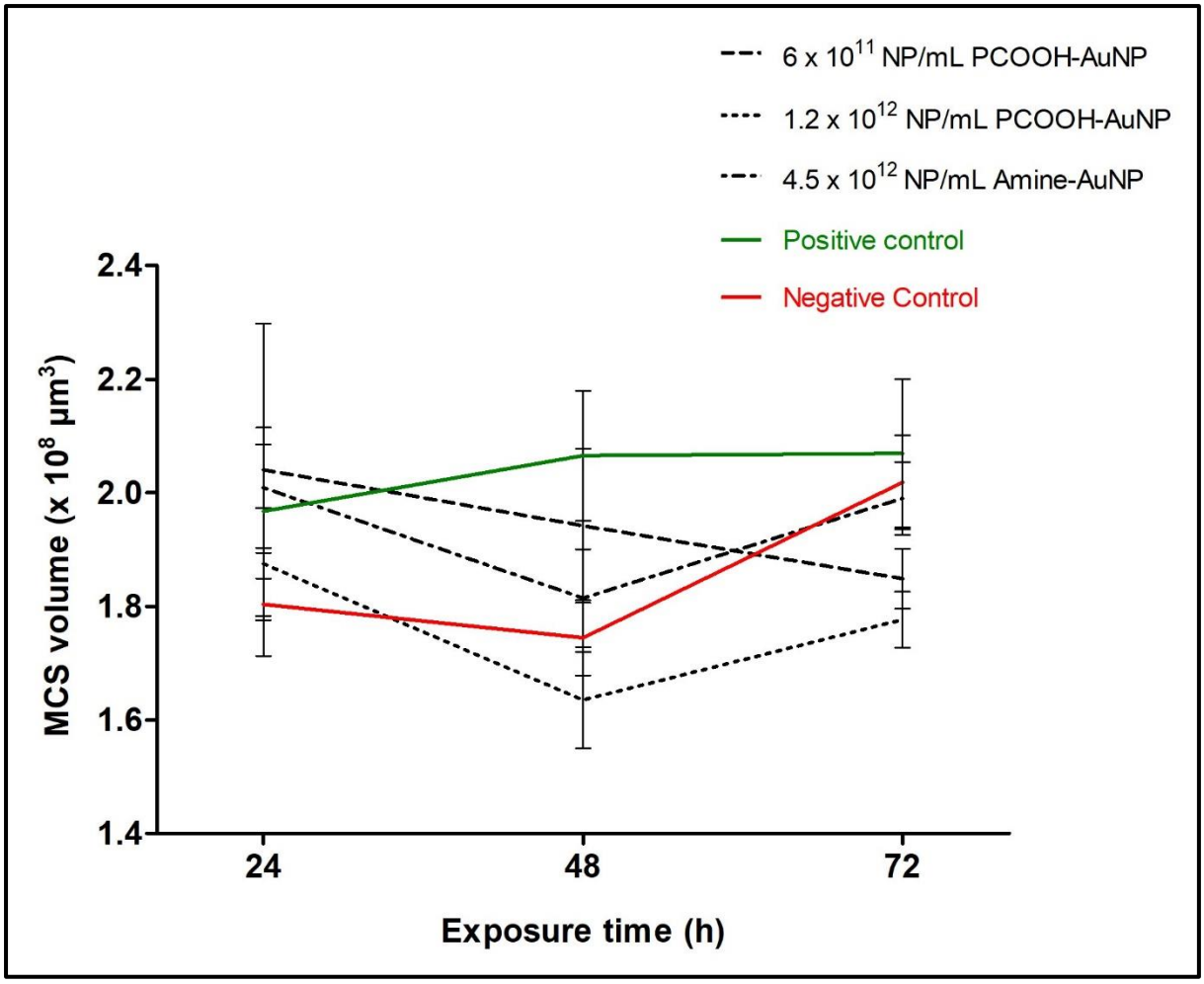

Figure 3.13: Effect of gold nanoparticles on the volume of multicellular spheroids over a 72 h exposure period. The positive control (1% saponin [indicated as a solid green line]) and the negative control (untreated multicellular spheroids [indicated as a solid red line]) were included for interpretation.

3.5.2. Effect of gold nanoparticles on A549 multicellular spheroid viability

The positive control significantly decreased ($p < 0.001$) APH activity by 78.49% at 24 h and plateaued thereafter (**Figure 3.14**). This indicates that the positive control reached its maximum activity by 24 h. The 6 x 10^{11} NP/mL PCOOH-AuNPs showed a non-significant ($p > 0.05$) decrease of 20.57% in APH activity between 24 h and 48 h (**Figure 3.14**). The APH activity returned to baseline at 72 h (**Figure 3.14**).

The 1.2 x 10^{12} NP/mL PCOOH-AuNPs initially showed a non-significant ($p > 0.05$) increase of 16.14% in APH activity, which returned to the original activity observed at 24 h, after 72 h (**Figure 3.14**). This might indicate an initial protective response by the cells, which then dissipates as the cytotoxic effect is diminished. These results

indicate that the PCOOH-AuNPs did not affect the APH activity in the MCSs, therefore suggesting a lack of cytotoxicity.

The APH activity of the 4.5 x 10^{12} NP/mL amine-AuNP-exposed MCSs after 24 h was similar to the negative control (**Figure 3.14**). A non-significant ($p > 0.05$) decrease of 28.34% in APH activity was observed after 48 h, which continued till 72 h (83.99%; $p < 0.001$) (**Figure 3.14**). It appears that the amine-AuNPs display time-dependent cytotoxicity.

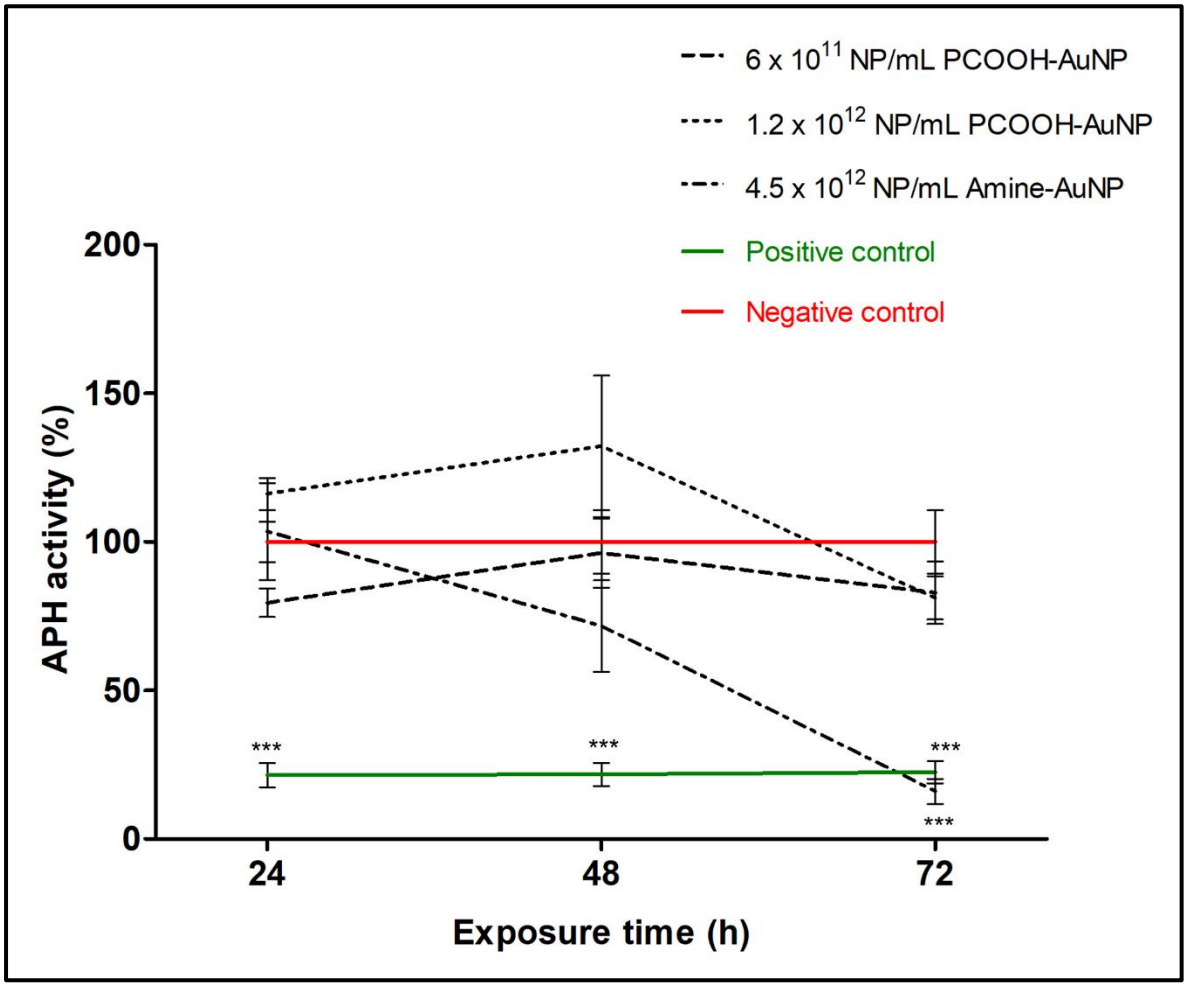

Figure 3.14: Multicellular spheroid acid phosphatase activity due to gold nanoparticle exposure over a 72 h exposure period. The positive control (1% saponin [indicated as a solid green line]) and the negative control (untreated multicellular spheroids [indicated as a solid red line]) were included for interpretation. Significance indicated as ***$p \leq 0.001$.

3.5.3. Effect of gold nanoparticles on protein content of A549 multicellular spheroids

The positive control significantly decreased ($p < 0.001$) the protein content by 95.48% after 24 h (**Figure 3.15**). After 48 h, the decrease was 50.81% (significant, $p < 0.001$), and an even more pronounced reduction of 80.56% (significant, $p < 0.001$) was observed after 72 h (**Figure 3.15**).

The lower concentration (6×10^{11} NP/mL) PCOOH-AuNPs caused a significant decrease of 34.40% ($p < 0.05$) after 24 h, and this effect plateaued till 48 h, after which protein content returned to baseline (**Figure 3.15**). This indicates that the effect of the PCOOH-AuNPs only lasted until the 48 h time point, after which the MCSs were able to synthesise protein again. This could indicate an active window for the PCOOH-AuNPs to elicit their response.

The higher concentration (1.2×10^{12} NP/mL) of PCOOH-AuNPs resulted in a significant decrease ($p < 0.01$) in protein content of 35.45% (**Figure 3.15**). This effect diminished over time and was comparable to the negative control at 72 h (**Figure 3.15**). This indicates that the higher concentration could not extend or increase the cytotoxicity of the PCOOH-AuNPs on the MCSs. The effect is not concentration-dependent, but rather time-dependent, since the lower concentration showed a similar effect that could be maintained for a longer time period.

The amine-AuNPs had a similar protein content to the negative control (non-significant, $p > 0.05$) after 48 h (**Figure 3.15**). By 72 h the protein content decreased non-significantly ($p > 0.05$) by 34.63%, suggesting that the effect might be dependent on the exposure time.

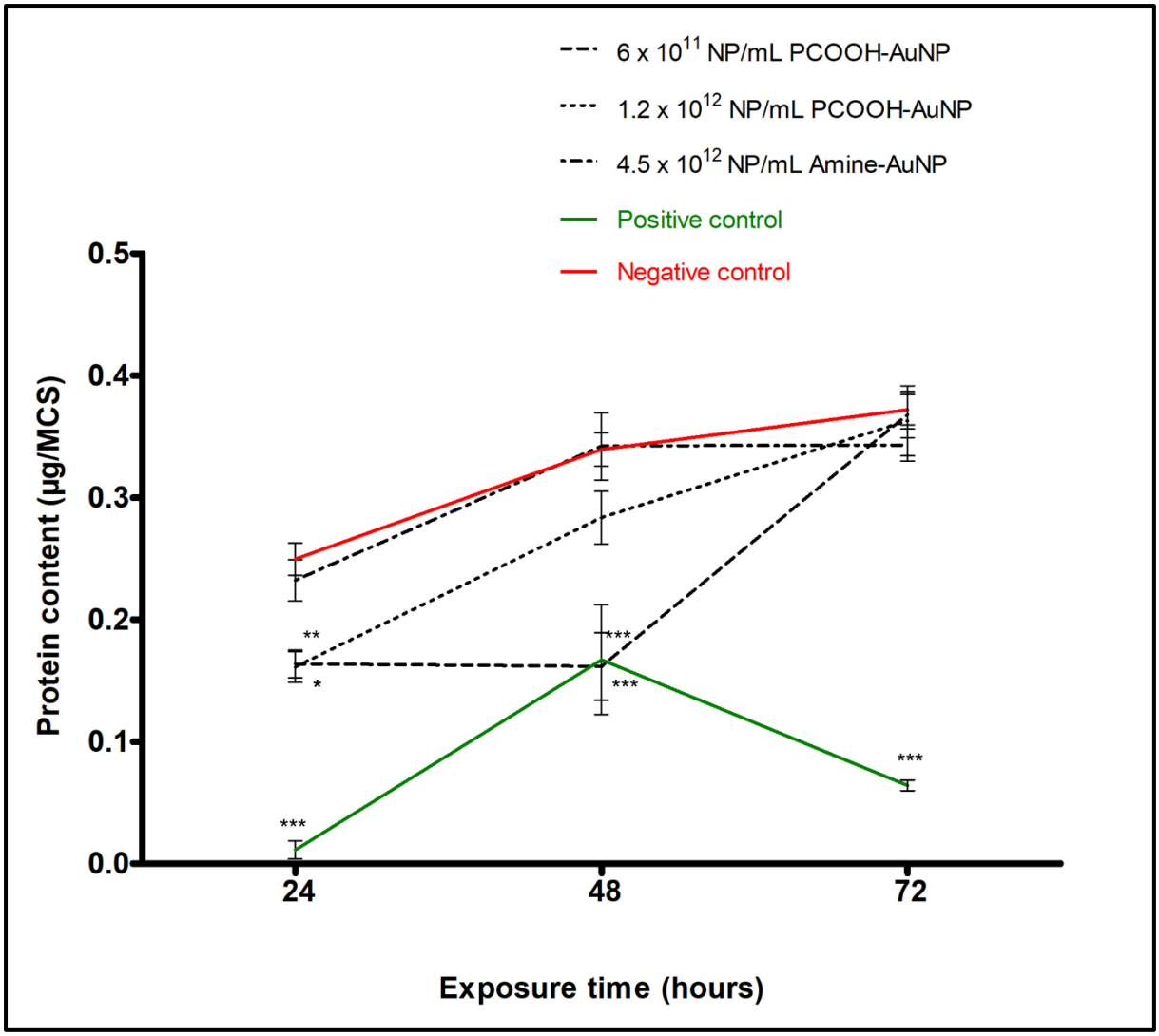

Figure 3.15: Effect of gold nanoparticles on the protein content of multicellular spheroids over a 72 h exposure period. The positive control (1% saponin [indicated as a solid green line]) and the negative control (untreated multicellular spheroids [indicated as a solid red line]) were included for interpretation. Significance indicated as *p ≤ 0.05; **p ≤ 0.01; ***p ≤ 0.001.

3.5.4. Effect of gold nanoparticles on cell cycle distribution within A549 multicellular spheroids

3.5.4.1. Baseline cell cycle distribution in A549 multicellular spheroids

Multicellular spheroids displayed a normal cellular distribution, with few cells (1.14%) in the sub-G_1 phase, the majority (84.61%) of cells in the G_0/G_1-phase, and a lower proportion (4.01%) of cells in the S-phase. The low number of cells in the sub-G_1 phase indicates that a low level of DNA degradation occurred. Over time, a greater proportion of cells transitioned into the G_0/G_1 phase, and less in S and G_2/M phase

(**Figure 3.16** and **Table 3.2**) with the progression of time. This could indicate more cells exiting the cell cycle and becoming quiescent.

Table 3.2: Summary of baseline cell cycle distribution of Day 7 A549 multicellular spheroids.

	Incubation time (h)		
Cell cycle phase	**24**	**48**	**72**
Sub-G_1 (%)	1.14 ± 0.35	0.57 ± 0.22	0.53 ± 0.14
G_0/G_1 (%)	84.61 ± 0.60	86.80 ± 0.26	87.89 ± 0.59
S (%)	4.01 ± 1.69	1.74 ± 0.40	1.81 ± 0.46
G_2/M (%)	10.23 ± 1.15	10.89 ± 0.36	9.77 ± 0.67

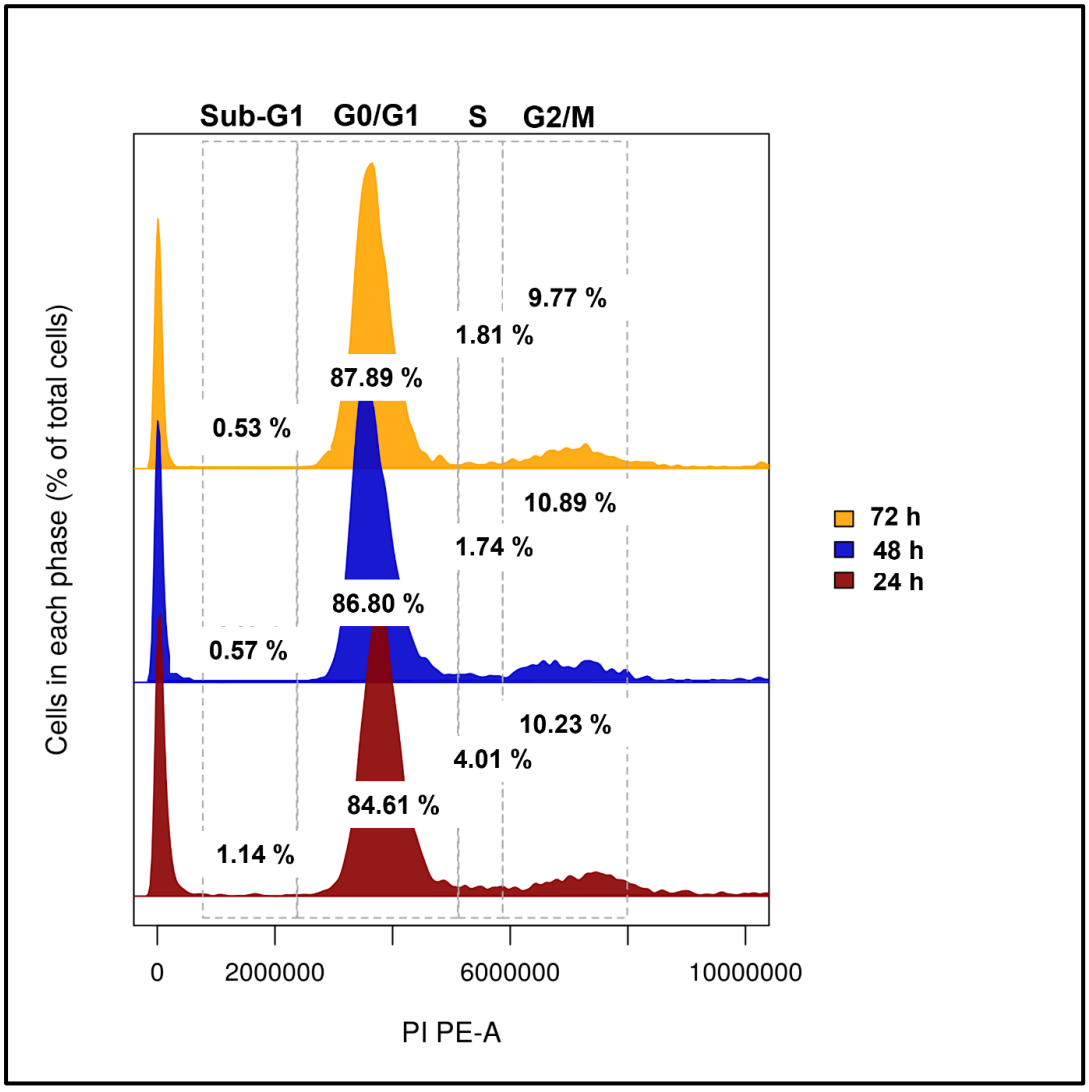

Figure 3.16: Baseline cell cycle distribution of Day 7 A549 multicellular spheroids after 24 h (red), 48 h (blue) and 72 h (yellow).

3.5.4.2. Carboxyl-polyethylene glycol-liganded gold nanoparticles

In comparison to the negative control (**Figures 3.17** and **3.18**; **Table 3.3 and 3.4**), no statistically significant ($p > 0.05$) differences in cell cycle distribution were observed for either the 6 x 10^{11} NP/mL or 1.2 x 10^{12} NP/mL PCOOH-AuNPs. The majority of cells (83.37%) were in the G_0/G_1-phase, with a low percentage cycling from S to G_2/M-phase over the 72 h exposure period (**Figures 3.17** and **3.18**, **Tables 3.3** and **3.4)**.

Table 3.3: Summary of cell cycle distribution of Day 7 A549 multicellular spheroids post-exposure to 6 x 10^{11} NP/mL carboxyl-polyethylene glycol-liganded gold nanoparticles.

	Incubation time (h)		
Cell cycle phase	**24**	**48**	**72**
Sub-G_1 (%)	1.27% ± 0.30	1.15% ± 0.50	0.44% ± 0.05
G_0/G_1 (%)	83.37% ± 0.12	84.43% ± 1.99	87.11% ± 0.61
S (%)	3.60% ± 1.02	2.52% ± 0.70	2.23% ± 0.67
G_2/M (%)	11.75% ± 1.14	11.91% ± 0.89	10.23% ± 0.44

Table 3.4: Summary of cell cycle distribution of Day 7 A549 multicellular spheroids post-exposure to 1.2 x 10^{12} NP/mL carboxyl-polyethylene glycol-liganded gold nanoparticles.

	Incubation time (h)		
Cell cycle phase	**24**	**48**	**72**
Sub-G_1 (%)	0.68% ± 0.13	0.89% ± 0.10	0.46% ± 0.06
G_0/G_1 (%)	83.87% ± 0.98	84.72% ± 0.98	87.70% ± 0.85
S (%)	3.86% ± 0.80	2.33% ± 0.61	1.56% ± 0.36
G_2/M (%)	11.59% ± 1.06	12.07% ± 0.50	10.29% ± 1.13

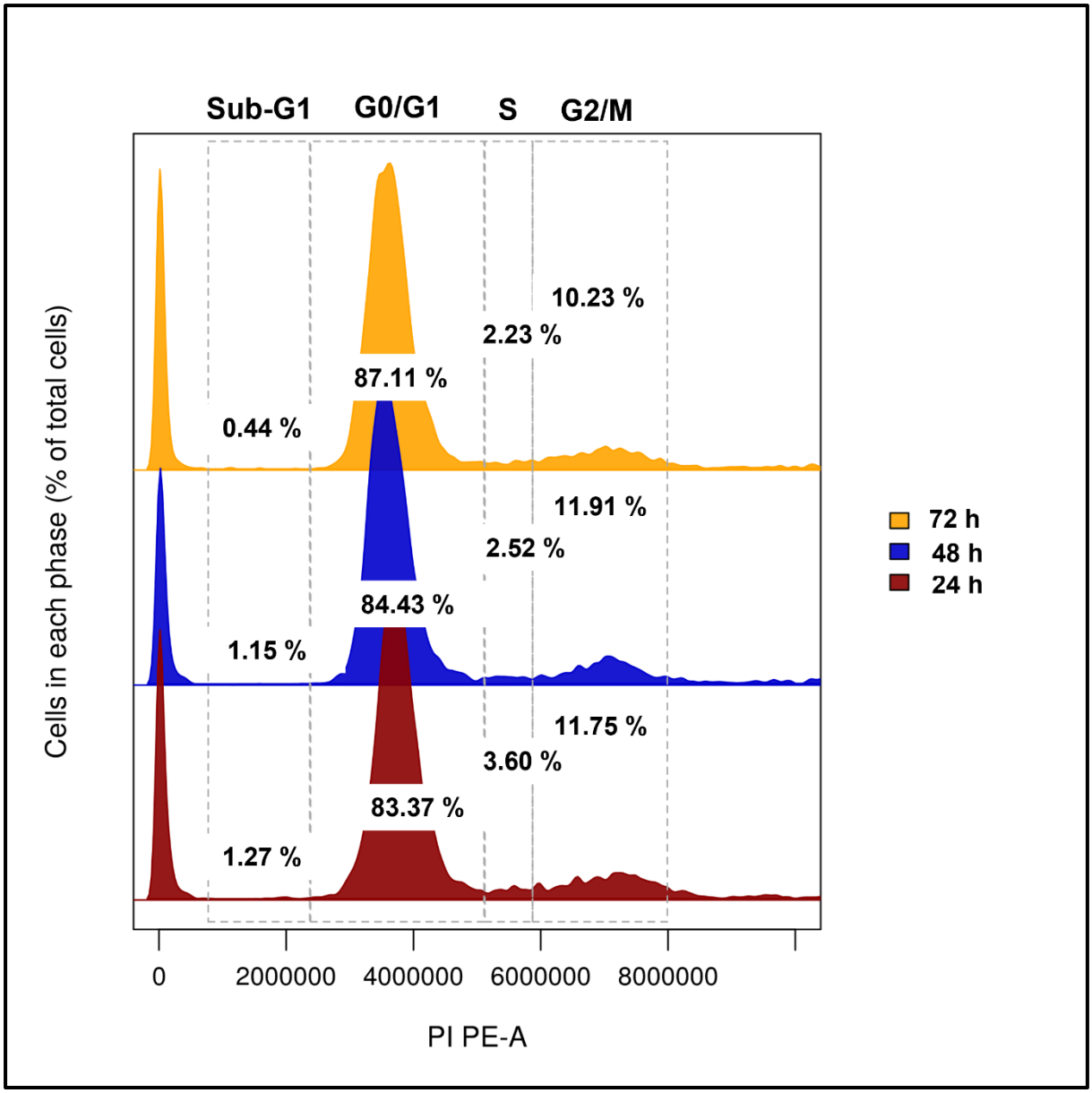

Figure 3.17: Cell cycle distribution of Day 7 A549 multicellular spheroids post-exposure to carboxyl-polyethylene glycol-liganded gold nanoparticles at 6 x 10^{11} NP/mL after 24 h (red), 48 h (blue) and 72 h (yellow).

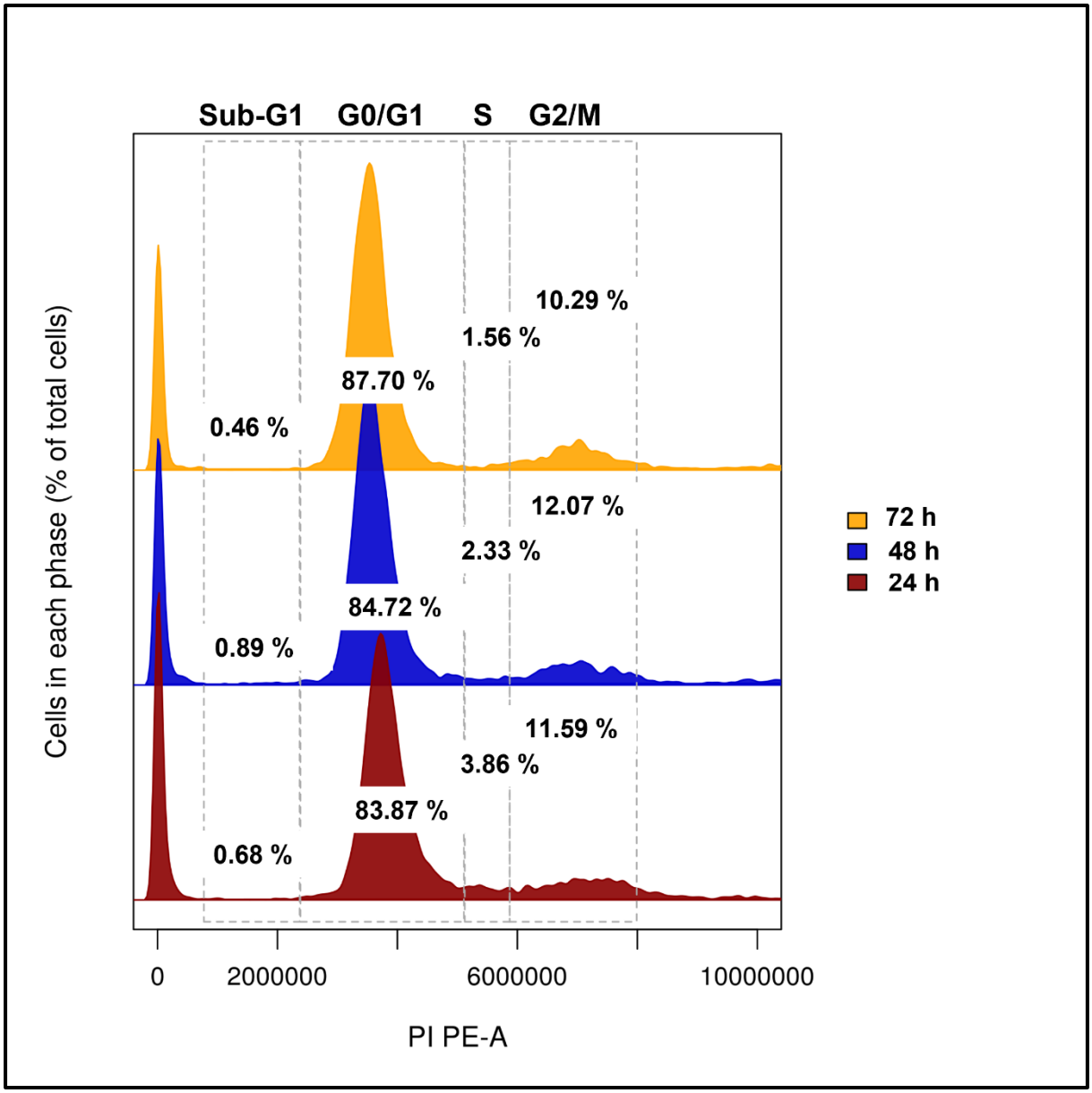

Figure 3.18: Cell cycle distribution of Day 7 A549 multicellular spheroids post-exposure to carboxyl-polyethylene glycol-liganded gold nanoparticles at 1.2 x 10^{12} NP/mL after 24 h (red), 48 h (blue) and 72 h (yellow).

3.5.4.3. Amine-liganded gold nanoparticles

In comparison to the negative control (**Figure 3.16** and **Table 3.2**), no statistically significant ($p > 0.05$) differences in the distribution of the cell cycle were observed after incubation with 2.3 x 10^{12} NP/L or 1.2 x 10^{12} NP/mL amine-AuNPs. The majority of cells (84.68%) were in the G_0/G_1-phase, with a low percentage cycling from G_2/M to S-phase over the 72 h exposure period (**Figure 3.19** and **Table 3.5**).

Table 3.5: Summary of cell cycle distribution of Day 7 A549 multicellular spheroids post-exposure to 2.3 x 10^{12} NP/mL amine-liganded gold nanoparticles.

	Incubation time (h)		
Cell cycle phase	**24**	**48**	**72**
Sub-G_1 (%)	1.67% ± 0.38	3.39% ± 0.45	2.71% ± 1.09
G_0/G_1 (%)	84.68% ± 1.03	84.0% ± 1.77	83.76% ± 2.02
S (%)	3.43% ± 1.55	2.53% ± 1.00	4.64% ± 2.73
G_2/M (%)	10.22% ± 1.40	10.08% ± 1.44	8.90% ± 0.78

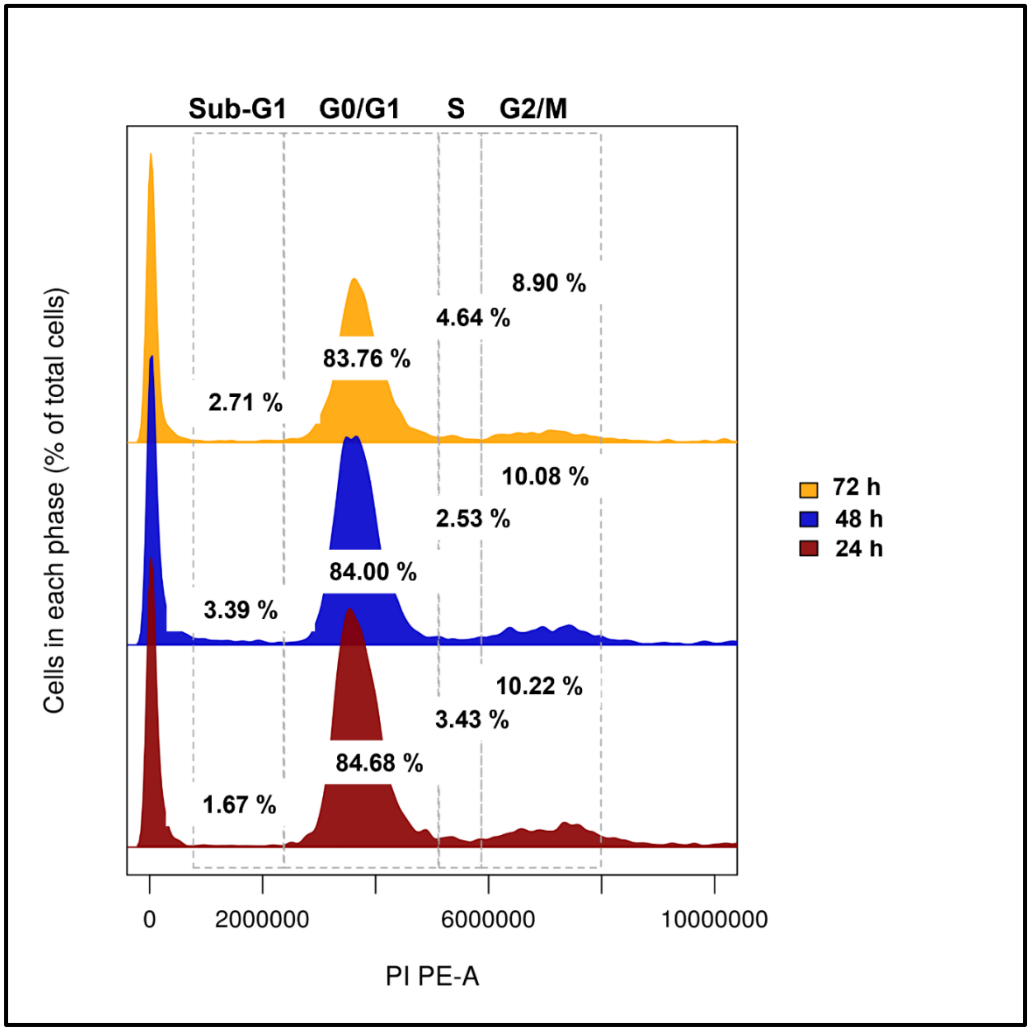

Figure 3.19: Cell cycle distribution of A549 multicellular spheroids post-exposure to amine-liganded gold nanoparticles at 2.3 x 10^{12} NP/mL after 24 h (red), 48 h (blue) and 72 h (yellow).

The 4.5 x 10^{12} NP/mL concentration of the amine-coated-AuNPs resulted in a time-dependent and significant increase ($p < 0.001$) of cells in the sub-G_1-phase, with a steady reduction in cells in the G_0/G_1 (significant; $p < 0.01$), S (non-significant, $p > 0.05$) and G_2/M-phases (only significant at the 72 h time point; $p < 0.01$) from 24 h onwards. As the amine-coated AuNPs did not exert this effect at a lower concentration, it appears that the effect may be dose-dependent (**Figure 3.20** and **Table 3.6**).

Table 3.6: Summary of cell cycle distribution of Day 7 A549 multicellular spheroids post-exposure to 4.5 x 10^{12} NP/mL amine-liganded gold nanoparticles.

	Incubation time (h)		
Cell cycle phase	**24**	**48**	**72**
Sub-G_1 (%)	12.68% ± 2.98	42.07% ± 8.69	78.0% ± 5.49
G_0/G_1 (%)	77.72% ± 2.42	52.66% ± 8.47	20.43% ± 5.10
S (%)	2.89% ± 0.54	2.28% ± 0.22	0.59% ± 0.34
G_2/M (%)	7.23% ± 1.28	2.99% ± 0.30	0.98% ± 0.52

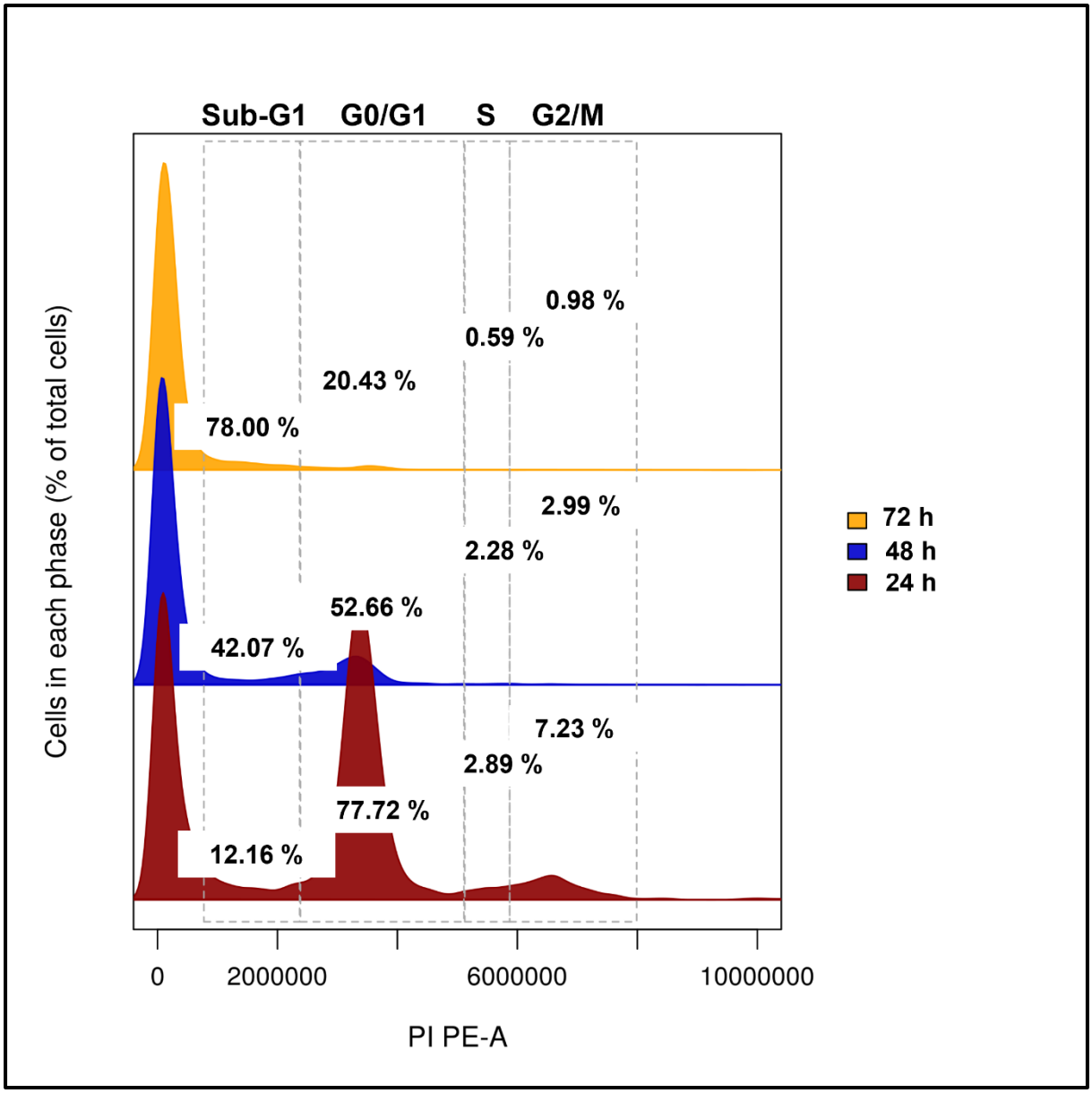

Figure 3.20: Cell cycle distribution of A549 multicellular spheroids post-exposure to amine-liganded gold nanoparticles at 4.5 x 10^{12} NP/mL after 24 h (red), 48 h (blue) and 72 h (yellow).

A summary of the effect of the AuNPs on the MCSs is provided in **Figure 3.21**. Overall, a significant effect was caused by the 4.5 x 10^{12} NP/mL amine-AuNPs on the proportion of cells in both the sub-G_1 and G_0/G_1-phases. At 24 h, the 4.5 x 10^{12} NP/mL amine-AuNPs caused a significant increase in sub-G_1 ($p < 0.001$) and decrease in G_0/G_1-phases ($p < 0.01$). At 48 h, the 4.5 x 10^{12} NP/mL amine-AuNPs caused a significant increase in sub-G_1 ($p < 0.001$) and decrease in G_0/G_1-phases ($p < 0.001$). Ratiometrically, the percentage of cells relative to the G_0/G_1 phase of each respective time point suggests that cells are not cycling into the S and G_2/M-phase, and thus the ratio of cells had increased in the G_0/G_1-phase, except at the 72 h time-point where the 4.5 x 10^{12} NP/mL amine-AuNPs produced the same effect with a significant increase in sub-G_1 phase ($p < 0.001$) and decrease in G_0/G_1-phase ($p < 0.001$), while at the same time causing a significant decrease in G_2/M-phase ($p < 0.01$).

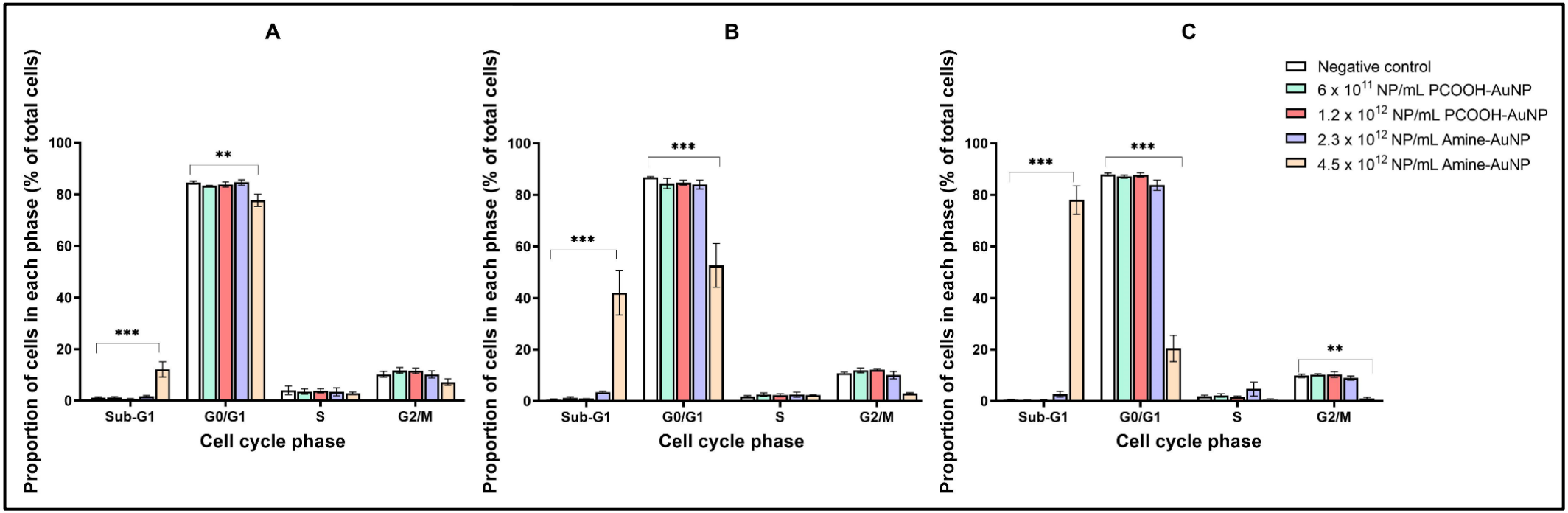

Figure 3.21: Effect of respective gold nanoparticle treatment groups on the distribution of cells within the cell cycle of Day 7 A549 multicellular spheroids after 24 h (A), 48 h (B) and 72 h (C). Significance indicated as **p ≤ 0.01; ***p ≤ 0.001.

3.5.5. Effect of gold nanoparticles on caspase-3/7 activation in A549 multicellular spheroids

The positive control resulted in a 0.14-fold increase ($p > 0.05$) in caspase-3/7 activity after 48 h (**Figures 3.22** and **3.23**). This may be indicative of the reduced susceptibility of the MCS to the control drug (100 µM cisplatin) since the chosen control is a known inducer of apoptosis in 2D cell cultures and an established control in the Departmental laboratory for the assay.

3.5.5.1. Carboxyl-polyethylene glycol-liganded gold nanoparticles

After 24 h, the caspase-3/7 activity was reduced, albeit non-significantly ($p > 0.05$) for both concentrations of PCOOH-AuNPs (**Figure 3.22**). From 48 h onwards, the caspase-3/7 activity returned to baseline for both concentrations of PCOOH-AuNPs (**Figure 3.22**). These results indicated that the PCOOH-AuNPs did not activate caspase-3/7 in A549 MCSs.

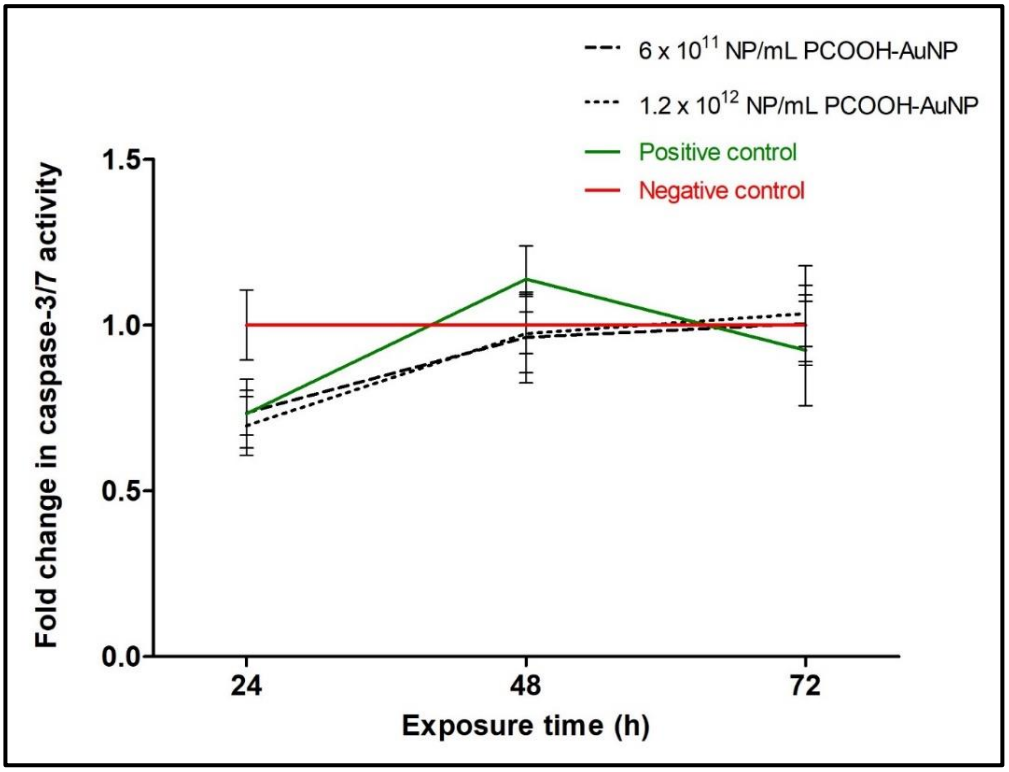

Figure 3.22: Fold-change in activation of caspase-3/7 in A549 multicellular spheroids, due to exposure to carboxyl-polyethylene glycol-liganded gold nanoparticles on Day 7 for 72-hours. The positive control (100 µM Cisplatin [indicated as a solid green line]) and the negative control (untreated multicellular spheroids [indicated as a solid red line]) were included for interpretation.

3.5.5.2. Amine-liganded gold nanoparticles

The lowest concentration (1.1 x 10^{12} NP/mL) of amine-AuNPs caused a non-significant ($p > 0.05$) decrease in caspase-3/7 activity over the first 48 h (**Figure 3.23**). The caspase-3/7 activity continued reducing over the exposure period with a significant reduction ($p < 0.05$) of 0.37-fold observed after 72 h (**Figure 3.23**).

The higher concentrations (2.3 x 10^{12} NP/mL and 4.5 x 10^{12} NP/mL) of amine-AuNPs caused a significant decrease ($p < 0.001$) in caspase-3/7 activity over the first 48 h (**Figure 32**). A further significant decrease ($p < 0.001$) of 0.82-fold in caspase-3/7 activity was observed with the 2.3 x 10^{12} NP/mL amine-AuNP treatment after 72 h (**Figure 32**). The 4.5 x 10^{12} NP/mL amine-AuNPs caused a significant increase ($p < 0.001$) of 0.13-fold in caspase-3/7 activity between 48 and 72 h (**Figure 3.23**).

The amine-AuNPs appeared to reduce the activity of caspase-3/7 at all concentrations over the 72 h period (**Figure 3.23**), suggesting that caspase-3/7 was not activated when the MCSs were exposed to the amine-AuNPs. The reduction in caspase-3/7 activity was more pronounced with an increase in the amine-AuNP concentration as well as with time of exposure, until approximately 48 h, suggesting a possible peak activation time or a dose- and time-dependent mechanism of action.

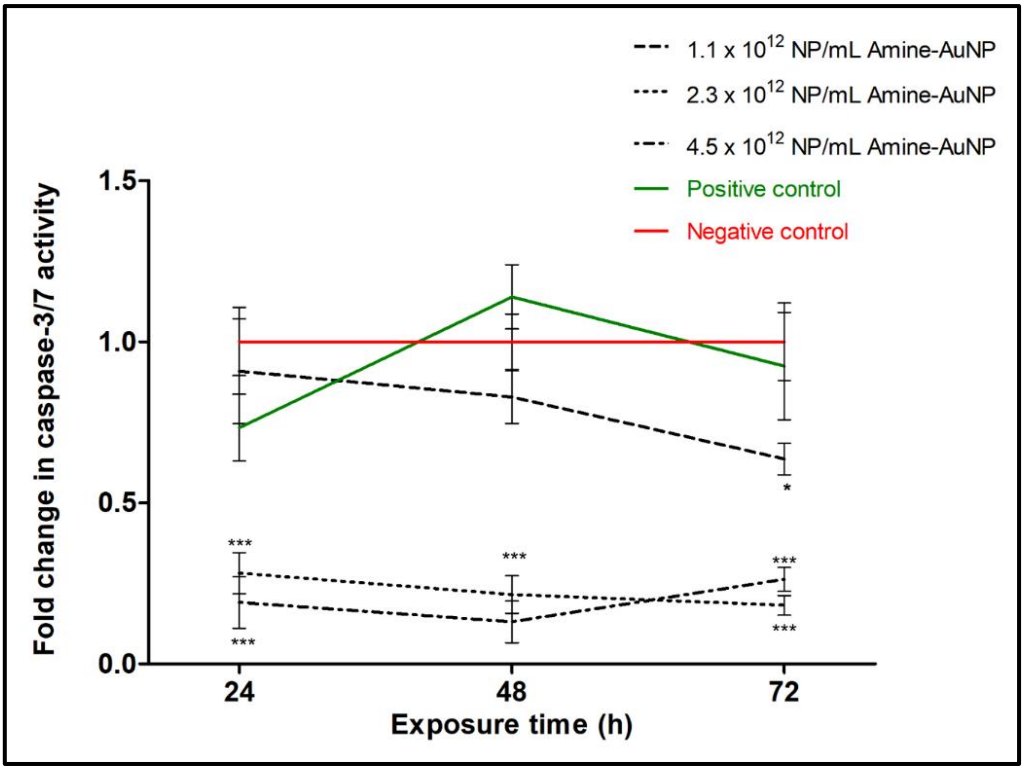

Figure 3.23: Fold-change in activation of caspase-3/7 in A549 multicellular spheroids, due to exposure to amine-liganded gold nanoparticles on Day 7 for 72 h. The positive control (100 µM cisplatin [indicated as a solid green line]) and the negative control (untreated multicellular spheroids [indicated as a solid red line]) were included for interpretation. Significance indicated as *p ≤ 0.05; ***p ≤ 0.001.

4. Chapter 4: Discussion

4.1. Establishing the optimal spheroid model

The cell line chosen for this study was the A549 alveolar carcinoma cell line due to its relevance in previous research conducted by the research group in pulmonary cells,[92] while showing evidence of successful 3D culturing.[93-94] Due to the global burden of lung cancer and heightened risk of occupational AuNP exposure in the South African mining sector, pulmonary cell lines need to be investigated.[101]

Initially, an established liquid overlay method, as described by Friedrich *et al*., was used to generate MCSs.[174] This method was successfully adapted for the uptake study of Fobian *et al.*[121] Liquid overlay is a scaffold-free MCS generation method where MCSs form by self-assembly. This method is more compatible with biological assays.[172] Although the classic liquid overlay method is scaffold-free and simple to use, the spheroids formed were often heterogenous in shape and size. In order to create a robust and reproducible model, homogenous MCSs are required for biological assays.[40] The classic method also proved to be time-consuming and not suitable for high-throughput MCS generation. A modified bulk generation liquid overlay method using polydimethylsiloxane moulds was employed to generate MCSs, whereby self-assembly occurs due to gravity in a low attachment environment.[172,192-193] This method proved more time-efficient and up to 81 homogenous MCSs could be formed per single agarose micro-mould. The latter enabled the establishment of a robust 3D model. The MCSs in the micro-moulds also endured less handling during the initial 24 h post-seeding, since the medium was added to the space surrounding the mould, rather than the space directly surrounding the MCS, as with the traditional method. The larger size of the wells containing the micro-moulds allowed more medium to be added per supplementation, thereby leading to the medium needing to be supplemented less often. This is known as a static cell culture system, where medium replenishment occurs in a batch-wise manner.[194] In the traditional method where the wells containing each individual MCS limits the amount of medium that can be replenished, more frequent medium supplementation is needed, introducing disturbances that could impact MCS growth and formation. Furthermore, the pores of

the agarose micro-mould are uniform in size and concavity, leading to the formation of less heterogenous MCSs. Contrary, when using agarose to coat each individual well of a 96-well plate (as was done in the classic method) more opportunity for variation in concavity of the plug existed, resulting in heterogenous MCSs.

Compact, robust MCSs were formed using the agarose micro-mould method, and growth was maintained for up to 21 days. The time-frames observed in this study are not uncommon for scaffold-free MCS generation. Prolonging the culture time that MCSs can be maintained for, would require the addition of specific growth factors,[195] or the use of complex microfluidic systems, specific to the chosen cell line,[196-197] or access to expensive equipment, including bioreactors, to maintain the MCSs.[198-199]

The cells self-assembled into stable MCSs, capable of being transferred after the fourth day of seeding. According to literature, the doubling time of the A549 cell line is 22 hours.[200] It would be expected that this time would increase for 3D cultures as the doubling time approximation is based on 2D cellular growth. It has been shown that the doubling time for cells in MCS are longer than that of cells in monolayer, and also that doubling time of cells in *in vivo* tumours is longer than in cultured cells.[201-202] Assembly of the MCS seems to take priority over cellular proliferation, especially in the initial stages of MCS formation.[202] The cells that make up MCSs are constantly migrating, attaching and detaching until the strongest bonds have been formed to strengthen the spheroid, which decreases the amount of energy (ATP) available in the cell for other functions, such as proliferation.[47] The Differential Adhesion Hypothesis (DAH) explains the phenomenon of adhesion exchange between cells to create the strongest bonds.[47,171] These inherent capabilities of 3D cell cultures require energy to be shifted away from unrestricted proliferation observed in 2D cultures, thus resulting in a decreased growth rate.[54]

In MCSs, the individual cells have more opportunity for cellular interaction and the formation of an ECM.[54] Formation of an ECM can act as a protective barrier by creating a micro-environment for the MCS that supports cellular survival.[203] The ECM is formed by varying expression of different cell-cell adhesion molecules, such as cadherins and integrins.[204] Cadherins are the main cellular adhesions believed to be involved in cellular binding. There are various types of cadherins, each type leads to cellular adhesion of different strengths. Cells exchange cadherins until the

strongest adhesions have been established.[47,171] Thus the increased doubling time observed could indicate that these cellular interactions and exchanges are taking precedent of cellular turnover, at least during the initial stages of MCS formation (Days 0 through 4).

The MCSs formed on the fourth day post-seeding had an average diameter of 538.71 µm, and an average volume of 2.18 x 10^8 μm^3. A MCS with a diameter > 500 µm generally shows a zonal differentiation that mimics that observed in *in vivo* tumours,[51] including the formation of gradients for nutrient absorption and waste expulsion.[54-55] The latter better reflects diffusion kinetics of tumours, leading to greater representation of *in vivo* tumours.[205] The rate of diffusion is highly influenced by spheroid circularity.[205] Circularity is a measure of how symmetric a MCS is. A value of 1 implies ideal symmetry, where the distance from the centre of the MCS to any point on the surface stays relatively constant.[205] Although circularity increased between Day 4 to Day 7, it remained the same until Day 14, and thereafter systematically decreased. Reduced circularity after Day 14 is suggestive of a gradual loss of integrity due to the inherent nature of scaffold-free formation.[54]

Fobian *et al*. reported that A549 MCSs grown using the classic liquid overlay method had an average diameter of 702 µm on Day 7,[121] while the diameter of MCS generated using the micro-mould method was 556.32 µm at the same time point. Theoretically, the size of MCSs would be expected to increase during formation due to growth kinetics,[206] however, the volume of Day 7 MCSs decreased. At the point when the necrotic core forms, the MCS will stop increasing in size, since the amount of actively proliferating cells start to decrease while the amount of quiescent cells start to increase, due to differential availability of oxygen, nutrients as well as waste expulsion capabilities.[206] Acid phosphatase activity increased by 31.93%, over this same time period which suggests that cells were growing and undergoing zonal differentiation.[54,206] A 30.00% increase in protein content was observed by Day 7, indicative thereof that the MCSs were growing. Given the reduced size, in conjunction with an increase in protein content, it appears that the MCSs were compacting over time. Cellular shrinkage is linked to MCS compaction.[207]

Compaction in MCSs is facilitated by cell-cell adhesion molecules, namely cadherins and integrins, which are known to be involved in ECM formation as discussed

above.[54,204] Compaction is an important phase of MCS formation as it correlates to tissue integrity.[208] Compaction in MCSs is a protective mechanism that can alter the level of exposure to extracellular elements, such as chemotherapeutic drugs.[203] It would appear as if the A549 MCSs were employing more than one protective action to evade chemotherapeutic destruction, namely compaction and ECM formation.

Cadherin expression has been linked to MCS compaction and cellular aggregation in cancerous cells.[203] It has been shown that MCS formation initially occurs due to the aggregation of cells, followed by compaction thereof. The time it takes for a MCS to reach the compaction phase varies between cell lines, as well as the compaction mechanism employed.[203,208] For example, in breast cancer cell lines, increased E-cadherin expression has been linked to MCS compaction,[209] while the levels of N-cadherin expression has been linked to compaction of MCSs from fibroblasts.[210] A study by Smyrek, *et al.* compared the phases of MCS formation over time of three cell lines.[208] It was found that HC11 cells reached the compaction phase at 18.5 h post-seeding, while 4T1 MCSs started compacting after 12 h post-seeding and T47D cells reached the compaction phase only after 29.5 h post-seeding.[208] The expression of the different adhesion molecules (e.g. cadherins and integrins) varies over the stages of MCS formation and specific molecules drive different phases of MCS formation.[208] Therefore, identifying which molecule is present at the highest level at a specific time point, might indicate what phase of formation the MCS is in.[208]

As this project was carried out in parallel to Fobian *et al*.[121] who assessed possible uptake mechanisms of AuNPs into A549 spheroids, it was important that the day of exposure was concurrent. Since the chosen exposure window lasted for 72 h, it was important to choose a time frame (in days) where the MCSs would remain relatively constant in terms of size and shape, while being the most representative of *in vivo* tumours as possible. Day 7 was chosen as the optimum day to start the exposure for biological assays as it still allowed for exposure within a timeframe where MCS remained stable in terms of the selected markers of assessment. Viability and growth assessment of the MCSs showed a decreased growth rate and reduced viability from Day 14 to Day 21. This is a common observation in 3D cell cultures, since the formation of the necrotic core reduces the overall amount of viable and actively proliferating cells.[54]

Although the micro-mould method enables less handling of the cultures compared to the classic liquid overlay, the method of medium replenishment still creates opportunity for contamination due to some handling still required.[194] To enable MCSs to be cultured for longer periods of time (beyond 21 days), perfusion methods are advantageous, since they continuously supply medium to ensure a stable culture environment and require no mechanical handling, reducing the possibility of contamination.[211-212]

4.2. Nanoparticle interference with assay substrates

The possibility of NPs interfering with biological assays is one of the major concerns when screening new NPs. Causes of interference can vary greatly and some examples include interference with light absorption, chemical reactions between the NPs and assay substrates, as well as dye adsorption to the NP surface.[213] Due to the high surface energy of NPs, it has been found that they are able to adsorb dyes to their surface, thereby distorting readings.[214] It has been found that the stability of some NPs are lower in culture medium than in water.[213] The DMEM used in this study contained the dye phenol red, which could be a possible explanation for some of the more significant changes in absorbance and fluorescence seen when the AuNPs were diluted in this medium. Culture medium contains various macromolecules that have also been observed to bind to NPs and create protein coronas around the NP, which affects the outcomes of biological assays.[213]

Serum may lower the interaction between cells and NPs as well as the NP uptake into cells, which can affect biological assays results.[215-216] Serum proteins adsorb onto the NP surface, which affects uptake into cells.[215] The DMEM used in the interference studies was not supplemented with FCS, Fobian *et al.* reported low penetration of PCOOH-AuNPs into the MCSs (4.5 µm), indicating the possibility of serum interference with AuNP uptake.[121] Although some significant interaction was observed for the APH assay, BCA assay, caspase-3/7 activation assay as well as some PI autofluorescence, these were measured with the assumption of full presence of AuNPs, which have been shown to be unlikely by Fobian *et al*.[121] Furthermore, washing of samples prior to assessment reduces the risk of interference by removal of AuNPs that have not been taken up by the spheroids. Although these will reduce the risk of interference, results will benefit from

comparative studies being assessed by label-free means, thus negating the effects of substrate or spectrometric influences.[116]

4.3. Cytotoxicity of gold nanoparticles

4.3.1. Morphological effects

The circularity index of MCSs was reduced significantly by amine-AuNPs. The amine-liganded AuNPs reduction thereof is indicative of cytotoxicity and a loss of integrity, which may be attributed to cell death processes such as apoptosis.[217] Although, cellular proliferation in the periphery may also reduce circularity due to newly formed cells' lacking dense compaction,[217] visual comparison clearly indicates loss of structural integrity, indicating cytotoxicity.

The PCOOH-AuNPs did not have a significant effect on MCS circularity, making them potentially attractive drug delivery vehicles, since circularity values closely correlate to diffusion within the MCS.[205] However, since Fobian *et al.*[121] found low penetration of these AuNPs in A549 MCSs, meaning they did not enter deeper cellular layers of the MCS, further analysis would be needed to ascertain the uptake potential in drug-delivery systems. The uptake mechanism of the amine-AuNPs are unknown, and this could explain the difference in cytotoxicity between the two types of AuNPs. The surface charge of NPs influences their behaviour and effects. It has been shown that surface charge influences opsonisation which affects plasma protein adsorption.[218] The PCOOH-AuNPs carried a slightly negative charge, while the amine-AuNPs carried a slightly positive charge. Cationic liposomes are known to have higher activation than neutral counterparts.[219] Harush-Frenkel *et al.* found positively charged NPs to internalise more rapidly.[124] The slightly cationic nature of the amine-AuNPs might explain the increased cytotoxicity observed, due to possible increased uptake compared to the PCOOH-AuNPs.

Volume is a reliable measurement for MCS viability, especially when used in conjunction with biological assays.[220] Increases in MCS volume were observed in all three treatment groups after 24 h. This may be indicative of a reduction in compaction of the spheroid and possible release of cellular connections, as well as expulsion of non-viable cells. An increase in the MCSs' volume has been linked to a surge in dead cells due to excessive amounts of debris being included in the

microscopic volume measurement,[220] which may be apparent here given the visual characteristics of the treated spheroids.

Microscopically, this excess debris expulsion and loss of cellular adhesion was evident for the amine-AuNP treatment group (**Appendix IV)**, but not for the PCOOH-AuNPs. From the PC images the effect of amine-AuNPs was found to be more similar to that of the cytotoxic (positive) control than the untreated (negative) control. The PCOOH-AuNPs did not cause significant debris formation, which is supported by Fobian *et al.* noted poor uptake of PCOOH-AuNPs after 24 h and penetration only into superficial layers of the MCS.[121]

The effect of the amine-AuNPs on MCS morphology increased after 48 h, suggesting further cell death, which may be a function of cell death mechanisms, such as apoptosis.[220] When apoptosis is initiated, cell shrinkage occurs and thus the overall volume of the MCS decreases.[220] Brüningk *et al.* found that reduced spheroid volume coincided with reduced viability in HCT116 cells.[221] In this study an increase in volume was observed. Due to the nature of the measurements conducted, using a macro for ImageJ, expelled debris were included as part of the overall volume measurement, which made the volume larger, especially for the amine-AuNP group. As seen in **Appendix IV** (positive control), when the MCS started to dissociate, they appeared larger and flatter. If debris and dead cells could be fully removed from the well before PC images were captured, the number of cells that aggregated would be very small. Since PC images were taken at 24 h intervals , this level of debris removal was not possible. Although washing may clear spheroids of debris, it was noted that too much washing disrupted the spheroid in its entirety, perturbing further analyses.

4.3.2. Viability

The interactions between cells and NPs have been shown to lead to denaturation of proteins.[222-223] Acid phosphatases are lysosomal enzymes that hydrolyse organic phosphates in acidic environments, are required for various cellular processes and are abundant in human cells.[224-226] Reduced acid phosphatase activity has been linked to cytotoxicity.[224-226] Both concentrations of the PCOOH-AuNPs did not cause significant changes in APH activity in the MCSs, indicating a lack of cytotoxicity. The viability results are supported by the lack of morphological changes, as well as by

the findings of Fobian *et al.* using the lactate dehydrogenase (LDH) assay, where it was observed that the PCOOH-AuNPs did not cause significant increases in the release of LDH over a 24 h exposure time at identical concentrations.[121] The poor penetration observed by Fobian *et al.* is the likely cause of the low cytotoxicity.[121] Vetten *et al.* also noted an absence of cytotoxicity with similar AuNPs in monolayer cultures of the BEAS-2B bronchial epithelial cell line.[92]

Apart from uptake considerations, the lack of cytotoxicity in the MCS could be due to the reduced chemo susceptibility of MCSs in relation to monolayer cultures.[25,43] *In vivo* tumours are often resistant to chemotherapy due to physical barriers preventing drug penetration into the tumour, which are mimicked in the MCS.[39] It has also been shown that PEGylated NPs show reduced cytotoxicity compared to non-PEGylated counterparts.[123] Since the PCOOH-AuNPs did not show innate cytotoxicity, they might have been an attractive target for chemotherapeutic drug delivery into the tumour. However, Fobian *et al.* found that since these AuNPs were taken up by the A549 MCSs primarily by clathrin-mediated endocytosis in the peripheral layer of the spheroid, they would likely be trafficked for lysosomal degradation.[121]

The amine-AuNPs caused a significant ($p \leq 0.001$) decrease in APH activity after 72 h exposure, suggesting time-dependent cytotoxicity. Studies on various types of NPs, e.g. comparing silver NPs to carbon nanotubules, as well as amine-coated polystyrene NPs, have found cytotoxicity to be time-dependent,[227-232] due to the uptake mechanism employed by the cell type, NP design and penetration, and activation of cytotoxic mechanisms.[227-228,231] It has been shown that amine-coating can assist in creating monodisperse NP solutions.[113] When using amines in the stabilisation of AuNPs, it has been found that the amines don't bind as strongly to gold as, e.g. thiols (which are also commonly used). This may be an advantage since the AuNP can then more easily detach from the amine molecule to perform its function.[113] As the amine-liganded AuNPs were considered cytotoxic at 4.5×10^{12} NP/mL, further mechanistic assessments as per **Sections 4.3.4** and **4.3.5** assessed lower concentrations to establish potential dose-dependency.

4.3.3. Protein content

The lower concentration PCOOH-AuNPs had a more prominent effect on protein content than the higher concentrations during the first 48 h. A decrease in total protein content could indicate protein degradation. Gold NPs have been known to interact with DNA, lipids and proteins in the cell, leading to various forms of cytotoxicity, including protein degradation.[233-234] The trend observed for PCOOH-AuNPs could indicate a possible dose-dependent effect. The size and viability were not reduced during the assay period, but the protein content decreased, indicating that the mechanism involved in reducing the amount of protein did not translate into visible reductions in viability. After 72 h, the protein content returned to baseline, this implies that if the reduction in protein content was due to the PCOOH-AuNPs, it would be reasonable to assume that the effect would not be sustained up to 72 h.

Aggregation is a known point of concern when working with small NPs, such as those in this study.[105-106] Since the PCOOH-AuNPs have been shown to be taken up in this model via clathrin-mediated endocytosis, albeit only within the peripheral layer of cells,[121] the higher concentration could possibly elicit the lysosomal degradation pathway faster due to more AuNPs being present in the cellular environment, or enable NP aggregation. Aggregates of AuNPs that were taken up by clathrin-mediated endocytosis were observed on lung fibroblasts, as well as agglomerates in lysosomes 72 h post-exposure.[127]

The amine-AuNPs did not have a significant effect on the protein content. Since the amine-AuNPs had a visible effect on morphology and viability, this finding was unexpected. Protein coronas have been known to form around NPs when they are exposed to biological fluids.[235] The synthetic medium used in cell culture closely resembles biological fluids due to the various additives. The proteins and other constituents in culture medium, interact with the NPs and form protein coronas.[235] Protein coronas can influence cellular uptake, targeting efficiency and distribution of NPs.[236-238] Covering the NP surface in PEG has been known to reduce protein deposition,[223,239] which could explain why there was a more significant initial decrease observed in protein content for the PCOOH-AuNPs, compared to the amine-AuNPs (which were not coated in PEG). The effect on protein content might also be explained by the cell cycle distribution discussed in **Section 4.3.4**, where an

increase in the number of cells in the sub-G_1 phase was observed. Gold NPs have been associated with increased expression of cleaved caspase proteins and concurrent accumulations of cells in the sub-G_1 phase.[240] Although no increase in caspase-3/7 expression was observed as discussed in **Section 4.3.5**, not all caspases were investigated.

4.3.4. Cell cycle distribution

The inherent cell cycle distribution of the MCSs confirmed the proposed zonal differentiation due to the high proportion of cells in the G_0/G_1 phase, indicating possible quiescent cells. Propidium iodide binds to DNA and staining with PI does not differentiate between the G_0 and G_1 phases.[241] The gating of the cells is only possible to differentiate based on the ploidy of the cells, with cells that have similar ploidy being undifferentiable.[241] Cells in both the G_1 and G_0-phases are diploid, while cells in G_2 and M-phases have 4n ploidy, meaning that these cells would essentially be twice as fluorescently intense than cells in G_0/G_1.[241]

G_0 is considered an exit point of the cell cycle, and thus relates to quiescence, while G_1 is the start of the cell cycle.[59] The PCOOH-AuNPs did not have any significant effect on the cell cycle distribution within the MCSs, confirming their lack of cytotoxicity observed in other biological assays. This again relates to the poor uptake and penetration of these PCOOH-AuNPs noted by Fobian *et al.*[121] The absence of an effect on the cell cycle distribution seems to support the notion that the changes in protein content due to the PCOOH-AuNPs are not indicative of cytotoxic effects.

The amine-AuNPs displayed dose-dependency on the cell cycle of the MCSs, where only the highest concentration tested yielded a perturbation of the cycle. This effect was also observed to increase as exposure time increased, leading to a possible time-dependent response. This may be related to the gradual inhibition of cell cycle checkpoint-factors.[147] Interestingly, the proportion of cells in sub-G_1 phase increased after exposure to the amine-AuNPs at high concentration, which indicates possible DNA fragmentation. DNA fragmentation has been reported as the mechanism of cytotoxicity of other AuNPs, either supporting apoptosis,[242] or as a hallmark of necrosis.[243] An increased proportion of cells in the sub-G_1 phase has been linked to DNA damage, protein degradation and cytotoxicity caused by AuNPs.[240] The effect on the cell cycle strengthens the outcomes from the viability and morphological

studies, where the amine-AuNPs, at high concentration, have a cytotoxic effect, although the exact mechanism is unknown.

4.3.5. Caspase-3/7 activity

Caspases are proteolytic enzymes involved in many cellular processes, most notably apoptosis and inflammation.[158] Apoptosis is a complex cell death mechanism and can be activated via various processes. Several caspases have been identified since their discovery, and they have been given unique numbers in order to differentiate them from one another. Mammalian caspases-2, -3, -7, -8, -9 and -10 are involved in apoptosis.[158] The caspase-dependent pathway is the classic apoptotic pathway in both extrinsic and intrinsic apoptosis and involves a cascade of caspase activation involving various caspase enzymes, including caspases-3, 7, 8, 9, and 12.[161] Initially, caspases are inactive pro-forms, but upon activation, caspases activate each other in a sequential approach by cleaving at the same sequences.[156] The different caspases act as either initiator caspases, or executioner caspases. Initiator caspases can initiate other caspases that then execute apoptosis, with caspase-3 being considered the most important. Any of the initiator caspases can activate caspase-3, eventually leading to apoptosis.[244] Caspase-3/7 expression is used as one possible indicator that apoptosis is being induced in a cell (however, it is not the only pathway apoptosis can follow).[161]

Although apoptotic cell death has been described for AuNPs,[245-247] the PCOOH-AuNPs did not significantly alter caspase-3/7 activity, which suggests a lack of pro-apoptotic effects. This is further corroborated by the lack of cytotoxicity described earlier, as well as the poor uptake and cellular penetration and absence of cytotoxicity described by Fobian *et al.*[121]

The amine-AuNPs caused significant ($p \leq 0.001$) decreases in caspase-3/7 activation at the two higher concentrations (2.3×10^{12} and 4.5×10^{12} NP/mL), suggesting an inhibition of caspase-dependent pathways, and thus ultimately a different cytotoxic mechanism. One possibility might be that cell death is being induced via a caspase-independent pathway.[159-160] The caspase-independent pathway of intrinsic apoptosis does not require the activation of caspase enzymes to induce apoptosis.[159-160] This pathway is activated when ligand binding causes a change in the membrane potential of the mitochondria.[161] This, in turn, increases the

cells ROS production which is the signal for apoptosis to occur.[161] Lui *et al.* found that AuNPs (13 nm in size) were able to induce cell death by various mechanisms, including caspase-independent mechanisms.[248] Different apoptotic mechanisms have been observed to be employed concurrently.[248] The amine-AuNPs also caused a shift in the distribution of cells resulting in a greater proportion of the cells in the sub-G_1 phase, especially at high concentrations. Gold NPs have been linked to the production of ROS and an increased expression of cleaved caspase proteins, accompanied by a high constituent of cells in the sub-G_1 phase.[240] It is known that a wide array of caspases are involved, depending on which apoptotic pathway is activated.[161] The increase in the amount of cells in the sub-G_1 phase may be indicative of a caspase-dependent pathway of apoptosis being activated, and not only the caspase-3/7 pathway based on the results observed in **Section 3.5.5**.

There were visible reductions in viability when the MCSs were exposed to amine-AuNPs, which were noted both morphologically, as well as by the changes in cell cycle distribution. However, these reductions did not seem to be linked to increased caspase-3/7 expression. Since MCSs are cultured to have contact with other cells and form an ECM, the MCS may benefit from protection from anoikis.[249] Anoikis is a specific type of programmed cell death that occurs upon loss of attachment to the ECM.[250] Resistance to anoikis is one of the emerging hallmarks of cancer and enables metastasis.[251] Loss of cellular contact and contact to the ECM (which was seen upon exposure to high concentrations of the amine-AuNPs, causing breakdown of the MCS [**Appendix IV**]), could have induced anoikis and subsequently apoptosis.[251]

Autophagy is an alternative method of cell death mediated through lysosomal activity.[153] Most often, autophagy is not the cause of cell death, but is rather associated with it.[162] Autophagy is often used by cells as a pro-survival response to stress. Therefore, if a cell is in a fatally stressful environment, autophagic processes may be stimulated in an attempt to improve cell survival.[252] It has been shown that AuNPs, quantum dots and carbon nanotubules can cause autophagy.[253] Human lung fibroblasts have been reported to employ autophagy as a cellular defence mechanism when exposed to AuNPs.[254]

Necrosis is a passive mechanism of cell death, typically characterised by adenosine triphosphate (ATP) depletion or membrane disruption in damaged or diseased cells, deters cell survival.[155,255] Necrosis is not associated with normal cellular development and is thus deemed pathological in nature.[155] Necrosis has characteristic morphological features including; vacuolation of the cytoplasm and breakdown of the plasma membrane. This leads to pro-inflammatory molecules and cell contents being released into the cytoplasm. The availability of these molecules in the cytoplasm induces inflammation which can be observed around the cell undergoing necrosis.[255]

Necrosis can be triggered by various factors, including DNA damage.[156] DNA fragmentation was possibly occurring in the MCSs as a result of exposure to high concentrations of amine-AuNPs (**Section 4.3.4**). Necrosis and apoptosis can be difficult to discern morphologically; often both may occur simultaneously, depending on the level of ATP depletion and the presence of caspase enzymes.[165] A cell that is actively undergoing apoptosis can be pushed into necrosis if there is an excessive decrease in the availability of caspases and ATP.[166] The examples in literature of NPs inducing necrosis is inconsistent due to the difficulty of morphological identification of necrosis.[156] Necrosis has been reported to be induced in hamster ovary cells by water-soluble germanium NPs with allylamine-conjugated surfaces.[256] Chen *et al.* found the death mechanism employed by HepG2 cells to be necrosis, rather than apoptosis after treatment with zinc oxide NPs.[257] Different NPs have been found to induce cell death in distinct cell lines via disparate mechanisms.[165-166,252,256,258]

5. Chapter 5: Conclusion, limitations and recommendations

The MCS model for A549 cells was successfully established and optimised via a high-throughput micro-mould system. The MCSs formed and started compacting by Day 4 and were able to be sustained until Day 21. The MCSs remained stable over the exposure period, and thus show potential for use in cytotoxicity determination. Assay selections were appropriate for the AuNPs used; however, further work should be done to optimise assays to ensure the full effect of interference is taken into consideration, or label-free means incorporated.

The PCOOH-AuNPs did not have any significant cytotoxic effect on A549 MCSs. Although this finding appears to make them attractive targets for drug delivery vehicles, their uptake and cellular penetration is too low.

Amine-AuNPs at high concentrations did significantly affect viability and growth measurements, indicating possible cytotoxicity. High concentrations of amine-AuNPs caused a shift in cell cycle distribution leading to an increase in the number of cells in the sub-G_1 phase. The latter may be indicative of apoptosis, however low levels of caspase-3/7 expression were observed, indicating either the involvement of different caspases or the caspase-independent pathway being activated.

The effects of amine-AuNP exposure creates potential for future studies to establish whether the A549 MCS would employ a different uptake mechanism, compared to the findings on the PCOOH-AuNPs. There is also potential to elucidate whether lower concentrations would show the same time-dependent trend in cytotoxic effects as was seen for high concentrations of amine-AuNPs. It would be beneficial to screen lower concentrations of the amine-AuNPs since for certain measurements only the highest concentration was screened. This would enable better applications for the amine-AuNPs, whether that be as direct cytotoxic agents or as drug delivery vehicles.

Studies to confirm MCS stability might strengthen the model for cytotoxicity screening. To further elucidate the extent and mechanism of DNA damage observed as a result of exposure to amine-AuNPs, studies such as the comet assay and gel electrophoresis can be performed to characterise the DNA damage. Oxidative stress

analysis could assist in elucidating the mechanism of action employed by amine-AuNPs to cause DNA damage. To elucidate the mechanism of cell death employed due to exposure to amine-AuNPs, an ATP/ADP ratiometry assay is suggested to determine the level of ATP depletion. Lower levels of ATP would indicate necrosis, whereas higher levels would lean towards apoptosis. Investigating the expression of specific caspases, e.g., initiator caspases (-2, -8, -9 and -10) may possibly elucidate the cell death mechanism employed.

Limitations of the study included a lack of standardisation of AuNP concentrations, especially during the morphological and viability investigations. Another limitation was not investigating the uptake mechanism or level of cellular uptake and penetration of amine-AuNPs into A549 MCSs. Another limitation was not characterising any proteins, e.g., as ECM proteins to relate it to MCS dysregulation. Characterising the proteins could be an interesting prospective future study to strengthen some of the theories in this study. Nanoparticle interference was also a limitation to the study. Some interference was noted, but given the experimental conditions the full impact of this interference could not be established, since it was impossible to ensure whether AuNPs would remain in the sample during washing steps. The low uptake of PCOOH-AuNPs (reported by Fobian *et al.*[113]) implies that the interference potential is low, however, label-free methods would be best suited for the investigations.

6. Chapter 6: References

1. Parvathaneni V, Kulkarni NS, Muth A, Gupta V. Drug repurposing: A promising tool to accelerate the drug discovery process. Drug Discovery Today. 2019; 24(10):2076-85.
2. DiMasi JA, Feldman L, Seckler A, Wilson A. Trends in risks associated with new drug development: Success rates for investigational drugs. Clinical Pharmacology and Therapeutics. 2010; 87(3):272-7.
3. Kola I. The state of innovation in drug development. Clinical Pharmacology and Therapeutics. 2008; 83(2):227-30.
4. Hay M, Thomas DW, Craighead JL, Economides C, Rosenthal J. Clinical development success rates for investigational drugs. Nature Biotechnology. 2014; 32(1):40-51.
5. Cohen FJ. Macro trends in pharmaceutical innovation. Nature Reviews Drug discovery. 2005; 4(1):78-84.
6. Takebe T, Imai R, Ono S. The current status of drug discovery and development as originated in United States academia: The influence of industrial and academic collaboration on drug discovery and development. Clinical and Translational Science. 2018; 11(6):597-606.
7. Turner MJ. The current state of drug discovery and what it might take to improve drug discovery outcomes and approval successes. Drug Discovery Today. 2015; 20(8):917-9.
8. DiMasi JA, Grabowski HG, Hansen RW. Innovation in the pharmaceutical industry: New estimates of R&D costs. Journal of Health Economics. 2016; 47:20-33.
9. Hopkins AL. Network pharmacology: The next paradigm in drug discovery. Nature Chemical Biology. 2008; 4(11):682-90.
10. Kola I, Landis J. Can the pharmaceutical industry reduce attrition rates? Nature Reviews Drug discovery. 2004; 3(8):711-5.
11. Hutchinson L, Kirk R. High drug attrition rates - where are we going wrong? Nature Reviews Clinical Oncology. 2011; 8(4):189-90.
12. Ocana A, Pandiella A, Siu LL, Tannock IF. Preclinical development of molecular-targeted agents for cancer. Nature Reviews Clinical Oncology. 2011; 8(4):200-9.
13. Cook D, Brown D, Alexander R, March R, Morgan P, Satterthwaite G, et al. Lessons learned from the fate of Astrazeneca's drug pipeline: A five-dimensional framework. Nature Reviews Drug Discovery. 2014; 13(6):419-31.
14. Breslin S, O'Driscoll L. Three-dimensional cell culture: The missing link in drug discovery. Drug Discovery Today. 2013; 18(5-6):240-9.
15. Imamura Y, Mukohara T, Shimono Y, Funakoshi Y, Chayahara N, Toyoda M, et al. Comparison of 2D- and 3D-culture models as drug-testing platforms in breast cancer. Oncology Reports. 2015; 33(4):1837-43.

16. Singh VK, Seed TM. How necessary are animal models for modern drug discovery? Expert Opinion on Drug Discovery. 2021; 16(12):1391-7.

17. Richmond A, Su Y. Mouse xenograft models vs GEM models for human cancer therapeutics. Disease Models & Mechanisms. 2008; 1(2-3):78-82.

18. Preskorn SH. The role of proof of concept (POC) studies in drug development using the EVP-6124 POC study as an example. Journal of Psychiatric Practice. 2014; 20(1):59-60.

19. Marx U, Sandig V. Drug testing in vitro: Breakthroughs and trends in cell culture technology. Weinheim: Wiley-VCH; 2007.

20. Antoni D, Burckel H, Josset E, Noel G. Three-dimensional cell culture: A breakthrough *in vivo*. International Journal of Molecular Sciences. 2015; 16(3):5517-27.

21. Zschenker O, Streichert T, Hehlgans S, Cordes N. Genome-wide gene expression analysis in cancer cells reveals 3D growth to affect ECM and processes associated with cell adhesion but not DNA repair. PLOS ONE. 2012; 7(4):e34279.

22. Szakács G, Gottesman MM. Comparing solid tumors with cell lines: Implications for identifying drug resistance genes in cancer. Molecular Interventions. 2004; 4(6):323-5.

23. Jensen C, Teng Y. Is it time to start transitioning from 2D to 3D cell culture? Frontiers in molecular biosciences. 2020; 7:33.

24. Kapałczyńska M, Kolenda T, Przybyła W, Zajączkowska M, Teresiak A, Filas V, et al. 2D and 3D cell cultures - a comparison of different types of cancer cell cultures. Archives of medical science : AMS. 2018; 14(4):910-9.

25. Dufau I, Frongia Cl, Sicard F, Dedieu L, Cordelier P, Ausseil FDR, et al. Multicellular tumor spheroid model to evaluate spatio-temporal dynamics effect of chemotherapeutics: Application to the gemcitabine/CHK1 inhibitor combination in pancreatic cancer. BMC Cancer. 2012; 12(1).

26. Edmondson R, Broglie JJ, Adcock AF, Yang L. Three-dimensional cell culture systems and their applications in drug discovery and cell-based biosensors. Assay and drug development technologies. 2014; 12(4):207-18.

27. Santini MT, Rainaldi G. Three-dimensional spheroid model in tumor biology. Pathobiology. 1999; 67(3):148-57.

28. Girigoswami K, Saini D, Girigoswami A. Extracellular matrix remodeling and development of cancer. Stem Cell Reviews and Reports. 2021; 17(3):739-47.

29. Lu P, Weaver VM, Werb Z. The extracellular matrix: A dynamic niche in cancer progression. The Journal of Cell Biology. 2012; 196(4):395-406.

30. Cox TR, Erler JT. Remodeling and homeostasis of the extracellular matrix: Implications for fibrotic diseases and cancer. Disease Models & Mechanisms. 2011; 4(2):165-78.

31. Abedin M, King N. Diverse evolutionary paths to cell adhesion. Trends in Cell Biology. 2010; 20(12):734-42.

32. Setargew Y, Wyllie K, Grant R, Chitty J, Cox T. Targeting lysyl oxidase family meditated matrix cross-linking as an anti-stromal therapy in solid tumours. Cancers. 2021; 13:491.

33. Sethi T, Rintoul RC, Moore SM, MacKinnon AC, Salter D, Choo C, et al. Extracellular matrix proteins protect small cell lung cancer cells against apoptosis: A mechanism for small cell lung cancer growth and drug resistance *in vivo*. Nature Medicine. 1999; 5(6):662-8.

34. Xian X, Gopal S, Couchman JR. Syndecans as receptors and organizers of the extracellular matrix. Cell and Tissue Research. 2010; 339(1):31-46.

35. Leitinger B, Hohenester E. Mammalian collagen receptors. Matrix Biology. 2007; 26(3):146-55.

36. Goldberga I, Li R, Duer MJ. Collagen structure-function relationships from solid-state NMR spectroscopy. Accounts of Chemical Research. 2018; 51(7):1621-9.

37. Erler JT, Weaver VM. Three-dimensional context regulation of metastasis. Clinical & Experimental Metastasis: Official Journal of the Metastasis Research Society. 2009; 26(1):35-49.

38. Pickup MW, Mouw JK, Weaver VM. The extracellular matrix modulates the hallmarks of cancer. BlackWell Publishing Ltd; 2014.

39. Antunes J, Gaspar VM, Ferreira L, Monteiro M, Henrique R, Jerónimo C, et al. In-air production of 3D co-culture tumor spheroid hydrogels for expedited drug screening. Acta Biomaterialia. 2019.

40. Achilli T-M, Meyer J, Morgan JR. Advances in the formation, use and understanding of multi-cellular spheroids. Expert Opinion on Biological Therapy. 2012; 12(10):1347-60.

41. Pampaloni F, Reynaud EG, Stelzer EH. The third dimension bridges the gap between cell culture and live tissue. Nature Reviews Molecular Cell Biology. 2007; 8(10):839-45.

42. Laurent J, Frongia C, Cazales M, Mondesert O, Ducommun B, Lobjois V. Multicellular tumor spheroid models to explore cell cycle checkpoints in 3D. BMC Cancer. 2013; 13:73.

43. Loessner D, Stok KS, Lutolf MP, Hutmacher DW, Clements JA, Rizzi SC. Bioengineered 3D platform to explore cell-ECM interactions and drug resistance of epithelial ovarian cancer cells. Biomaterials. 2010; 31(32):8494-506.

44. Karlsson H, Fryknäs M, Larsson R, Nygren P. Loss of cancer drug activity in colon cancer HCT-116 cells during spheroid formation in a new 3-D spheroid cell culture system. Experimental Cell Research. 2012; 318(13):1577-85.

45. Tibbitt MW, Anseth KS. Hydrogels as extracellular matrix mimics for 3D cell culture. Biotechnology and Bioengineering. 2009; 103(4):655-63.

46. Cooke MJ, Phillips SR, Shah DSH, Athey D, Lakey JH, Przyborski SA. Enhanced cell attachment using a novel cell culture surface presenting functional domains from extracellular matrix proteins. Cytotechnology. 2008; 56(2):71-9.

47. Foty RA, Steinberg MS. The differential adhesion hypothesis: A direct evaluation. Developmental Biology. 2005; 278(1):255-63.

48. Lee JM, Mhawech-Fauceglia P, Lee N, Parsanian LC, Lin YG, Gayther SA, et al. A three-dimensional microenvironment alters protein expression and chemosensitivity of epithelial ovarian cancer cells *in vitro*. Laboratory Investigation; A Journal of Technical Methods and Pathology. 2013; 93(5):528-42.

49. Griffith LG, Swartz MA. Capturing complex 3D tissue physiology *in vitro*. Nature reviews. Molecular Cell Biology. 2006; 7(3):211-24.

50. Kim JB. Three-dimensional tissue culture models in cancer biology. Seminars in Cancer Biology. 2005; 15(5):365-77.

51. Khaitan D, Chandna S, Arya MB, Dwarakanath BS. Establishment and characterization of multicellular spheroids from a human glioma cell line; implications for tumor therapy. Journal of Translational Medicine. 2006; 4:12.

52. Sant S, Johnston PA. The production of 3D tumor spheroids for cancer drug discovery. Drug Discovery Today. Technologies. 2017; 23:27-36.

53. Vinci M, Gowan S, Boxall F, Patterson L, Zimmermann M, Court W, et al. Advances in establishment and analysis of three-dimensional tumor spheroid-based functional assays for target validation and drug evaluation. BMC Biology. 2012; 10(1):1-21.

54. Zanoni M, Piccinini F, Arienti C, Zamagni A, Santi S, Polico R, et al. 3D tumor spheroid models for in vitro therapeutic screening: A systematic approach to enhance the biological relevance of data obtained. Scientific Reports. 2016; 6(1).

55. Nath S, Devi GR. Three-dimensional culture systems in cancer research: Focus on tumor spheroid model. Pharmacology and Therapeutics. 2016; 163:94-108.

56. Mueller-Klieser W, Freyer JP, Sutherland RM. Influence of glucose and oxygen supply conditions on the oxygenation of multicellular spheroids. British Journal of Cancer. 1986; 53(3):345-53.

57. Lazzari G, Couvreur P, Mura S. Multicellular tumor spheroids: A relevant 3D model for the in vitro preclinical investigation of polymer nanomedicines. Polymer Chemistry. 2017; 8(34):4947-69.

58. Reynaud-Bougnoux A, Lespinasse F, Malaise EP, Guichard M. Partial hypoxia as a cause of radioresistance in a human tumor xenograft: Its influence illustrated by the sensitizing effect of misonidazole and hyperbaric oxygen. International Journal of Radiation Oncology, Biology, Physics. 1986; 12(8):1283-6.

59. Katzman SDB, Alessandra L; Higgings, Rebecca; Talley, Jennell; Hurst-Kennedy, Jennifer. Fundementals of cell biology. Athens, Georgia: University System of Georgia; 2020.

60. Morin PJ. Drug resistance and the microenvironment: Nature and nurture. Drug Resistance Updates. 2003; 6(4):169-72.

61. Hodkinson PS, Mackinnon AC, Sethi T. Extracellular matrix regulation of drug resistance in small-cell lung cancer. International Journal of Radiation Biology. 2007; 83(11-12):733-41.

62. Williams GH, Stoeber K. The cell cycle and cancer. The Journal of Pathology. 2012; 226(2):352-64.

63. Gottesman MM. Mechanisms of cancer drug resistance. Annual Review of Medicine. 2002; 53:615-27.

64. Ghosh P, Han G, De M, Kim CK, Rotello VM. Gold nanoparticles in delivery applications. Advanced Drug Delivery Reviews. 2008; 60(11):1307-15.

65. Royal Societies. Nanoscience and nanotechnologies: Opportunities and uncertainties: Summary and recomendations: Royal Society; 2004.

66. Singh R, Lillard JW, Jr. Nanoparticle-based targeted drug delivery. Experimental and Molecular Pathology. 2009; 86(3):215-23.

67. De Jong WH, Borm PJA. Drug delivery and nanoparticles: Applications and hazards. International Journal of Nanomedicine. 2008; 3(2):133-49.

68. Conde J, Doria G, Baptista P. Noble metal nanoparticles applications in cancer. Journal of Drug Delivery. 2012; 2012:1-12.

69. Friedman AD, Claypool SE, Liu R. The smart targeting of nanoparticles. Current Pharmaceutical Design. 2013; 19(35):6315-29.

70. Vu MN, Kelly HG, Kent SJ, Wheatley AK. Current and future nanoparticle vaccines for COVID-19. eBioMedicine. 2021; 74:103699.

71. Perrie Y, Crofts F, Devitt A, Griffiths HR, Kastner E, Nadella V. Designing liposomal adjuvants for the next generation of vaccines. Advanced Drug Delivery Reviews. 2016; 99:85-96.

72. Schwenk MH. Ferumoxytol: A new intravenous iron preparation for the treatment of iron deficiency anemia in patients with chronic kidney disease. Pharmacotherapy. 2010; 30(1):70-9.

73. Abo-Zeid Y, Ismail NSM, McLean GR, Hamdy NM. A molecular docking study repurposes FDA approved iron oxide nanoparticles to treat and control COVID-19 infection. European journal of pharmaceutical sciences: official journal of the European Federation for Pharmaceutical Sciences. 2020; 153:105465.

74. Sperling RA, Rivera Gil P, Zhang F, Zanella M, Parak WJ. Biological applications of gold nanoparticles. Chemical Society Reviews. 2008; 37(9):1896-908.

75. Varshosaz J, Farzan M. Nanoparticles for targeted delivery of therapeutics and small interfering RNAs in hepatocellular carcinoma. World Journal of Gastroenterology. 2015; 21(42):12022-41.

76. Lim Z-ZJ, Li J-EJ, Ng C-T, Yung L-YL, Bay B-H. Gold nanoparticles in cancer therapy. Acta Pharmacologica Sinica. 2011; 32(8):983-90.

77. Liu R, Kay BK, Jiang S, Chen S. Nanoparticle delivery: Targeting and nonspecific binding. MRS Bulletin. 2009; 34(6):432-40.

78. Hermanson GT. Bioconjugate techniques. San Diego: Academic Press; 1996.

79. Ds A, Mj S. Nanotechnology: The risks and benefits for medical diagnosis and treatment. Journal of Nanomedicine & Nanotechnology. 2016; 7(4).

80. Akbarzadeh A, Rezaei-Sadabady R, Davaran S, Joo SW, Zarghami N, Hanifehpour Y, et al. Liposome: Classification, preparation, and applications. Nanoscale Research Letters. 2013; 8(1):1-9.

81. Kelly C, Jefferies C, Cryan S. Targeted liposomal drug delivery to monocytes and macrophages. Journal of Drug Delivery2010.

82. Pattni BS, Chupin VV, Torchilin VP. New developments in liposomal drug delivery. Chemical Reviews. 2015; 115(19):10938-66.

83. Barenholz Y. Doxil® — the first FDA-approved nano-drug: Lessons learned. Journal of Controlled Release. 2012; 160(2):117-34.

84. LaVan DA, McGuire T, Langer R. Small-scale systems for *in vivo* drug delivery. Nature Biotechnology. 2003; 21(10):1184-91.

85. Chen X, Wong STC. Cancer theranostics: An introduction: Elsevier Inc.; 2014.

86. Perry JL, Herlihy KP, Napier ME, Desimone JM. Print: A novel platform toward shape and size specific nanoparticle theranostics. Accounts of Chemical Research. 2011; 44(10):990-8.

87. Saha K, Agasti SS, Kim C, Li X, Rotello VM. Gold nanoparticles in chemical and biological sensing. Chemical Reviews. 2012; 112(5):2739-79.

88. Daniel MC, Astruc D. Gold nanoparticles: Assembly, supramolecular chemistry, quantum-size-related properties, and applications toward biology, catalysis, and nanotechnology. Chemical reviews. 2004; 104(1):293.

89. Edwards PP, Thomas JM. Gold in a metallic divided state - from Faraday to present-day nanoscience. Angewandte Chemie International Edition. 2007; 46(29):5480-6.

90. Das M, Shim KH, An SSA, Yi DK. Review on gold nanoparticles and their applications. Toxicology and Environmental Health Sciences. 2011; 3(4):193-205.

91. Torrisi L. Gold nanoparticles enhancing protontherapy efficiency. Recent patents on nanotechnology. 2015; 9(1):51-60.

92. Vetten M, Gulumian M. Differences in uptake of 14 nm peg-liganded gold nanoparticles into beas-2b cells is dependent on their functional groups. Toxicology and Applied Pharmacology. 2019; 363:131-41.

93. Yan X, Luo H, Zhou X, Zhu B, Wang Y, Bian X. Identification of CD90 as a marker for lung cancer stem cells in A549 and H446 cell lines. Oncology Reports. 2013; 30(6):2733-40.

94. Sun F-F, Hu Y-H, Xiong L-P, Tu X-Y, Zhao J-H, Chen S-S, et al. Enhanced expression of stem cell markers and drug resistance in sphere-forming non-small cell lung cancer cells. International Journal of Clinical and Experimental Pathology. 2015; 8(6):6287-300.

95. Barta JA, Powell CA, Wisnivesky JP. Global epidemiology of lung cancer. Annals of global health. 2019; 85(1).

96. Miller KD, Nogueira L, Devasia T, Mariotto AB, Yabroff KR, Jemal A, et al. Cancer treatment and survivorship statistics, 2022. CA: A Cancer Journal for Clinicians. 2022; 72(5):409-36.

97. Siegel RL, Miller KD, Jemal A. Cancer statistics, 2019. CA: A Cancer Journal for Clinicians. 2019; 69(1):7-34.

98. Cathcart-Rake EJ, Sangaralingham LR, Henk HJ, Shah ND, Riaz IB, Mansfield AS. A population-based study of immunotherapy-related toxicities in lung cancer. Clinical Lung Cancer. 2020; 21(5):421-7.e2.

99. Suresh K, Voong KR, Shankar B, Forde PM, Ettinger DS, Marrone KA, et al. Pneumonitis in non–small cell lung cancer patients receiving immune checkpoint immunotherapy: Incidence and risk factors. Journal of Thoracic Oncology. 2018; 13(12):1930-9.

100. Lansdown ABG. Gold: Human exposure and update on toxic risks. Critical Reviews in Toxicology. 2018; 48(7):596-614.

101. Gulumian M, Verbeek J, Andraos C, Sanabria N, de Jager P, Xu BE. Systematic review of screening and surveillance programs to protect workers from nanomaterials. PLOS ONE2016.

102. Rizvi SAA, Saleh AM. Applications of nanoparticle systems in drug delivery technology. Saudi Pharmaceutical Journal: SPJ: the Official Publication of the Saudi Pharmaceutical Society. 2018; 26(1):64-70.

103. Buzea C, Pacheco II, Robbie K. Nanomaterials and nanoparticles: Sources and toxicity. Biointerphases2007. p. MR17-MR71.

104. Prokop A, Davidson JM. Nanovehicular intracellular delivery systems. Journal of Pharmaceutical Sciences. 2008; 97(9):3518-90.

105. Li D, Kaner RB. Shape and aggregation control of nanoparticles: Not shaken, not stirred. Journal of the American Chemical Society. 2006; 128(3):968-75.

106. Hotze EM, Phenrat T, Lowry GV. Nanoparticle aggregation: Challenges to understanding transport and reactivity in the environment. Journal of Environmental Quality. 2010; 39(6):1909-24.

107. Bantz C, Koshkina O, Lang T, Galla HJ, Kirkpatrick CJ, Stauber RH, et al. The surface properties of nanoparticles determine the agglomeration state and the size of the particles under physiological conditions. Beilstein Journal of Nanotechnology. 2014; 5:1774-86.

108. Kou L, Sun J, Zhai Y, He Z. The endocytosis and intracellular fate of nanomedicines: Implication for rational design. Asian Journal of Pharmaceutical Sciences. 2013; 8(1):1-10.

109. Araujo L, Löbenberg R, Kreuter J. Influence of the surfactant concentration on the body distribution of nanoparticles. Journal of Drug Targeting. 1999; 6(5):373-85.

110. Labhasetwar V, Song C, Humphrey W, Shebuski R, Levy RJ. Arterial uptake of biodegradable nanoparticles: Effect of surface modifications. Journal of Pharmaceutical Sciences. 1998; 87(10):1229-34.

111. Angra PK, Rizvi SAA, Oettinger CW, D'Souza MJ. Novel approach for preparing nontoxic stealth microspheres for drug delivery. European Journal of Chemistry. 2011; 2(2):125-9.

112. Li S-D, Huang L. Stealth nanoparticles: High density but sheddable PEG is a key for tumor targeting. Journal of Controlled Release. 2010; 145(3):178-81.

113. Rak MJ, Saade NK, Friscic T, Moores A. Mechanosynthesis of ultra-small monodisperse amine-stabilized gold nanoparticles with controllable size. Green Chemistry. 2014; 16(1):86-9.

114. Ramirez E, Jansat S, Philippot K, Lecante P, Gomez M, Masdeu-Bultó AM, et al. Influence of organic ligands on the stabilization of palladium nanoparticles. Journal of Organometallic Chemistry. 2004; 689(24):4601-10.

115. Ong KJ, MacCormack TJ, Clark RJ, Ede JD, Ortega VA, Felix LC, et al. Widespread nanoparticle-assay interference: Implications for nanotoxicity testing. PloS One. 2014.

116. Sanabria NM, Vetten M, Andraos C, Boodhia K, Gulumian M, Antopolsky ME. Gold nanoparticle interference study during the isolation, quantification, purity and integrity analysis of RNA. PloS One. 2014.

117. Stone V, Johnston H, Schins RPF. Development of *in vitro* systems for nanotoxicology: Methodological considerations. Critical Reviews in Toxicology. 2009; 39(7):613-26.

118. Douglas KL, Tabrizian M, Piccirillo CA. Cell line-dependent internalization pathways and intracellular trafficking determine transfection efficiency of nanoparticle vectors. European Journal of Pharmaceutics and Biopharmaceutics. 2008; 68(3):676-87.

119. Shang L, Nienhaus G, Nienhaus K. Engineered nanoparticles interacting with cells: Size matters. Journal of Nanobiotechnology. 2014. p. 1-11.

120. Dagmar AK, Dimitri V, Benjamin M, Fabian B, Peter G, Alke P-F, et al. Different endocytotic uptake mechanisms for nanoparticles in epithelial cells and macrophages. Beilstein Journal of Nanotechnology. 2014. p. 1625-36.

121. Fobian S-F, Petzer M, Vetten M, Steenkamp V, Gulumian M, Cordier W. Mechanisms facilitating the uptake of carboxyl–polythene glycol-functionalized gold nanoparticles into multicellular spheroids. Journal of Pharmacy and Pharmacology. 2022:rgac017.

122. Iversen T-G, Skotland T, Sandvig K. Endocytosis and intracellular transport of nanoparticles: Present knowledge and need for future studies. Nano Today. 2011; 6(2):176-85.

123. Thiruppathi R, Mishra S, Ganapathy M, Padmanabhan P, Gulyás B. Nanoparticle functionalization and its potentials for molecular imaging. Advanced Science. 2017; 4(3):1600279.

124. Harush-Frenkel O, Debotton N, Benita S, Altschuler Y. Targeting of nanoparticles to the clathrin-mediated endocytic pathway. Biochemical and Biophysical Research Communications. 2007; 353(1):26-32.

125. Albanese A, Chan WC. Effect of gold nanoparticle aggregation on cell uptake and toxicity. ACS Nano. 2011; 5(7):5478-89.

126. Chithrani BD, Chan WC. Elucidating the mechanism of cellular uptake and removal of protein-coated gold nanoparticles of different sizes and shapes. Nano Letters. 2007; 7(6):1542-50.

127. Ng CT, Tang FM, Li JJ, Ong C, Yung LL, Bay BH. Clathrin-mediated endocytosis of gold nanoparticles *in vitro*. Anatomical Record. 2015; 298(2):418-27.

128. Hao X, Wu J, Shan Y, Cai M, Shang X, Jiang J, et al. Caveolae-mediated endocytosis of biocompatible gold nanoparticles in living hela cells. Journal of Physics: Condensed Matter. 2012; 24(16):164207.

129. Mironava T, Hadjiargyrou M, Simon M, Jurukovski V, Rafailovich MH. Gold nanoparticles cellular toxicity and recovery: Effect of size, concentration and exposure time. Nanotoxicology. 2010; 4(1):120-37.

130. Goodman CM, McCusker CD, Yilmaz T, Rotello VM. Toxicity of gold nanoparticles functionalized with cationic and anionic side chains. Bioconjugate Chemistry. 2004; 15(4):897-900.

131. Montes-Fonseca SL, Orrantia-Borunda E, Aguilar-Elguezabal A, González Horta C, Talamás-Rohana P, Sánchez-Ramírez B. Cytotoxicity of functionalized carbon nanotubes in J774A macrophages. Nanomedicine: Nanotechnology, Biology and Medicine. 2012; 8(6):853-9.

132. Savolainen K, Alenius H, Norppa H, Pylkkänen L, Tuomi T, Kasper G. Risk assessment of engineered nanomaterials and nanotechnologies - a review. Toxicology. 2010; 269(2):92-104.

133. Vetten MA, Tlotleng N, Tanner Rascher D, Skepu A, Keter FK, Boodhia K, et al. Label-free *in vitro* toxicity and uptake assessment of citrate stabilised gold nanoparticles in three cell lines. Particle and Fibre Toxicology. 2013; 10(1):50.

134. Shvedova AA, Castranova V, Kisin ER, Schwegler-Berry D, Murray AR, Gandelsman VZ, et al. Exposure to carbon nanotube material: Assessment of nanotube cytotoxicity using human keratinocyte cells. Journal of Toxicology and Environmental Health. Part A. 2003; 66(20):1909-26.

135. Brown DM, Donaldson K, Borm PJ, Schins RP, Dehnhardt M, Gilmour P, et al. Calcium and ROS-mediated activation of transcription factors and TNF-alpha cytokine gene expression in macrophages exposed to ultrafine particles. American Journal of Physiology. Lung Cellular and Molecular Physiology. 2004; 286(2):344-53.

136. Dai L, Liu Y, Wang Z, Guo F, Shi D, Zhang B. One-pot facile synthesis of PEGylated superparamagnetic iron oxide nanoparticles for MRI contrast enhancement. Materials Science and Engineering: C. 2014; 41:161-7.

137. Tasso M, Singh MK, Giovanelli E, Fragola A, Loriette V, Regairaz M, et al. Oriented bioconjugation of unmodified antibodies to quantum dots capped with copolymeric ligands as versatile cellular imaging tools. ACS Applied Materials & Interfaces. 2015; 7(48):26904-13.

138. Powell AC, Paciotti GF, Libutti SK. Colloidal gold: A novel nanoparticle for targeted cancer therapeutics. Cancer nanotechnology: Humana Press: Totowa, NJ. 2010. p. 375-84.

139. Chithrani BD, Ghazani AA, Chan WC. Determining the size and shape dependence of gold nanoparticle uptake into mammalian cells. Nano Letters. 2006; 6(4):662-8.

140. Connor EE, Mwamuka J, Gole A, Murphy CJ, Wyatt MD. Gold nanoparticles are taken up by human cells but do not cause acute cytotoxicity. Small. 2005; 1(3):325-7.

141. Patra HKM, Banerjee SM, Chaudhuri UMD, Lahiri PP, Dasgupta AKP. Cell selective response to gold nanoparticles. Nanomedicine: Nanotechnology, Biology, and Medicine. 2007; 3(2):111-9.

142. Pan Y, Leifert A, Ruau D, Neuss S, Bornemann J, Schmid G, et al. Gold nanoparticles of diameter 1.4 nm trigger necrosis by oxidative stress and mitochondrial damage. Small. 2009; 5(18):2067-76.

143. Schafer KA. The cell cycle: A review. Veterinary Pathology. 1998; 35(6):461-78.

144. Johnson DG, Walker CL. Cyclins and cell cycle checkpoints. Annual Review of Pharmacology and Toxicology. 1999; 39:295-312.

145. Kung AL, Zetterberg A, Sherwood SW, Schimke RT. Cytotoxic effects of cell cycle phase specific agents: Result of cell cycle perturbation. Cancer Research. 1990; 50(22):7307-17.

146. Liu L, Michowski W, Kolodziejczyk A, Sicinski P. The cell cycle in stem cell proliferation, pluripotency and differentiation. Nature Cell Biology. 2019; 21(9):1060-7.

147. Panagopoulos A, Altmeyer M. The hammer and the dance of cell cycle control. Trends in Biochemical Sciences. 2021; 46(4):301-14.

148. Oki T, Nishimura K, Kitaura J, Togami K, Maehara A, Izawa K, et al. A novel cell-cycle-indicator, mVenus-p27k−, identifies quiescent cells and visualizes G_0–G_1 transition. Scientific Reports. 2014; 4(1):4012.

149. Beaumont KA, Anfosso A, Ahmed F, Weninger W, Haass NK. Imaging- and flow cytometry-based analysis of cell position and the cell cycle in 3D melanoma spheroids. Journal of visualized experiments: JoVE. 2015; (106):e53486-e.

150. Olofsson K, Carannante V, Takai M, Önfelt B, Wiklund M. Single cell organization and cell cycle characterization of DNA stained multicellular tumor spheroids. Scientific Reports. 2021; 11(1):17076.

151. Malumbres M, Barbacid M. Cell cycle, CDKs and cancer: A changing paradigm. Nature reviews. Cancer. 2009; 9(3):153-66.

152. Collins K, Jacks T, Pavletich NP. The cell cycle and cancer. Proceedings of the National Academy of Sciences of the United States of America. 1997; 94(7):2776-8.

153. Edinger AL, Thompson CB. Death by design: Apoptosis, necrosis and autophagy. Current Opinion in Cell Biology. 2004; 16(6):663-9.

154. Mizushima N. Autophagy in protein and organelle turnover. Cold Spring Harbor Symposia on Quantitative Biology. 2011; 76(0):397-402.

155. Fawthrop DJ, Boobis AR, Davies DS. Mechanisms of cell death. Archives of Toxicology. 1991; 65(6):437-44.

156. Fulda S, Debatin KM. Extrinsic versus intrinsic apoptosis pathways in anticancer chemotherapy. Oncogene. 2006; 25(34):4798-811.

157. Elmore S. Apoptosis: A review of programmed cell death. Toxicologic Pathology. 2007; 35(4):495-516.

158. Shalini S, Dorstyn L, Dawar S, Kumar S. Old, new and emerging functions of caspases. Cell Death and Differentiation. 2015; 22(4):526-39.

159. Kumar S. Caspase function in programmed cell death. Cell Death and Differentiation. 2007; 14(1):32-43.

160. De Stefano D, Carnuccio R, Maiuri MC. Nanomaterials toxicity and cell death modalities. Journal of Drug Delivery. 2012; 2012:167896-.

161. Hongmei Z. Extrinsic and intrinsic apoptosis signal pathway review. Apoptosis and medicine: InTech; 2012.

162. Tait SWG, Ichim G, Green DR. Die another way – non-apoptotic mechanisms of cell death. Journal of Cell Science. 2014; 127(10):2135.

163. Green DR, Kroemer G. The pathophysiology of mitochondrial cell death. Science. 2004; 305(5684):626-9.

164. Bissell MJ, Rizki A, Mian IS, Lawrence Berkeley National Lab BCA. Tissue architecture: The ultimate regulator of breast epithelial function. Current Opinion in Cell Biology. 2005; 15.

165. Ahamed M, Akhtar MJ, Siddiqui MA, Ahmad J, Musarrat J, Al-Khedhairy AA, et al. Oxidative stress mediated apoptosis induced by nickel ferrite nanoparticles in cultured A549 cells. Toxicology. 2011; 283(2-3):101-8.

166. Yoo KC, Yoon CH, Kwon D, Hyun KH, Woo SJ, Kim RK, et al. Titanium dioxide induces apoptotic cell death through reactive oxygen species-mediated FAS upregulation and BAX activation. International Journal of Nanomedicine. 2012; 7:1203-14.

167. Frens G. Controlled nucleation for the regulation of the particle size in monodisperse gold suspensions. Nature Physical Science. 1973; 241(105):20-2.

168. Turkevich J, Stevenson PC, Hillier J. A study of the nucleation and growth processes in the synthesis of colloidal gold. Discussions of the Faraday Society. 1951; 11:55-75.

169. Tomita K, Ishioka T, Harata A. Development of an anion probe: Detection of sulfate ion by two-photon fluorescence of gold nanoparticles. Analytical sciences: the International Journal of the Japan Society for Analytical Chemistry. 2012; 28(12):1139-44.

170. Karaman O, Yaralı Z. Determination of minimum serum concentration to develop scaffold free micro-tissue. The European Research Journal. 2017.

171. Duguay D, Foty RA, Steinberg MS. Cadherin-mediated cell adhesion and tissue segregation: Qualitative and quantitative determinants. Developmental Biology. 2003; 253(2):309-23.

172. Kelm JM, Fussenegger M. Microscale tissue engineering using gravity-enforced cell assembly. Trends in Biotechnology. 2004; 22(4):195-202.

173. Anderer U, Libera J. In vitro engineering of human autogenous cartilage. Journal of Bone and Mineral Research. 2002; 17(8):1420-9.

174. Friedrich J, Seidel C, Ebner R, Kunz-Schughart LA. Spheroid-based drug screen: Considerations and practical approach. Nature Protocols. 2009; 4(3):309-24.

175. De Moor L, Merovci I, Baetens S, Verstraeten J, Kowalska P, Krysko DV, et al. High-throughput fabrication of vascularized spheroids for bioprinting. Biofabrication. 2018; 10(3):035009.

176. Gevaert E, Dollé L, Billiet T, Dubruel P, van Grunsven L, van Apeldoorn AA, et al. High throughput micro-well generation of hepatocyte micro-aggregates for tissue engineering. PloS One. 2014; 9(8).

177. Richards OW. Phase microscopy 1954-56. Science. 1956; 124(3226):810-4.

178. Zernike F. How i discovered phase contrast. Science. 1955; 121(3141):345-9.

179. Ayers GD, McKinley ET, Zhao P, Fritz JM, Metry RE, Deal BC, et al. Volume of preclinical xenograft tumors is more accurately assessed by ultrasound imaging than manual caliper measurements. Journal of Ultrasound in Medicine. 2010; 29(6):891-901.

180. Schindelin J, Arganda-Carreras I, Frise E, Kaynig V, Longair M, Pietzsch T, et al. Fiji: An open-source platform for biological-image analysis. Nature methods. 2012; 9(7):676-82.

181. Yang TT, Sinai P, Kain SR. An acid phosphatase assay for quantifying the growth of adherent and nonadherent cells. Analytical Biochemistry. 1996; 241(1):103-8.

182. Smith PK, Krohn RI, Hermanson GT, Mallia AK, Gartner FH, Provenzano MD, et al. Measurement of protein using bicinchoninic acid. Analytical Biochemistry. 1985; 150(1):76-85.

183. Han X, Gelein R, Corson N, Wade-Mercer P, Jiang J, Biswas P, et al. Validation of an LDH assay for assessing nanoparticle toxicity. Toxicology. 2011; 287(1-3):99-104.

184. Holder AL, Goth-Goldstein R, Lucas D, Koshland CP. Particle-induced artifacts in the MTT and LDH viability assays. Chemical Research in Toxicology. 2012; 25(9):1885-92.

185. Mayilo S, Kloster MA, Wunderlich M, Lutich A, Klar TA, Nichtl A, et al. Long-range fluorescence quenching by gold nanoparticles in a sandwich immunoassay for cardiac troponin t. Nano Letters. 2009; 9(12):4558-63.

186. Nunez R. DNA measurement and cell cycle analysis by flow cytometry. Current Issues in Molecular Biology. 2001; 3(3):67-70.

187. Molinari M. Cell cycle checkpoints and their inactivation in human cancer. Cell Proliferation. 2000; 33(5):261-74.

188. Cordier W. *In vitro* hepatotoxicity and herb-drug interactions of selected african plant extracts. Pretoria: University of Pretoria; 2016.

189. Grässer U, Bubel M, Sossong D, Oberringer M, Pohlemann T, Metzger W. Dissociation of mono- and co-culture spheroids into single cells for subsequent flow cytometric analysis. Annals of anatomy = Anatomischer Anzeiger: official organ of the Anatomische Gesellschaft. 2018; 216:1-8.

190. van Tonder J. Development of an in vitro mechanistic toxicity screening model using cultured hepatocytes: University of Pretoria; 2011.

191. Biologics C [Internet] BCA and Bradford protein assays. 2018.

192. Napolitano AP, Chai P, Dean DM, Morgan JR. Dynamics of the self-assembly of complex cellular aggregates on micromolded nonadhesive hydrogels. Tissue Engineering. 2007; 13(8):2087-94.

193. Ferreira LP, Gaspar VM, Mano JF. Bioinstructive microparticles for self-assembly of mesenchymal stem cell-3D tumor spheroids. Biomaterials. 2018; 185:155-73.

194. Wu M-H, Huang S-B, Lee G-B. Microfluidic cell culture systems for drug research. Lab on a Chip. 2010; 10(8):939-56.

195. Tong JZ, De Lagausie P, Furlan V, Cresteil T, Bernard O, Alvarez F. Long-term culture of adult rat hepatocyte spheroids. Experimental Cell Research. 1992; 200(2):326-32.

196. Zuchowska A, Kwapiszewska K, Chudy M, Dybko A, Brzozka Z. Studies of anticancer drug cytotoxicity based on long-term HepG2 spheroid culture in a microfluidic system. Electrophoresis. 2017; 38(8):1206-16.

197. Ziółkowska K, Kwapiszewski R, Stelmachowska A, Chudy M, Dybko A, Brzózka Z. Development of a three-dimensional microfluidic system for long-term tumor spheroid culture. Sensors and Actuators B: Chemical. 2012; 173:908-13.

198. Tostões RM, Leite SB, Serra M, Jensen J, Björquist P, Carrondo MJT, et al. Human liver cell spheroids in extended perfusion bioreactor culture for repeated-dose drug testing. Hepatology. 2012; 55(4):1227-36.

199. Ahmed HMM, Salerno S, Piscioneri A, Khakpour S, Giorno L, De Bartolo L. Human liver microtissue spheroids in hollow fiber membrane bioreactor. Colloids and Surfaces B: Biointerfaces. 2017; 160:272-80.

200. [Internet] A549 cell line: Cell cuture and transfection protocol. 2022. Available from: https://www.a549.com/cell-subculture-protocol/.

201. Risinger AL, Dybdal-Hargreaves NF, Mooberry SL. Breast cancer cell lines exhibit differential sensitivities to microtubule-targeting drugs independent of doubling time. Anticancer Research. 2015; 35(11):5845-50.

202. Freyer JP. Role of necrosis in regulating the growth saturation of multicellular spheroids. Cancer Research. 1988; 48(9):2432-9.

203. Shield K, Ackland ML, Ahmed N, Rice GE. Multicellular spheroids in ovarian cancer metastases: Biology and pathology. Gynecologic Oncology. 2009; 113(1):143-8.

204. Waleh NS, Gallo J, Grant TD, Murphy BJ, Kramer RH, Sutherland RM. Selective down-regulation of integrin receptors in spheroids of squamous cell carcinoma1. Cancer Research. 1994; 54(3):838-43.

205. Leung BM, Lesher-Perez SC, Matsuoka T, Moraes C, Takayama S. Media additives to promote spheroid circularity and compactness in hanging drop platform. Biomaterials science. 2015; 3(2):336-44.

206. Lu H, Stenzel MH. Multicellular tumor spheroids (mcts) as a 3D *in vitro* evaluation tool of nanoparticles. Small. 2018; 14(13):1702858.

207. Lin R-Z, Chou L-F, Chien C-CM, Chang H-Y. Dynamic analysis of hepatoma spheroid formation: Roles of e-cadherin and β1-integrin. Cell and Tissue Research. 2006; 324(3):411-22.

208. Smyrek I, Mathew B, Fischer SC, Lissek SM, Becker S, Stelzer EHK. E-cadherin, actin, microtubules and FAK dominate different spheroid formation phases and important elements of tissue integrity. Biology Open. 2019; 8(1):bio037051.

209. Ivascu A, Kubbies M. Diversity of cell-mediated adhesions in breast cancer spheroids. International Journal of Oncology. 2007; 31(6):1403-13.

210. Kim YJ, Sauer C, Testa K, Wahl JK, Svoboda RA, Johnson KR, et al. Modulating the strength of cadherin adhesion: Evidence for a novel adhesion complex. Journal of Cell Science. 2005; 118(Pt 17):3883-94.

211. Wu MH, Urban JPG, Cui Z, Cui ZF. Development of PDMS microbioreactor with well-defined and homogenous culture environment for chondrocyte 3D culture. Biomedical Microdevices. 2006; 8(4):331-40.

212. Sittinger M, Schultz O, Keyszer G, Minuth WW, Burmester GR. Artificial tissues in perfusion culture. The International Journal of Artificial Organs. 1997; 20(1):57-62.

213. Costa C, Brandão F, Bessa MJ, Costa S, Valdiglesias V, Kiliç G, et al. *In vitro* cytotoxicity of superparamagnetic iron oxide nanoparticles on neuronal and glial cells. Evaluation of nanoparticle interference with viability tests. Journal of Applied Toxicology. 2016; 36(3):361-72.

214. Kroll A, Pillukat MH, Hahn D, Schnekenburger Jr. Interference of engineered nanoparticles with *in vitro* toxicity assays. Archives of Toxicology. 2012; 86(7):1123-36.

215. Geys J, Nemery B, Hoet PHM. Assay conditions can influence the outcome of cytotoxicity tests of nanomaterials: Better assay characterization is needed to compare studies. Toxicology in Vitro. 2010; 24(2):620-9.

216. Fröhlich E. Cellular targets and mechanisms in the cytotoxic action of non-biodegradable engineered nanoparticles. Current Drug Metabolism. 2013. p. 976-88.

217. Gong X, Lin C, Cheng J, Su J, Zhao H, Liu T, et al. Generation of multicellular tumor spheroids with microwell-based agarose scaffolds for drug testing. PloS One. 2015; 10(6):e0130348.

218. Zhao Z, Ukidve A, Krishnan V, Mitragotri S. Effect of physicochemical and surface properties on *in vivo* fate of drug nanocarriers. Advanced Drug Delivery Reviews. 2019; 143:3-21.

219. Semple SC, Chonn A, Cullis PR. Interactions of liposomes and lipid-based carrier systems with blood proteins: Relation to clearance behaviour *in vivo*. Advanced Drug Delivery Reviews. 1998; 32(1):3-17.

220. Ivanov DP, Parker TL, Walker DA, Alexander C, Ashford MB, Gellert PR, et al. Multiplexing spheroid volume, resazurin and acid phosphatase viability assays for high-throughput screening of tumour spheroids and stem cell neurospheres. PloS One. 2014.

221. Brüningk SC, Rivens I, Box C, Oelfke U, ter Haar G. 3D tumour spheroids for the prediction of the effects of radiation and hyperthermia treatments. Scientific Reports. 2020; 10(1):1653.

222. Cedervall T, Lynch I, Lindman S, Berggard T, Thulin E, Nilsson H, et al. Understanding the nanoparticle-protein corona using methods to quantify exchange rates and affinities of proteins for nanoparticles. Proceedings of the National Academy of Sciences of the United States of America. 2007; 104(7):2050.

223. Lynch I, Cedervall T, Lundqvist M, Cabaleiro-Lago C, Linse S, Dawson KA. The nanoparticle-protein complex as a biological entity; a complex fluids and surface science challenge for the 21st century. Advances in Colloid and Interface Science. 2007; 134-135:167-74.

224. Bodansky O. Acid phosphatase. Advances in Clinical Chemistry. 1972; 15:43-147.

225. Bozzo GG, Raghothama KG, Plaxton WC. Structural and kinetic properties of a novel purple acid phosphatase from phosphate-starved tomato (lycopersicon esculentum) cell cultures. The Biochemical Journal. 2004; 377(Pt 2):419-28.

226. Moradi S, Shareghi B, Saboury AA, Farhadian S. Evaluation of the effect of $MnFe_2O_4$ nanoparticles on the activity parameters and stability of acid phosphatase. Monatshefte für Chemie - Chemical Monthly. 2021; 152(1):175-84.

227. Salesa B, Assis M, Andrés J, Serrano-Aroca Á. Carbon nanofibers versus silver nanoparticles: Time-dependent cytotoxicity, proliferation, and gene expression. Biomedicines. 2021; 9(9).

228. Paknijadi M, Bayat M, Salimi M, Razavilar V. Concentration- and time-dependent cytotoxicity of silver nanoparticles on normal human skin fibroblast cell line. Iranian Red Crescent Medical Journal. 2018.

229. Manna SK, Sarkar S, Barr J, Wise K, Barrera EV, Jejelowo O, et al. Single-walled carbon nanotube induces oxidative stress and activates nuclear transcription factor-κb in human keratinocytes. Nano Letters. 2005; 5(9):1676-84.

230. Cui D, Tian F, Ozkan CS, Wang M, Gao H. Effect of single wall carbon nanotubes on human HEK293 cells. Toxicology Letters. 2005; 155(1):73-85.

231. Efeoglu E, Casey A, Byrne HJ. In vitro monitoring of time and dose dependent cytotoxicity of aminated nanoparticles using raman spectroscopy. The Analyst. 2016; 141(18):5417-31.

232. Suliman Y AO, Ali D, Alarifi S, Harrath AH, Mansour L, Alwasel SH. Evaluation of cytotoxic, oxidative stress, proinflammatory and genotoxic effect of silver nanoparticles in human lung epithelial cells. Environmental Toxicology. 2015; 30(2):149-60.

233. Kus-Liśkiewicz M, Fickers P, Ben Tahar I. Biocompatibility and cytotoxicity of gold nanoparticles: Recent advances in methodologies and regulations. International Journal of Molecular Sciences. 2021; 22(20).

234. Tee JK, Ong CN, Bay BH, Ho HK, Leong DT. Oxidative stress by inorganic nanoparticles. WIREs Nanomedicine and Nanobiotechnology. 2016; 8(3):414-38.

235. Mirshafiee V, Kim R, Mahmoudi M, Kraft ML. The importance of selecting a proper biological milieu for protein corona analysis *in vitro*: Human plasma versus human serum. The International Journal of Biochemistry & Cell Biology. 2016; 75:188-95.

236. Salvati A, Pitek AS, Monopoli MP, Prapainop K, Bombelli FB, Hristov DR, et al. Transferrin-functionalized nanoparticles lose their targeting capabilities when a biomolecule corona adsorbs on the surface. Nature nanotechnology. 2013; 8(2):137-43.

237. Sobczynski DJ, Charoenphol P, Heslinga MJ, Onyskiw PJ, Namdee K, Thompson AJ, et al. Plasma protein corona modulates the vascular wall interaction of drug carriers in a material and donor specific manner. PloS One. 2014.

238. Lazarovits J, Chen YY, Sykes EA, Chan WCW. Nanoparticle–blood interactions: The implications on solid tumour targeting. Chemical Communications. 2015; 51(14):2756-67.

239. Norde W, Gage RA. Interaction of bovine serum albumin and human blood plasma with PEO-tethered surfaces: Influence of PEO chain length, grafting density and temperature. Langmuir. 2004; 20(10):4162-7.

240. Coulter JA, Jain S, Butterworth KT, Taggart LE, Dickson GR, McMahon SJ, et al. Cell type-dependent uptake, localization, and cytotoxicity of 1.9 nm gold nanoparticles. International Journal of Nanomedicine. 2012; 7:2673-85.

241. Khurana L, ElGindi M, Tilstam PV, Pantouris G. Chapter seventeen - elucidating the role of an immunomodulatory protein in cancer: From protein expression to functional characterization. In: Galluzzi L, Rudqvist N-P, editors. Methods in Enzymology: Academic Press; 2019. p. 307-60.

242. Geetha R, Ashokkumar T, Tamilselvan S, Govindaraju K, Sadiq M, Singaravelu G. Green synthesis of gold nanoparticles and their anticancer activity. Cancer Nanotechnology. 2013; 4(4):91-8.

243. El-Kassas HY, El-Sheekh MM. Cytotoxic activity of biosynthesized gold nanoparticles with an extract of the red seaweed corallina officinalis on the MCF-7 human breast cancer cell line. Asian Pacific Journal of Cancer Prevention. 2014; 15(10):4311-7.

244. Tapan Kumar P, Smruti Ranjan M. Caspases: An apoptosis mediator. Journal of Advanced Veterinary and Animal Research. p. 18-22.

245. Lee B, Lee DG. Synergistic antibacterial activity of gold nanoparticles caused by apoptosis-like death. Journal of Applied Microbiology. 2019; 127(3):701-12.

246. Kang B, Mackey MA, El-Sayed MA. Nuclear targeting of gold nanoparticles in cancer cells induces DNA damage, causing cytokinesis arrest and apoptosis. Journal of the American Chemical Society. 2010; 132(5):1517-9.

247. Pan Y, Neuss S, Leifert A, Fischler M, Wen F, Simon U, et al. Size-dependent cytotoxicity of gold nanoparticles. Small. 2007; 3(11):1941-9.

248. Liu M, Gu X, Zhang K, Ding Y, Wei X, Zhang X, et al. Gold nanoparticles trigger apoptosis and necrosis in lung cancer cells with low intracellular glutathione. Journal of Nanoparticle Research. 2013; 15(8):1745.

249. Paoli P, Giannoni E, Chiarugi P. Anoikis molecular pathways and its role in cancer progression. Biochimica et Biophysica Acta (BBA) - Molecular Cell Research. 2013; 1833(12):3481-98.

250. Malagobadan S, Nagoor NH. Anoikis. In: Boffetta P, Hainaut P, editors. Encyclopedia of cancer (third edition). Oxford: Academic Press; 2019. p. 75-84.

251. Chiarugi P, Giannoni E. Anoikis: A necessary death program for anchorage-dependent cells. Biochemical Pharmacology. 2008; 76(11):1352-64.

252. Leist M, Single B, Castoldi AF, Kühnle S, Nicotera P. Intracellular adenosine triphosphate (ATP) concentration: A switch in the decision between apoptosis and necrosis. The Journal of Experimental Medicine. 1997; 185(8):1481-6.

253. Ma Y-H, Huang C-P, Tsai J-S, Shen M-Y, Li Y-K, Lin L-Y. Water-soluble germanium nanoparticles cause necrotic cell death and the damage can be attenuated by blocking the transduction of necrotic signaling pathway. Toxicology Letters. 2011; 207(3):258-69.

254. Li JJ, Hartono D, Ong C-N, Bay B-H, Yung L-YL. Autophagy and oxidative stress associated with gold nanoparticles. Biomaterials. 2010; 31(23):5996-6003.

255. Mora-Huertas CE, Fessi H, Elaissari A. Polymer-based nanocapsules for drug delivery. International Journal of Pharmaceutics. 2010; 385(1-2):113-42.

256. Zeiss CJ. The apoptosis-necrosis continuum: Insights from genetically altered mice. Veterinary Pathology. 2003; 40(5):481-95.

257. Chen P, Wang H, He M, Chen B, Yang B, Hu B. Size-dependent cytotoxicity study of Zn) nanoparticles in HepG2 cells. Ecotoxicology and Environmental Safety. 2019; 171:337-46.

258. Reisetter AC, Stebounova LV, Baltrusaitis J, Powers L, Gupta A, Grassian VH, et al. Induction of inflammasome-dependent pyroptosis by carbon black nanoparticles. The Journal of biological chemistry. 2011; 286(24):21844-52.

7. Appendix I: Ethical approval

UNIVERSITEIT VAN PRETORIA
UNIVERSITY OF PRETORIA
YUNIBESITHI YA PRETORIA

Faculty of Health Sciences

Institution: The Research Ethics Committee, Faculty Health Sciences, University of Pretoria complies with ICH-GCP guidelines and has US Federal wide Assurance.
- FWA 00002567. Approved dd 18 March 2022 and Expires 18 March 2027.
- IORG #: IORG0001762 OMB No. 0990-0278 Approved for use through August 31, 2023

Faculty of Health Sciences **Research Ethics Committee**

11 November 2022

Approval Certificate
Annual Renewal

Dear Ms M Petzer,

Ethics Reference No.: 690/2019 – Line 3
Title: Multicellular spheroids as a platform for cytotoxicity assessment of gold nanoparticles

The **Annual Renewal** as supported by documents received between 2022-10-26 and 2022-11-09 for your research, was approved by the Faculty of Health Sciences Research Ethics Committee on 2022-11-09 as resolved by its quorate meeting.

Please note the following about your ethics approval:
- Renewal of ethics approval is valid for 1 year, subsequent annual renewal will become due on 2023-11-11.
- Please remember to use your protocol number (690/2019) on any documents or correspondence with the Research Ethics Committee regarding your research.
- Please note that the Research Ethics Committee may ask further questions, seek additional information, require further modification, monitor the conduct of your research, or suspend or withdraw ethics approval.

Ethics approval is subject to the following:
- The ethics approval is conditional on the research being conducted as stipulated by the details of all documents submitted to the Committee. In the event that a further need arises to change who the investigators are, the methods or any other aspect, such changes must be submitted as an Amendment for approval by the Committee.

We wish you the best with your research.

Yours sincerely

On behalf of the FHS REC, Professor Werdie (CW) Van Staden
MBChB, MMed(Psych), MD, FCPsych(SA), FTCL, UPLM
***Chairperson**: Faculty of Health Sciences Research Ethics Committee*

The Faculty of Health Sciences Research Ethics Committee complies with the SA National Act 61 of 2003 as it pertains to health research and the United States Code of Federal Regulations Title 45 and 46. This committee abides by the ethical norms and principles for research, established by the Declaration of Helsinki, the South African Medical Research Council Guidelines as well as the Guidelines for Ethical Research: Principles Structures and Processes, Second Edition 2016 (Department of Health)

Research Ethics Committee
Room 1 68, Level 1, Tswelopele Building
University of Pretoria, Private Bag x323
Gezina 0031, South Africa
Tel: 27 (0)12 356 3084
Email: deepika.behari@up.ac.za
www.up.ac.za

Fakulteit Gesondheidswetenskappe
Lefapha la Litsebenzi tša Maphelo

8. Appendix II: Reagent preparation and storage

1. Nanoparticles

The AuNPs sourced from the NIOH (Johannesburg, South Africa) were refrigerated at 4°C until needed. The PCOOH-AuNPs were received at a stock concentration of 2.5 x 10^{12} NP/mL and the amine-liganded AuNPs were received at a stock concentration of 1.8 x 10^{14} NP/mL. The AuNPs made up to the chosen concentrations by diluting the stock in FCS-free DMEM.

2. Maintenance of cell cultures and MCS generation

2.1. Ethanol

Absolute ethanol was sourced from Merck (Johannesburg, South Africa) and can be stored at room temperature until use. Dilution of the ethanol was achieved using distilled water.

2.2. A549 alveolar carcinoma cell line

A549 cells (ATCC® CCL-185™) were obtained from the American Type Culture Collection (Virginia, United States). 96-well and 12-well plates, as well as Corning® T75 culture flasks were obtained from Merck (Johannesburg, South Africa).

2.3. Dulbecco's Modified Eagle's Medium (DMEM)

Dulbecco's Modified Eagle's Medium (DMEM) was obtained from Merck (Johannesburg, South Africa) and refrigerated at 4°C until use. Medium (495 mL) was supplemented with 5 mL penicillin/streptomycin (100%) to achieve a 1% dilution in-reaction. To aid cell growth, medium (450 mL) was fortified with 50 mL heat-inactivated FCS to achieve a 10% solution in-reaction.

2.4. Foetal calf serum

Foetal calf serum (FCS) was purchased from Merck (Johannesburg, South Africa) and kept frozen until use.

2.5. Penicillin/Streptomycin

Penicillin/streptomycin solution was obtained from the Merck (Johannesburg, South Africa) and kept frozen until use.

3. Freezing of cell stock

3.1. Freezing medium

Freezing medium (50 mL) was prepared by adding 37 mL of FCS-negative DMEM (1% Penicillin/streptomycin and 1% Glutamine fortified) to a 50 mL flask and adding 10 mL FCS and 2.5 mL pure DMSO. Freezing medium was stored at 4°C for up to one month.

3.2. FTA hemagluttination buffer

FTA hemagluttination buffer was purchased from BD Biosciences (Sandton, South Africa) and used to prepare PBS. To prepare PBS, 9.23 g powder was dissolved in 1 L distilled water. The PBS solution was autoclaved before use to ensure sterility and stored at room temperature.

3.3. TrypLE™ Express

TrypLE™ Express was obtained from ThermoFisher Scientific (Centurion, South Africa) and refrigerated at 4°C until use.

3.4. Trypan blue counting solution

Trypan blue powder was obtained from Merck (Johannesburg, South Africa). To prepare a 0.1% solution, 1 mg powder was dissolved in 100 mL PBS. The stain was stored at room temperature until use.

3.5. Agarose

Agarose powder was obtained from Merck (Johannesburg, South Africa) and stored at room temperature until use. To prepare 1% agarose, 10 mg powder was dissolved in 100 mL FCS-free medium. The agarose was autoclaved to assist with dissolution and to sterilise it. After autoclaving the agarose was refrigerated at 4°C until use. Prior to use, agarose was melted using a microwave.

4. Microwell system for MCS generation

The 9 x 9 array negative polydimethylsiloxane moulds (MicroTissues® 3D Petri Dish®) were obtained from Merck (Johannesburg, South Africa) and were autoclaved prior to each generation of microwells to ensure sterility.

5. Determination of spheroid growth and viability

5.1. Acid phosphatase assay

5.1.1. Citrate buffer

Sodium citrate dihydrate and citric acid was obtained from Merck (Johannesburg, South Africa). A 0.04 mM sodium citrate dihydrate and 0.06 M citric acid solution was prepared by dissolving 12.044 g sodium citrate dihydrate and 11.341 g citric acid with 800 mL distilled water. The pH was adjusted to approximately 6 (using NaOH to increase the pH and HCl to decrease the pH) and the volume was constituted to 1 L using distilled water. The buffer was autoclaved before use to ensure sterility. It was refrigerated at 4°C until needed.

5.1.2. Assay buffer

The assay buffer was prepared by dissolving 20 mg para-nitrophenylphosphate (2 mg/mL) with 100 µL Triton X-100 by reverse pipette method (0.1% v/v) and making it up to a final volume of 100 mL in citrate buffer (0.1 M). All reagents were obtained from Merck (Johannesburg, South Africa). The buffer was refrigerated at 4°C until use.

5.1.3. Saponin (1%)

Saponin was obtained from Merck (Johannesburg, South Africa) and stored at room temperature until needed. A 1% w/v solution was prepared by dissolving 1 g of saponin powder in 100 mL distilled water. The solution was autoclaved after dilution as sterilisation step, after which it was stored in the dark at 4°C.

5.1.4. Sodium hydroxide

A 10 M stock solution was prepared by dissolving 40 g NaOH pellets in 100 mL distilled water. Dilution of 1/10 (1 mL 10 M stock with 9 mL distilled water) resulted in a 1 M solution. The solution was stored at room temperature.

6. Bicinchoninic acid assay

6.1. Bovine serum albumin standards

Bovine serum albumin (BSA) powder was obtained from Merck (Johannesburg, South Africa) and stored at 4°C until use. A BSA stock solution of 2 mg/mL was prepared by dissolving 2 mg of BSA powder in 1 mL of PBS. From this stock solution further dilutions were prepared with PBS: 0.1, 0.2, 0.25, 0.5, 1.0, and 1.5 mg/mL. Solutions were freshly prepared for each assay.

6.2. Radioimmunoprecipitation assay buffer

The radioimmunoprecipitation assay **(**RIPA) buffer was obtained from Merck (Johannesburg, South Africa) and stored at -20°C until use. Once the container was opened it was stored upright at 4°C.

6.3. Bicinchoninic acid assay working solution

The working solution was prepared by individually preparing the two components of the working solution; reagent A and reagent B, after which they were mixed at a volumetric ratio of 50:1 (reagent A:reagent B) immediately before carrying out the assay.

All salts required for preparation of BCA reagent A was purchased from Merck (Johannesburg, South Africa). Reagent A was prepared by dissolving 1 g BCA disodium hydrate salt, 0.95 g sodium bicarbonate, 2 g sodium carbonate, 0.4 g sodium hydroxide and 0.16 g sodium tartrate to a final volume of 100 mL in distilled water. The pH of the solution was adjusted to 11.25 and the solution was stored at 4°C. BCA reagent B was prepared by dissolving 0.4 g copper II sulphate pentahydrate (Merck, Johannesburg, South Africa) to a final volume of 10 mL in distilled water. The solution was protected from light and stored at 4°C.

7. Cell cycle analysis

7.1. Propidium iodide (interference study)

Propidium iodide (PI) powder was obtained from Merck (Johannesburg, South Africa) and stored between 2°C and 8°C until required. A 160 mg/mL stock solution was prepared by dissolving 160 mg of PI powder in 1 mL of DMSO and storing the

solution at -80°C until needed. Dilutions for in-reaction concentrations of 2 mg/mL and 5 mg/mL for interference studies were prepared in PBS.

7.2. Accutase

Accutase® solution was obtained from Merck (Johannesburg, South Africa) and stored at -80°C until needed for MCS dissociation.

7.3. Propidium iodide staining solution

Propidium iodide powder, RNaseA and Triton X-100 was sourced from Merck (Johannesburg, South Africa). All reagents were stored at room temperature, except for the RNaseA, which was kept refrigerated at 4°C until the solution was prepared. To prepare 10 mL of staining solution, 0.4 mg of PI powder and 1 mg of RNaseA was dissolved in 100 µL of Triton X-100 and 10 mL of distilled water. The solution was prepared fresh before each assay.

8. Caspase-3/7 activity

8.1. Acetyl-Asp-Glu-Val-Asp-7-amido-4-methylcoumarin (Ac-DEVD-AMC)

Ac-DEVD-AMC powder was obtained from Merck (Johannesburg, South Africa). A 5 mM stock solution was prepared by dissolving 5 mg Ac-DEVD-AMC powder in 1.48 mL pure DMSO. This stock was stored at -80°C in 10 µL aliquots.

8.2. Phenylmethylsulfonyl fluoride (PMSF)

The PMSF powder was obtained from Sigma-Aldrich (St. Louis, USA). A 100 mM stock solution was prepared by dissolving 17.4 mg PMSF in 1 mL pure DMSO. The stock was stored at -80°C in 50 µL aliquots in Eppendorf tubes.

8.3. 4-(2-hydroxyethyl)-1-piperazineethanesulfonic acid (HEPES)

4-(2-hydroxyethyl)-1-piperazineethanesulfonic acid (HEPES) powder was obtained from Merck (Johannesburg, South Africa) and stored at room temperature until needed to prepare the buffers.

8.4. Ethylenediaminetetraacetic acid (EDTA)

Ethylenediaminetetraacetic acid (EDTA) powder was obtained from Merck (Johannesburg, South Africa) and stored at room temperature until needed to prepare the buffers.

8.5. 3-[(3-cholamidopropyl)-dimethylammonio]-1-propanesulfate (CHAPS)

The CHAPS powder was procured from Merck (Johannesburg, South Africa) and stored at 4°C until needed to prepare the buffers.

8.6. β-mercaptoethanol

A 14.3 M solution was purchased from Merck (Johannesburg, South Africa) and stored at room temperature, in the dark, until needed to prepare the buffers.

8.7. Lysis buffer

A solution consisting of 10 mM HEPES, 2 mM CHAPS, 5 mM EDTA, 0.5 mM PMSF and 4.3 mM β-mercaptoethanol was prepared. The incomplete lysis buffer was prepared by dissolving 238.3 mg HEPES, 122.98 mg CHAPS and 146.12 mg EDTA in 100 mL distilled water. This incomplete buffer was stored at 4°C until needed. Thirty min before the start of each experiment a 50 µL aliquot of PMSF (100 mM) was added to 10 mL of the refrigerated incomplete buffer as well as 3 µL β-mercaptoethanol (14.3 M).

8.8. Assay buffer

A solution consisting of 20 mM HEPES, 2 mM EDTA, 0.5 mM PMSF, 4.3 mM β-mercaptoethanol and 5 µM Ac-DEVD-AMC was prepared. The incomplete assay buffer was prepared by dissolving 476.6 mg HEPES and 58.4 mg EDTA in 100 mL distilled water. This incomplete buffer was stored at 4°C until needed. Thirty min before the start of each experiment a 50 µL aliquot of PMSF (100 mM) and 10 µL aliquot of Ac-DEVD-AMC (5 mM) was added to 10 mL of the refrigerated incomplete buffer as well as 3 µL β-mercaptoethanol (14.3 M).

8.9. Cisplatin control

Cisplatin powder was obtained from Merck (Johannesburg, South Africa) and frozen until needed. A 10 mM stock solution was prepared by dissolving 3.01 mg cisplatin in 1 mL of pure DMSO. Aliquots (100 µL) were frozen at -80°C until needed. The cisplatin was made up to desired in-reaction concentrations using FCS-free DMEM.

9. Appendix III: Gold nanoparticles documentation

Sterility reports:

NATIONAL INSTITUTE FOR OCCUPATIONAL HEALTH
Division of the National Health Laboratory Service

Immunology & Microbiology Section
25 Hospital Street, Constitution Hill, Johannesburg, 2000
Tel: +27 (0)11 712 6475 Fax: +27 (0)11 712 6426
Tanusha.singh@nioh.nhls.ac.za

TEST REPORT			
LAB/REPORT NO. :	**IM100-107/18**	**REPORT DATE; TIME:**	**June 6, 2018; 08:02**
REFERRING PERSON:	**n/a**	**CONSULTATION DATE:**	**n/a**
SAMPLE CONDITION:	**good**	**SAMPLE RECEIPT DATE:**	**01 June 2018**
CONTACT DETAILS:			
COMPANY NAME:	**NIOH**	**CONTACT PERSON:**	**Melissa Vetten**
ADDRESS:	**25 Hospital Street Johannesburg**		
TEL:	**011 712 6400**	**FAX:**	**-**
PATIENT DETAILS:			
PATIENT NAME:	**n/a**		
AGE:	**n/a**	**SEX:**	**n/a**
TESTS REQUESTED:	**Sterility testing for bacteria (NIOH0292)**		

Dear Ms Melissa Vetten

RE: Testing for bacterial contamination of nanoparticle samples

Laboratory analysis of samples

The Laboratory received eight nanoparticle samples for testing for bacterial contamination on the 01 June 2018. Samples were cultured on Tryptic soy agar (TSA) and incubated at 37°C±2 for 3 days to support bacterial growth. The final results are recorded on the table 1.

Quality Control

Aseptic techniques were followed and TSA culture plates were checked for sterility before analyses were performed. A sterile plate was streaked with *E.coli* specie as a positive control, and sterile TSA plate was treated as a negative control. Control plates were incubated together with the test samples for quality control purposes and growth of *E. coli* as positive control, and no growth for sterile agar plate indicated that the media used for the test was not contaminated.

TEST REPORT			
LAB/REPORT NO. :	**IM560-564/18**	**REPORT DATE:**	**September 27, 2018**
REFERRING PERSON:	**n/a**	**CONSULTATION DATE:**	**n/a**
SAMPLE CONDITION:	**good**	**SAMPLE RECEIPT DATE:**	**21 September 2018**
CONTACT DETAILS:			
COMPANY NAME:	**NIOH**	**CONTACT PERSON:**	**Melissa Vetten**
ADDRESS:	**25 Hospital Street Johannesburg**		
TEL:	**011 712 6400**	**FAX:**	**-**
PATIENT DETAILS:			
PATIENT NAME:	**n/a**		
AGE:	**n/a**	**SEX:**	**n/a**
TESTS REQUESTED:	**Sterility testing for bacteria (NIOH0292)**		

Dear Ms Melissa Vetten

RE: Testing for bacterial contamination of nanoparticle samples

Laboratory analysis of samples

The Laboratory received five nanoparticle samples for testing for bacterial contamination on the 21 September 2018. Samples were cultured on Tryptic soy agar (TSA) and incubated at 37°C±2 for 3 days to support bacterial growth. The final results are recorded on the table 1.

Quality Control

Aseptic techniques were followed and TSA culture plates were checked for sterility before analyses were performed. A sterile plate was streaked with *E.coli* specie as a positive control, and sterile TSA plate was treated as a negative control. Control plates were incubated together with the test samples for quality control purposes and growth of *E. coli* as positive control, and no growth for sterile agar plate indicated that the media used for the test was not contaminated.

Certificate of Analysis:

NP0138

MINTEK
Specialists in mineral and metallurgical technology

ISO 9001 QUALITY MANAGEMENT SYSTEM
ISO 17025 TESTING AND CALIBRATION LABORATORY
ISO 14001 ENVIRONMENTAL MANAGEMENT SYSTEM
OHSAS 18001 OCCUPATIONAL HEALTH AND SAFETY MANAGEMENT SYSTEM

CERTIFICATE OF ANALYSIS

MINTEK GOLD NANOPARTICLES

Product : [100%PC000II14GJ
Batch number : [20180515SC052]
Production date : [15 May 2018]
Expiry date : [April 2019]
Form : [2x 50 mL Au nanoparticles in milli-Q water]

Properties and Test Methods

Property	Units	Typical Values (as in the SOP)	Results
UV Absorbance	nm	[e.g. 517 - 522 nm]	522 nm
Concentration (OD)	-	[e.g. 0.8 – 1.2]	1.01
½ OD	nm	[e.g. < 599]	585
Citrate concentration	%	[e.g. 0.01 – 0.05 %]	0.03 %

Manufacturing procedure: [Standard citrate reduction method]

Sterilisation method/s: [N/A]

Particle size (Method Used): [14±2 nm; TEM]
Surface Charge (Method used): [-58.2 mV (ζ-potential measured using Malvern Zetasizer)]

Concentration: 3.6 nM; 2.2 x 10^{12} nps/ml

28/05/2018
Date

Caroline Mphela
(SHEQ office – Mintek AMD)

28/05/2018
Date

Dr Lucky Sikhwivhilu
(Head - Nanotechnology group)

200 Malibongwe Drive (Formerly Hans Strijdom Drive), Randburg
Tel: 011 709 4111 Fax: 011 793 2413 http://www.mintek.co.za
Telegrams: Mintekse, Johannesburg Telex: 4-24867 SA
All correspondence to: Private Bag X3015, Randburg, 2125, South Africa

10. Appendix IV: Phase contrast images

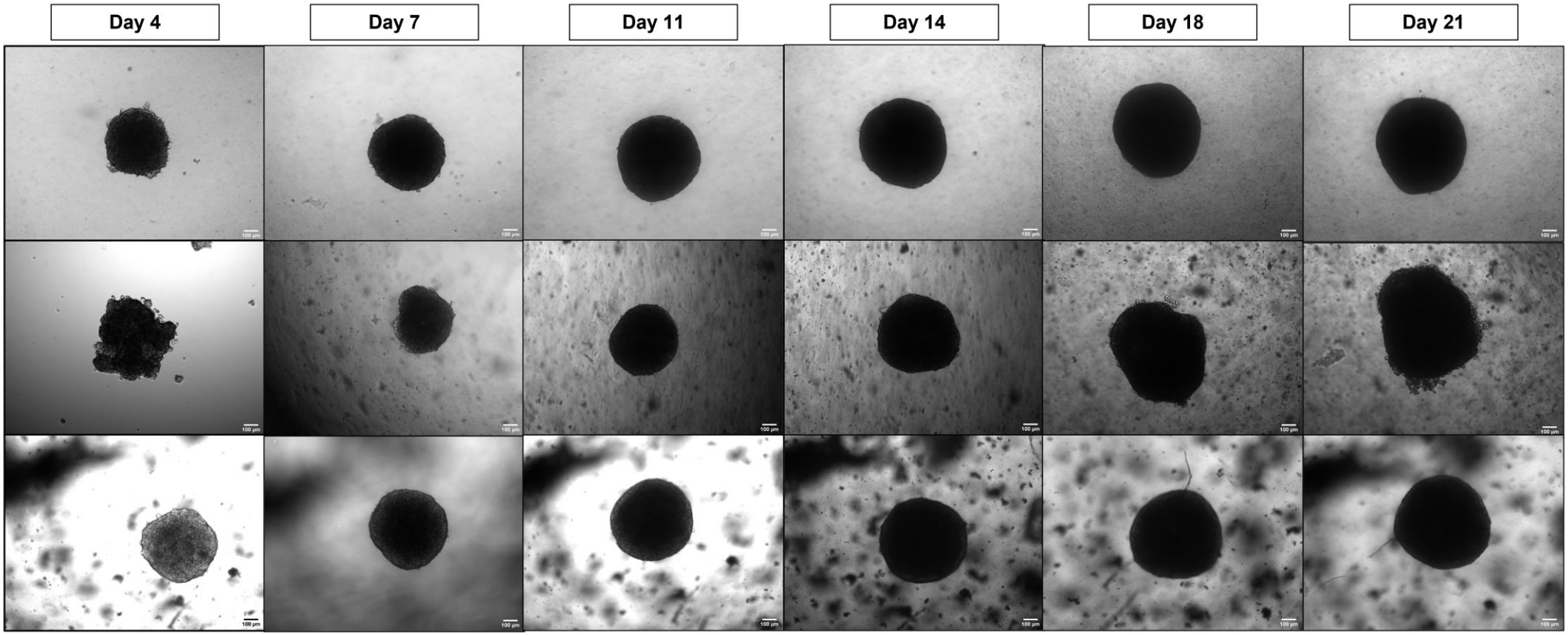

Figure 10.1: Phase-contrast images taken at 4 x magnification at three-day intervals of A549 multicellular spheroids from Day 4 until Day 21. Three sets of images are shown with one set per row. Scale bar = 100 µm.

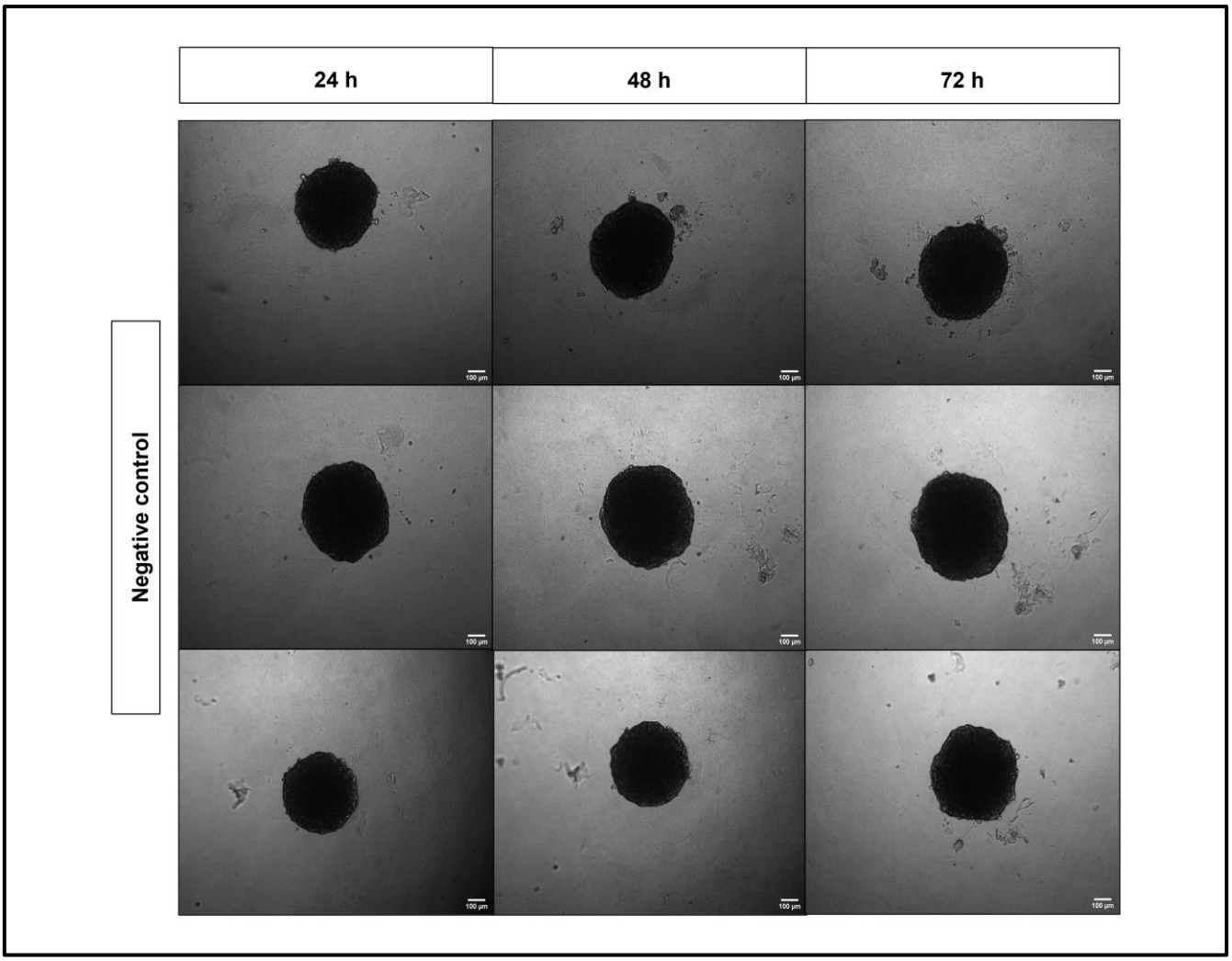

Figure 10.2: Triplicate images taken at 4 x magnification of the negative control of Day 7 A549 multicellular spheroids at 24 h (column 1), 48 h (column 2) and 72 h (column 3). Scale bar = 100 µm.

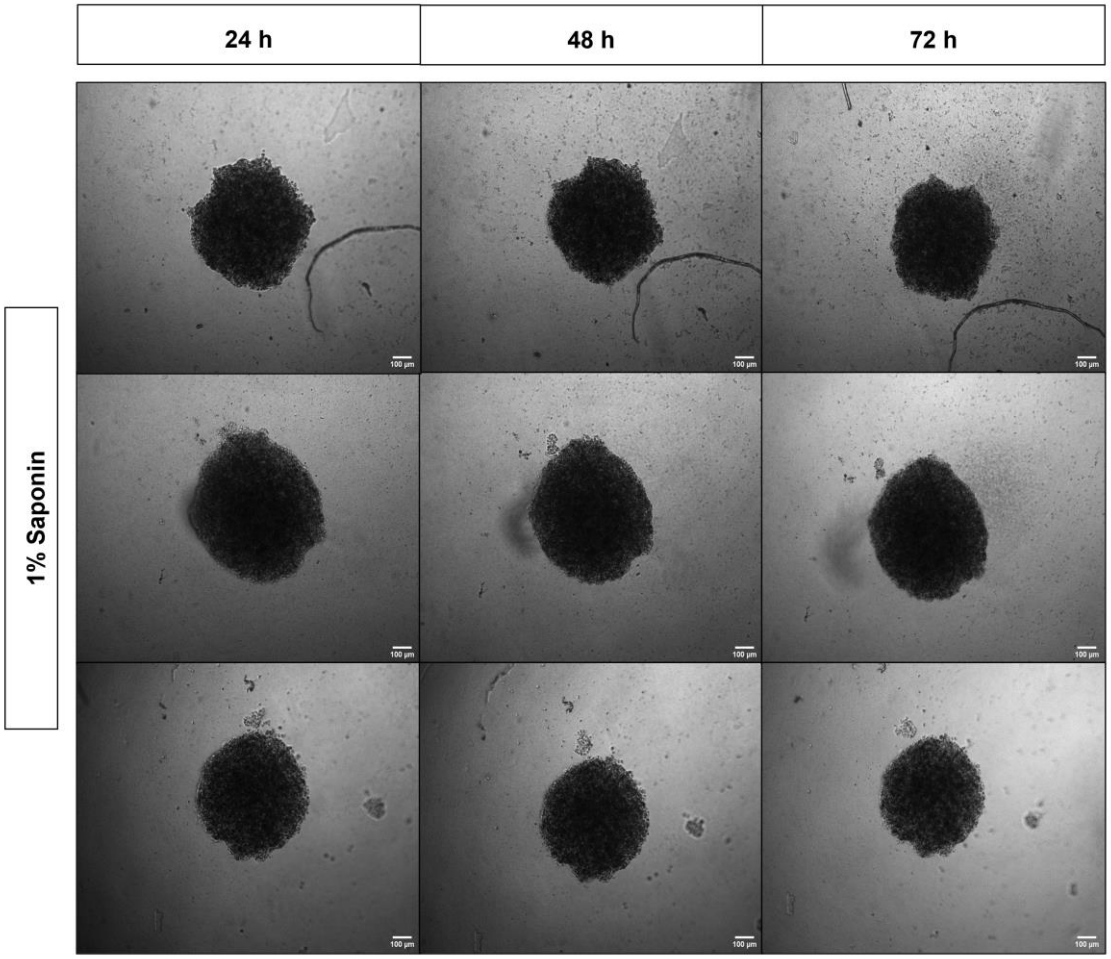

Figure 10.3: Triplicate images taken at 4 x magnification of the positive control of Day 7 A549 multicellular spheroids after exposure to 1% saponin for 24 h (column 1), 48 h (column 2) and 72 h (column 3). Scale bar = 100 µm.

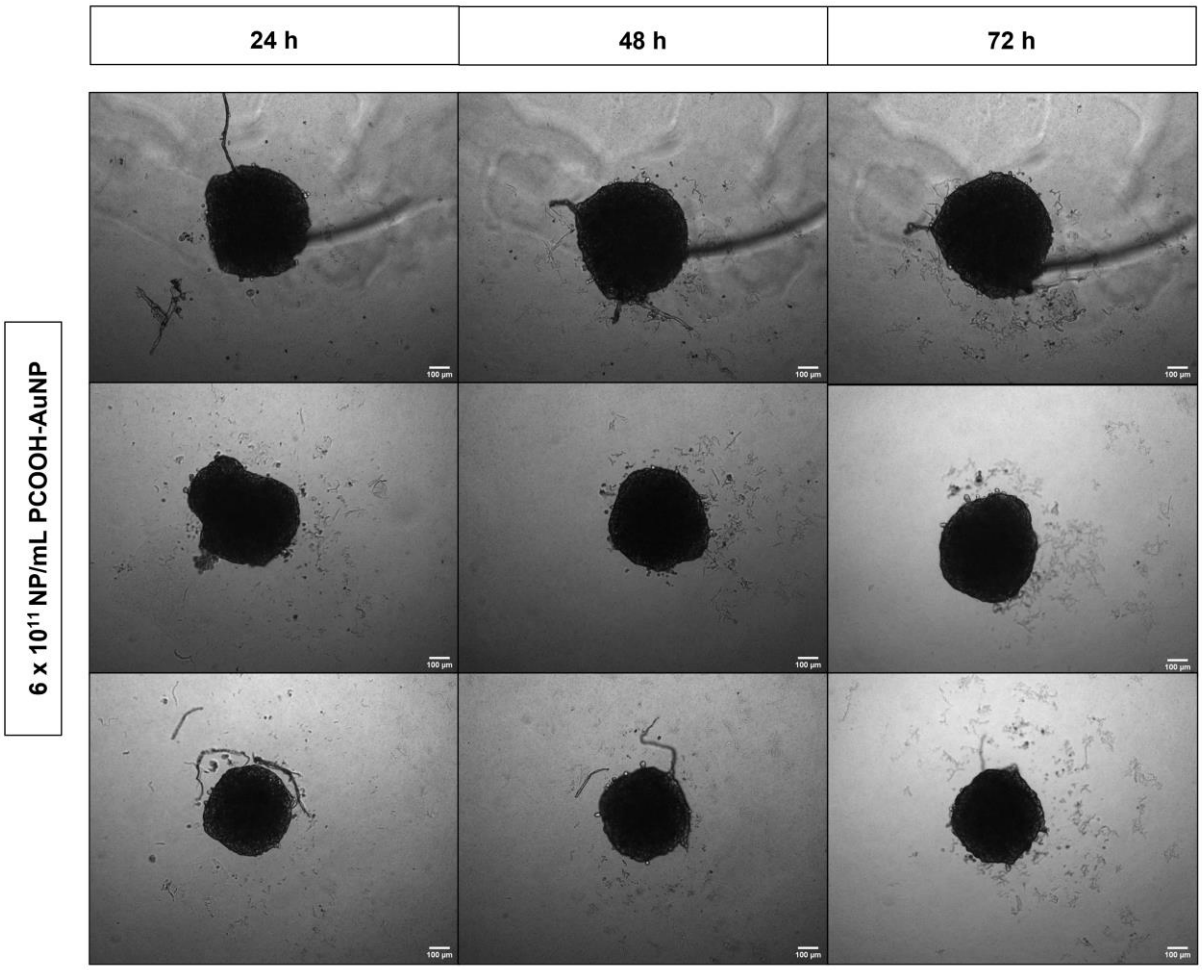

Figure 10.4: Triplicate images taken at 4 x magnification of Day 7 A549 multicellular spheroids exposed to 6 x 10^{11} NP/mL PCOOH-AuNPs for 24 h (column 1), 48 h (column 2) and 72 h (column 3). Scale bar = 100 µm.

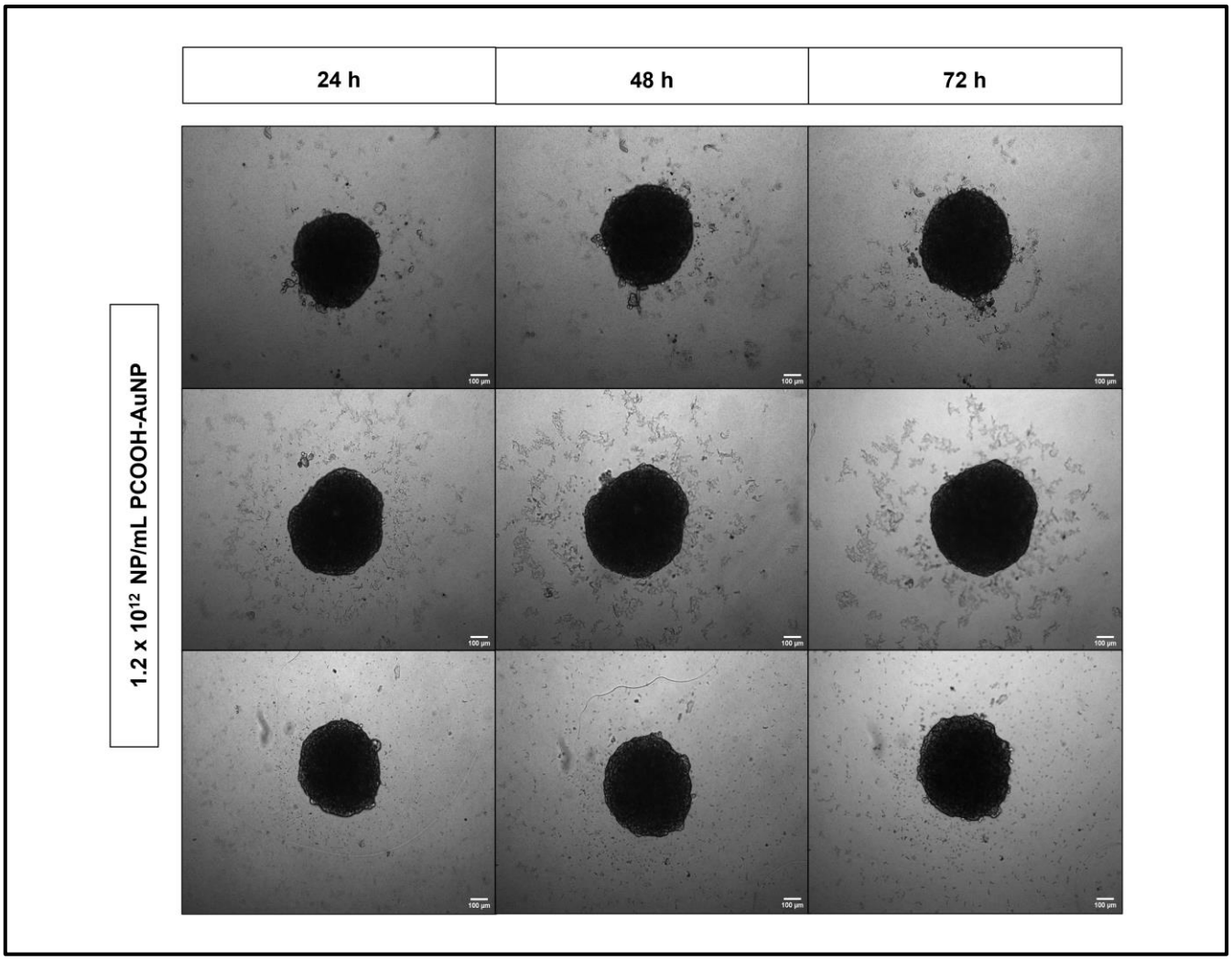

Figure 10.5: Triplicate images taken at 4 x magnification of Day 7 A549 multicellular spheroids exposed to 1.2 x 10^{12} NP/mL PCOOH-AuNPs for 24 h (column 1), 48 h (column 2) and 72 h (column 3). Scale bar = 100 µm.

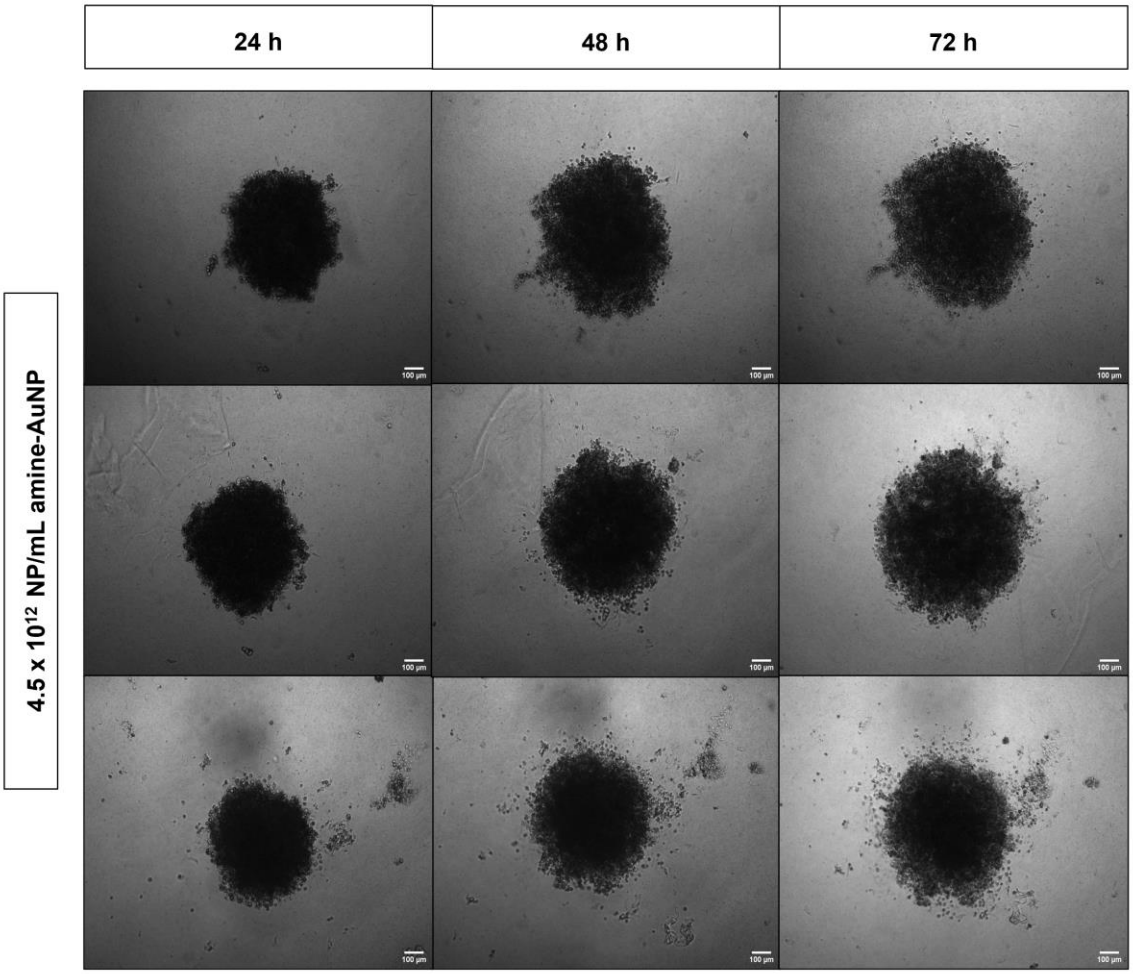

Figure 10.6: Triplicate images taken at 4 x magnification of Day 7 A549 multicellular spheroids exposed to 4.5 x 10^{12} NP/mL amine-AuNPs for 24 h (column 1), 48 h (column 2) and 72 h (column 3). Scale bar = 100 µm.